İSTANBUL TECHNICAL UNIVERSITY ★ INSTITUTE OF SCIENCE AND TECHNOLOGY

AN EXPERIMENTAL STUDY ON RECTANGULAR TWIN JETS

Ph.D. Thesis by

Duygu ERDEM, M.Sc.

(511942001)

Date of submission : 13 April 2001

Date of defence examination: 26 October 2001

Supervisor (Chairman): Prof.Dr. Veysel ATLI (EÜ)

Members of the Examining Committee Prof.Dr. M. Fevzi ÜNAL

Prof.Dr. İ. Bedii ÖZDEMİR

Assoc.Prof.Dr. M. Şerif KAVSAOĞLU(ODTÜ)

Assoc.Prof.Dr. M. Zafer GÜL (MÜ)

OCTOBER 2001

ACKNOWLEDGMENTS

I would like to thank my advisor, Prof. Dr. Veysel ATLI, for his support, guidance and encouragement throughout this study. I am grateful to him for giving me the motivation to complete my PhD study.

I also wish to thank my co-advisor Prof. Dr. Fevzi ÜNAL for his contributions and advice.

I am thankful to my colleagues Asst. Prof. Dr. Hayri ACAR and Asst. Prof. Dr. N. L. Okşan ÇETİNER-YILDIRIM for their friendship and valuable help.

I would like to extend my special thanks to Technicians Aliosman TABANLI and Ercan BAŞARIR for their valuable contributions.

Finally, many thanks to my family who provided an excellent background for my education, especially to my mother for her patience and understanding during my PhD study.

April, 2001 Duygu ERDEM

İstanbul

CONTENTS

ABBREVIATIONS

CTA	: Constant Temperature Anemometer
HWA	: Hot Wire Anemometer
STOL	: Short Take-off and Landing
VTOL	: Vertical Take-off and Landing

LIST OF TABLES

LIST OF FIGURES

LIST OF SYMBOLS

C_P	: Pressure coefficient
f	: Frequency
h	: Nozzle exit height
h/ℓ	: Jet aspect ratio
H^-	: S-h
H^+	: S+h
ℓ	: Nozzle exit length
ℓ	: Mixing length
M_0	: Momentum flux (at the nozzle exit)
Re	: Reynolds number
Re_h	: Reynolds number based on nozzle exit height
S	: Jet spacing
S/h	: Spacing ratio
St	: Strouhal number
S_{xx}	: Auto-spectral density
u'	: Fluctuating streamwise velocity component
$\bar{u}$, U	: Mean streamwise velocity
U_j	: Mean velocity at the nozzle exit
U_m	: Maximum streamwise velocity
x,y,z	: coordinate system
X_{cp}	: Combined point
X_{ip}	: Impingement point
X_{mp}	: Merging point
X_p	: Vortex pairing location
Y	: Distance from the nozzle exit to the impingement surface
$y_{1/2}$	: Local jet half width of velocity profile along the y axis
$z_{1/2}$	: Local jet half width of velocity profile along the z axis
δ	: Boundary layer thickness
δ^*	: Displacement thickness
ε	: Kinematic eddy viscosity
ρ	: Density
Q	: Mass flow
θ	: Momentum thickness
ψ	: Stream function

AN EXPERIMENTAL STUDY ON RECTANGULAR TWIN JETS

SUMMARY

Interaction of two incompressible rectangular jets and impingement of twin jets on a flat surface are investigated experimentally in the present study. Five different twin jet geometries are used to perform the measurements.

Detailed analysis of initial flow characteristics as the initial boundary layer, turbulence level and the initial spectral distribution of the velocity fluctuations are presented first. Twin jet flow characteristics are examined by using three different Reynolds numbers based on the nozzle exit height. Flow pattern is investigated on lateral and spanwise directions. Following the twin jet experiments, results are compared with those of offset jet flow. Then, the effect of a convex surface between two jet exits on the flow development is examined.

Twin jet impingement on a flat surface is investigated. To examine the effect of the non-dimensional nozzle to plate distance (Y/H^+) on the flow, experiments are performed for three different nozzle to plate distances (Y/H^+=2, 4, 8). Resultant velocity and turbulence intensity profiles and pressure distributions on the plate are measured.

The mean velocity and turbulence intensities are measured by using constant temperature hot-wire anemometry. Flow visualization techniques as smoke visualization and surface oil film technique are used for qualitative investigation of flow pattern. Pressure distributions on the impingement plate are measured by means of the pressure tabs on the surface and a micro manometer.

This study consists of five chapters. Chapter 1 is the introduction which outlines the objectives and the means of the study. Chapter 2 describes basic principles of the turbulent, incompressible jet flow structure and gives literature review of the experimental studies and recent advances on the characteristics of the flow. Experimental flow facility, instrumentation and experimental procedures are described in Chapter 3. Experimental results are presented in Chapter 4. Finally, conclusions are given in Chapter 5.

DİKDÖRTGEN KESİTLİ ÇİFT JETLER ÜZERİNE DENEYSEL BİR ÇALIŞMA

ÖZET

Bu çalışmada sıkıştırılamaz akışlarda iki dikdörtgen jetin birbirleri ile etkileşimi ve çift jetlerin düz yüzeye çarpması hali deneysel olarak incelenmiştir. Ölçümlerin gerçekleştirilmesinde beş farklı çift jet geometrisi kullanılmıştır.

İlk olarak sınır tabaka, türbülans seviyesi ve hız çalkantılarının spectral dağılımı gibi akımın başlangıç şartlarının detaylı analizi verilmiştir. Çift jet akım karakteristikleri üç farklı, çıkış kesidi yüksekliğine bağlı Reynolds sayısında, yapılan deneylerle araştırılmıştır. Akım yapısı, yatay ve dikey eksenlerde incelenmiştir. Çift jet deneylerini takiben, sonuçlar offset jet deney sonuçları ile karşılaştırılmıştır. Ardından iki jet çıkış kesidi arasına yerleştirilen dışbükey yapının akım gelişimine etkisi araştırılmıştır.

Düzlemsel yüzeye çarpan çift jet yapısı incelenmiştir. Boyutsuz plaka uzaklığının (Y/H^{+}) akıma etkisini incelemek için üç farklı plaka uzaklığında ($Y/H^{+}=2, 4, 8$) deney yapılmıştır. Plaka üzerindeki hız ve türbülans profilleri ile basınç dağılımı ölçülmüştür.

Ortalama hız ve türbülans değerleri sabit sıcaklık sıcak-tel anemomtresi ile ölçülmüştür. Duman ile akım görüntüleme ve yüzey yağ tekniği ile akım görüntüleme yöntemleri akımın yapısının kalitatif incelemesi için kullanılmıştır. Çarpma yüzeyi üzerindeki basınç dağılımı yüzey üzerindeki basınç pirizleri ve bir mikromanometre vasıtasıyla ölçülmüştür.

Bu çalışma beş bölümden meydana gelmiştir. Bölüm 1 çalışmanın amacını ve yöntemini taslak olarak veren giriş bölümüdür. Bölüm 2 türbülanslı, sıkıştırılamaz jet akışlarının temel prensiplerini tanımlarken deneysel çalışmaların literatür özetleri ve konu hakkındaki son gelişmeleri vermektedir. Deney düzeneği, deney aletleri ve deneysel prosedürler Bölüm 3' te tanımlanmıştır. Deneysel sonuçlar Bölüm 4 ve yorumlar Bölüm 5' te verilmiştir.

1. INTRODUCTION

Jet flow, having many engineering applications, like in turbines, jet engines for vertical take off and short take off, burners and ejectors, attracted attention of researchers since the first half of the 20th century. That is why, the scientific and technical literature on this area is abundant. The amount of the work in this area has, however, not diminished; indeed it seems to be increasing.

Jet flows can be classified according to many aspects, one of them is their interaction with another flow or structure. If the flow, issuing from a nozzle, is sufficiently far from the objects and boundaries around it so that they do not have any effect on it, it is called a free jet. Free jets have been of major interest in the field of turbulent shear flows. Free jet flows have been extensively investigated by many researchers [1-30]. These investigations brought in to light that the shape of the exit nozzle is very important in mixing and entrainment phenomenon.

Jets bounded with solid bodies can be classified in to three types: wall jet, where the fluid is discharged parallel to a wall; offset jet, parallel to a wall with a gap between jet axis and solid boundary and impinging jet, directed towards a solid wall.

The turbulent wall jets, are of great engineering importance with many applications as cooling of combustion chamber of gas turbines, mass transfer modification in defrosters of automobiles. The turbulent wall jet is a basic flow of fundamental interest for researchers because of its two scale character. The inner layer of the plane wall jet is similar to that of turbulent boundary layer, while the outer layer resembles of a free jet.

Combustion chambers of gas turbines, environmental dischargers, heat exchangers, boilers and fuel injection systems are strongly governed by the behavior of offset jets. Investigations on offset jet flow are not sufficiently numerous despite its importance [31-38].

Impinging jets are widely used to enhance heat and mass transfer in many industrial processes as surface cooling, liquid atomization and mixing, surface coating. The increasing interest in vertical take-off and landing military aircraft, is directed the jet flow investigations to this area. Extensive studies have been done on the ground effects of impinging jets [39-54].

Jets, bounded with another flow field, are called with different names such as; coaxial jets, dual jets, multiple jets, etc. Multiple jet configuration has many advantages over a single jet having better mixing and noise reduction [55]. Multiple jets are used in wide variety of engineering applications and subjected to many research studies. In some gas burners the gas stream emerges from various parallel jets. The flame length and width of gas burners are affected by the mutual interaction of jets. A common industrial application of multiple jets is the drying of diverse products such as papers, textiles, peat pots and on moving beds by the impingement of hot air issuing from rows of plane nozzles. Multiple jets are also used for cleaning and dispersing the materials in industry.

Parallel turbulent jets, having various technological applications have been investigated by many researchers [55-74]. The turbulent mixing of jets can be applied in a variety of fluid as in burners, in trust augmenting ejectors of VTOL and STOL aircrafts, fluidics, and injection systems. Studies on parallel turbulent jets have been concentrated on two dimensional flow field. However, studies on multiple three dimensional jets are very limited [55-59].

In multi-jet studies, the mutual influence of the neighboring jets on each other requires clear understanding and hence twin jet studies become important.

The number of studies on twin jet flow is very limited. Previous twin jet studies are mainly focused on two dimensional parallel jets [60-74]. Lin and Sheu [62, 64] investigated interaction of two plane parallel unventilated jets. Measurements of mean velocity components, turbulence intensities, and Reynolds shear stresses were made with a split film probe. Tanaka [60, 61], measured mean velocity and turbulence intensities of two dimensional parallel jets with single hot-wire. Eleven nozzle distance were provided for experiments. Nasr and Lai [68], investigated the flow field characteristics and effects of acoustic excitation. They show that the two dimensionality of the flow was enhanced by the installation of side plates. The studies of Marsters [71] and Elbanna et al. [69], deal with the ventilated twin jets. Elbanna and Sabbagh [70,72], investigated effects of the velocity ratio of the two jets on the flow field. A study on the confluence of two jets, issuing from inclined nozzles is presented by Murai et al. [66].

Although the practical applications are mostly three dimensional there is a lack of documentation on the interaction of rectangular twin jets. The present study aims to investigate experimentally the flow structure of incompressible unventilated rectangular twin jets. Similarity of flow structure with other jet flow structure is examined. An active control of twin jet was proposed by Nasr and Lai [68]. They have shown that acoustic excitation is reduced the size of potential core, recirculation zone, merging length and combined length however, enhanced jet spreading, streamwise velocity decay and volume entrainment. In the present work, a passive control mechanism is proposed to obtain a similar flow enhancement: A cylindrical convex surface is inserted between the two jet exit slots.

In the present study, twin rectangular jet flow is investigated experimentally. Detailed experiments were carried out for five different exit geometries of twin jet.

Characteristics of twin jet flow have been examined by using hot wire anemometer (HWA). A blower type wind tunnel was employed to obtain twin jet flow. Jet flow exit velocity was 30 m/s and turbulence intensity was about 0.7-0.8 % for all jet configurations. On the other hand, for a passive control mechanism, a cylindrical body is placed between the nozzles. The coanda effect forces two jets to merge and changes the flow characteristics like merging point, converging point and spreading rate.

For dual jet configuration above-mentioned, the impingement phenomenon is also investigated. The impingement plate is placed normally to the jet axis, in different streamwise locations: $Y/H^+ = 2, 4, 8$. The effect of the convex surface curvature on the impingement flow has been also studied.

First, the qualitative flow measurements have been performed. In the present study smoke method and surface oil-film technique have been used as flow visualization techniques. All these flow visualization tests have been recorded on a CCD camera.

Flow velocity and turbulence characteristics have been investigated by using hot wire technique. Hot wire anemometry (HWA) is based on convective heat transfer from a heated wire or film element placed in a fluid flow. Any change in fluid flow condition that affects the heat transfer from a heated element will be detected instantaneously by a constant temperature HWA system.

HWA is likely to remain the principal research tool for most turbulent air/gas flow studies. A standard hot wire probe operated with a modern constant temperature anemometer (CTA) has very high frequency response in comparison with LDA[75]. Measurements up to several hundred kilohertz are therefore easy to obtain. Measuring volume of a hot wire probe is also very small. A typical hot wire sensor is about 5 μm in diameter and 1.25 mm long. HWAs have very wide velocity range and good accuracy. One of the most important advantages of HWA is the continuous analogue signal output of the system. Consequently, conditionally sampled time domain and frequency domain analysis can be carried out. HWAs have very low noise level [75]. The use of two or more spatially separated probes enables the measurements of spatial-temporal correlation of turbulent fluctuations. HWA systems are relatively cheap and simple to operate in comparison with LDA. All these aforementioned advantages, is the cause of the extensive use of HWA in experimental fluid mechanics. HWA is often the ideal tool for providing the required information related both to mean velocity and temperature field and the magnitude and distribution of turbulence for complex flow studies. HWA also remains the principal tool for basic studies of the physics of turbulent flows.

Surface pressure measurements are performed by using a diaphragm gage type micro-manometer.

The format of the present study is as follows: Chapter 1 is the introduction which outlines the objectives and the means of the study. Chapter 2 describes basic principles of the turbulent, incompressible jet flow structure. Some of the theoretical equations, developed by several researchers in the last century, are presented in this chapter. Furthermore, literature review of the experimental studies and recent advances on the characteristics of the flow, vortex structure development in the mixing layer of jets, non-circular (especially rectangular) and multiple jet flows; are presented. Experimental flow facility, instrumentation and experimental procedures are described in Chapter 3. Experimental results are presented in Chapter 4. This chapter consists of seven substantial parts. Followed by an introduction, in the second part, initial jet conditions as initial velocity and turbulence profiles and spectral distributions are presented. Reynolds number effect for a specific jet configuration is investigated in the third part. In the fourth part, twin jet flow measurements are presented. Five different twin jet configurations are used in the experiments. The twin jet results are compared with offset jet flow measurements in the next part. The influence of the convex surface between jets is examined in the sixth part. Last of all, twin jet impingement on a flat plate is investigated. Pressure distributions and velocity profiles on the plate are presented. Finally, conclusions are given in Chapter 5.

2. FLOW STRUCTURE OF TURBULENT JETS

2.1 Introduction

A comprehensive review of recent studies and knowledge on jet flow structure is necessary for better understanding of twin jet flows and its impingement on a flat surface. In this chapter, flow structure of two-dimensional single jets and some theories developed in the 20th century are cited. Then, experimental studies on three dimensional circular and non-circular jets are outlined. Finally, three dimensional dual jet flow structure and jet impingement studies are presented.

2.2 General Properties of Turbulent Jets

The fluid flow issuing from a nozzle into a surrounding medium is called a jet. The flow velocity at nozzle is approximately uniform. A growing boundary layer appears, which is limited at its inner side by the potential core where no mean velocity gradient exists, and at its outer side it has free boundaries. The region of finite thickness contains eddies moving both along and across the stream which brings out an exchange of matter between surrounding flow. This entrainment and mixing effect leads to an increase in cross section of boundary and on the other hand, to a graduate vanishing of potential core. The schematic of flow field is given in Figure 2.1.

The part of the jet in which there is a core of potential flow is termed the initial region or the potential core region. After this region, flow relaxes in to its final stage of development along the transition region and becomes fully developed at main region where the self-similarity is reached in the flow (Figure 2.2).

Free jet flows are investigated experimentally by several authors from different points of view. Early studies deal with two dimensional plane jets to improve new theoretical approaches for the turbulent jet theory and to understand the turbulence mechanism of jets [3, 6, 11-15]. Numerous studies on circular jet flows are done since 1950's [1-5, 7-10]. The objective of these studies was to understand the nature of large-scale structures in the near field and the mixing and development characteristics as the growth rate, maximum velocity decay rate, self-similarity etc. in the far field.

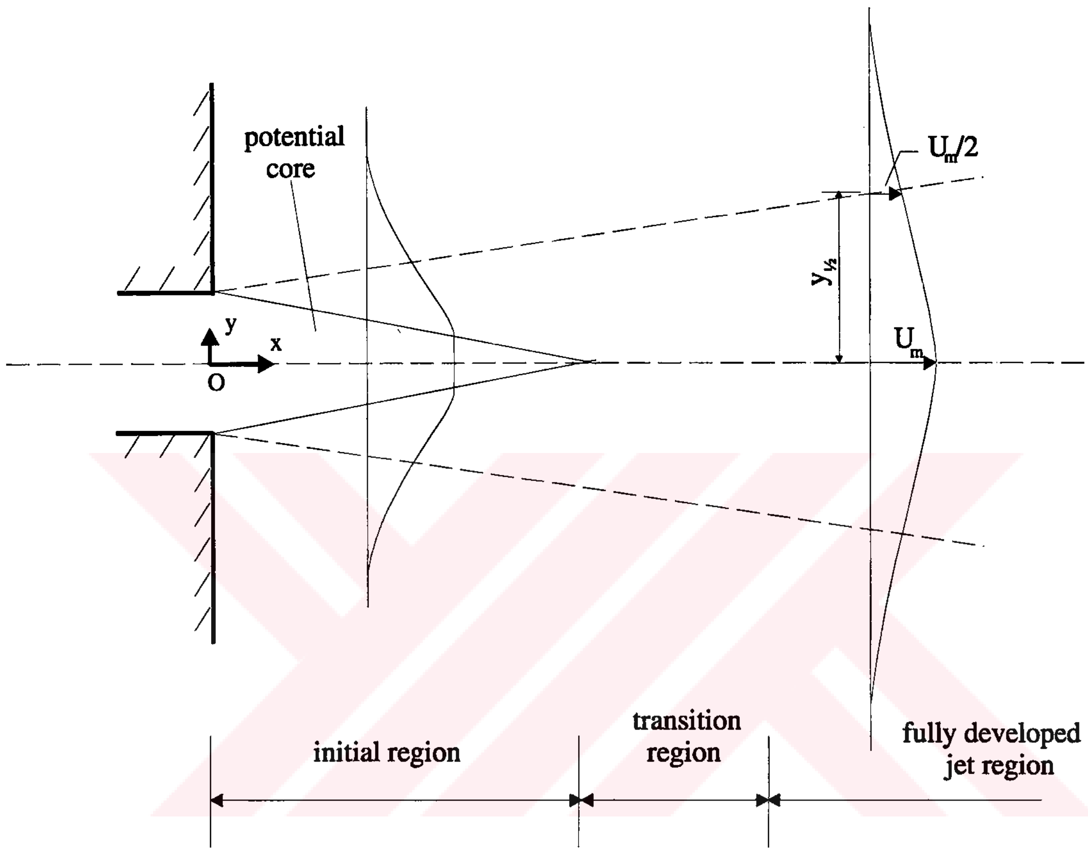

Figure 2.1 Schematic of a free jet flow

If the x axis is aligned with the axis of symmetry of the stream, $y_{1/2}$ is the distance between jet axis and the point where the velocity is equal to half of the maximum velocity ($U_m/2$). Growth rate of a jet is determined by the development of jet half-width $y_{1/2}$ along the jet axis x. Plane and round jets expand linearly with axial distance according to experimental results of Abramovich[1].

Similarity of boundary layers, in different cross sections has been established by a large number of experiments. When the velocity profiles are plotted in non-

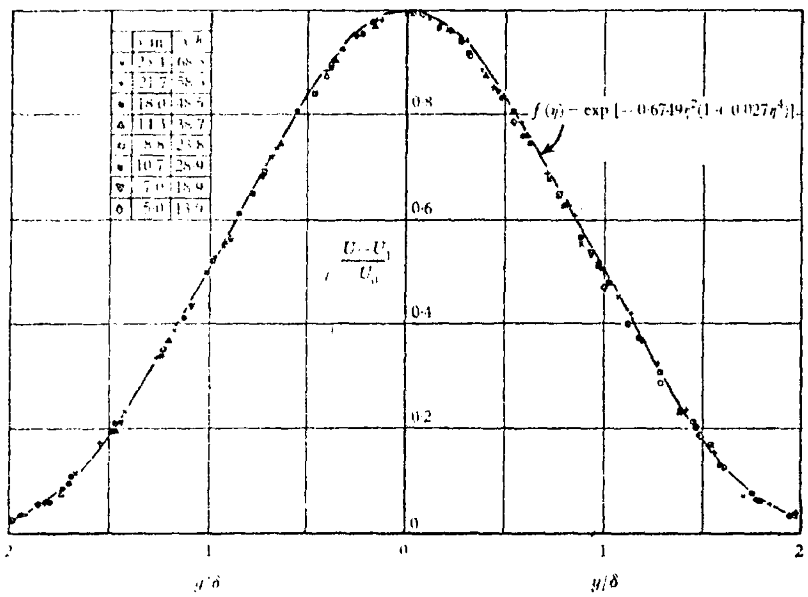

Figure 2.2 Mean velocity profiles in the fully turbulent jet [15]

dimensional coordinates, they coincide on each other. Hence the non-dimensional velocity $\bar{u}/\bar{u}_m$ is function of only the relative position of the point in cross section of the jet $y/y_{1/2}$ as seen in Equation 2.1.

$$\frac{\bar{u}}{\bar{u}_m} = f\left(\frac{y}{y_{1/2}}\right) \qquad (2.1)$$

This property is called 'self-similarity of jets' in the literature.

A characteristic feature of a turbulent jet is the smallness of transverse velocity components in any section of the jet compared with the longitudinal velocity u. Hence transverse components can be neglect in many engineering applications.

If $\partial\bar{u}/\partial y$ is the mean transverse velocity gradient mixing length theory can be rewritten as,

$$u' = \ell \frac{\partial \bar{u}}{\partial y} \qquad (2.2)$$

where ℓ is mixing length (mean free path of a fluid particle).

It is usually assumed that the transverse perturbations in velocity v', are proportional to the streamwise perturbations u' with opposite sign;

$$-v' \approx u'; -v' \approx \ell \frac{\partial \bar{u}}{\partial y} \tag{2.3}$$

Prandtl's mixing length theory for free turbulence advances the hypothesis of constant mixing length in each transverse section of the flow;

$$\ell(y) = \text{const.} \tag{2.4}$$

The similarity of boundary layers may be expected between the dimensionless mixing lengths

$$\frac{\ell_1}{(y_{1/2})_1} = \frac{\ell_2}{(y_{1/2})_2} = ... = \text{const.} \tag{2.5}$$

Prandtl assumes the growth of the jet is controlled by the transverse perturbation velocity

$$\frac{dy_{1/2}}{dt} \approx v' \tag{2.6}$$

Derivation of equation (2.1) gives;

$$\frac{\partial \bar{u}}{\partial y} \approx \frac{\bar{u}_m}{y_{1/2}} \tag{2.7}$$

From equations (2.4),(2.5),(2.6) and (2.7);

$$\frac{dy_{1/2}}{dt} \approx \bar{u}_m \tag{2.8}$$

and using;

$$\frac{dy_{1/2}}{dt} = \frac{\partial y_{1/2}}{\partial x}\frac{\partial x}{\partial t} \approx \frac{\partial y_{1/2}}{\partial x}\bar{u}_m \tag{2.9}$$

equations (2.8) and (2.9) provides;

$$\frac{\partial y_{1/2}}{\partial x} = \text{const.} \quad ; \quad y_{1/2} = \text{const.}\,x \quad ; \quad \ell = \text{const.}\,x \tag{2.10}$$

The linear law for the increase in jet thickness and the mixing length derived above can be applied to jets of different shapes as plane jet and circular jet.

Several theories have been established on turbulent jet flow. A special characteristic of turbulent free jet is the absence of solid boundaries of flow, and consequently a laminar sublayer, which makes it possible to neglect completely the influence of viscosity. This property explains self similarity of turbulent jets, independent of Reynolds number over a very broad range [1]. For two dimensional steady jets the general form of momentum and continuity equations are;

$$\bar{u}\frac{\partial \bar{u}}{\partial x} + \bar{v}\frac{\partial \bar{u}}{\partial y} = \frac{1}{\rho}\frac{\partial \tau}{\partial y} \tag{2.11}$$

$$\frac{\partial \bar{u}}{\partial x} + \frac{\partial \bar{v}}{\partial y} = 0 \tag{2.12}$$

It is necessary to establish a hypothesis on the behavior of the shear stress. Several theories and hypothesis on turbulent stress have been produced since 1925. Prandtl's mixing theory was issued in 1925, which assumes according to Boussinesq's definition;

$$\tau_{xy} = \rho\varepsilon\frac{\partial \bar{u}}{\partial y} \quad ; \quad \varepsilon = \ell^2\left|\frac{\partial \bar{u}}{\partial y}\right| \tag{2.13}$$

ε should be null when $\frac{\partial \bar{u}}{\partial y} = 0$. However, at this point experimental results do not agree with theory. Because of this inconsistency, Prandtl has announced in 1942 a new free turbulence hypothesis. This hypothesis proposes,

$$\varepsilon = k y_{1/2}(\bar{u}_{max} - \bar{u}_{min}) \tag{2.14}$$

Considering a fully developed jet flowing through the fluid at rest ($\bar{u}_{min}=0$)

$$\varepsilon = k y_{1/2} \bar{u}_m \tag{2.15}$$

Several other free turbulence hypothesis have been put forward, in order to obtain better agreement with experimental results like Taylor's hypothesis, Tollmien's hypothesis and Reichadt's hypothesis [1].

Starting from Prandtl's second hypothesis Gortler solved the problem of plane and circular jets. In this chapter two dimensional fully developed turbulent plane and circular jet solution of Gortler are represented.

Considering momentum M_0, issuing from the nozzle keeps a constant value in any section of a plane jet;

$$M_0 = 2\rho\int_0^\infty \bar{u}^2 dy \approx 2\rho \bar{u}_m{}^2 x \approx \text{const.} \tag{2.16}$$

$$\bar{u}_m \approx \frac{1}{\sqrt{x}} \frac{\sqrt{M_0}}{\sqrt{\rho}} \tag{2.17}$$

in similar manner for circular jets;

$$M_0 = 2\rho\pi\int_0^\infty \bar{u}^2 y dy \approx 2\rho\pi \bar{u}_m{}^2 x^2 \approx \text{const.} \tag{2.18}$$

$$\bar{u}_m \approx \frac{1}{x} \frac{\sqrt{M_0}}{\sqrt{\rho}} \tag{2.19}$$

from (2.1) and (2.17) one obtains for plane jets;

$$\bar{u} \approx \frac{1}{\sqrt{x}} f\left(\frac{y}{y_{1/2}}\right) \tag{2.20}$$

and from (2.14) and (2.17);

$$\varepsilon \approx \sqrt{x} \tag{2.21}$$

It is possible to find $\bar{u}$, by assuming stream function of the form;

$$\psi = kx^{1/2} f(\eta) \tag{2.22}$$

where;

$$\eta = \frac{y}{y_{1/2}} = \frac{\sigma y}{x} \quad ; \quad \sigma = \frac{1}{c} \tag{2.23}$$

Finally, velocity components can be found for plane jets;

$$\bar{u} = \frac{\sqrt{3}}{2}\sqrt{\frac{M_0 \sigma}{\rho x}} \sec h^2 \sigma \frac{y}{x} \tag{2.24}$$

$$\bar{v} = \frac{\sqrt{3}}{4}\sqrt{\frac{M_0 \sigma}{\rho x}} \left[\frac{2\rho y}{x} \sec h^2 \sigma \frac{y}{x} - \text{tgh} \sigma \frac{y}{x} \right] \tag{2.25}$$

The constant σ is called the spread parameter. This constant has been found by Reichardt through experiments: σ =7.67.

The mass flow is ;

$$Q = \sqrt{\frac{3M_0 \rho x}{\sigma}} \tag{2.26}$$

The axisymmetric fully developed jets can be studied, by the Prandtl's second hypothesis. In this case, momentum equation gives the expression (2.19) which shows a proportional relation between $\bar{u}_m$ and x^{-1}. Therefore ε is constant. This signifies that the problem may be solved in an identical way to the analogous laminar problem. The solution of the problem in this way gives;

$$\bar{u} = \frac{3M_0}{8\pi\rho\varepsilon x (1 + \eta^2 / 4)^2} \tag{2.27}$$

where;

$$\eta = \frac{1}{4\varepsilon}\left(\frac{3M_0}{\pi\rho}\right)^{1/2}\frac{y}{x} \qquad (2.28)$$

The constant $\varepsilon\left(\frac{M_0}{\rho}\right)^{-1/2}$ found by Reichardt is 0.0161.

The mass flow is,

$$Q = 0.404\sqrt{M_0\rho}.x \qquad (2.29)$$

2.3 Vortex Street Structure of Turbulent Jets

Near field structure of turbulent jets, has attracted attention of researchers since 1950's. After Second World War, jet engines has taken a very important role as power plant of civil transportation. Nevertheless, it is realized soon after that jet engines have many limitations because of the noise from their jet exhaust. The exhausts from the jet engine generate severe acoustic environments in the wake of aircraft. The severity of acoustic environment generally augments with increasing vehicle size and performance. In general, the acoustic pressure due to jet exhaust is characterized by a broad spectral distribution over the audible and sub-audible frequency range. At resonant frequencies, skin and substructures absorb considerable amount of acoustic energy resulting in significant vibratory response [76].

After 1950's the studies tends to explore the characteristics of jet noise and means for its reduction [77-87]. As a first step, it would be necessary to understand the mechanism by which noise is generated. Such an understanding would come out with a more definitive description of the jet structure.

The earliest works by Bradshaw, Ferris and Johnson [2], brought to light that the flow in the noise producing region of a circular jet is dominated by a group of large eddies. They suggested that the augmentation of these large eddies could be used to increase the mixing rate and permit the reduction of jet noise. They discovered that the spectra of hot-wire signals in the potential core had a narrow band appearance. It was further argued that, the source of the regular patterns which has been detected by hot-wire would most probably be situated in the mixing layer.

Winant and Browand [77], investigated the mechanism of turbulent mixing in a mixing layer which is formed by two streams of water moving at different velocities. Two-dimensional vortical structures are observed by injecting dye between two streams just before they are brought together. The growth of mixing layer by pairing has been visualized. In the very early stages, the flow field is laminar and small waves are formed. In cases where the instability is mechanically forced, the frequency of the wave is fixed by the frequency at which the forcing mechanism is driven. In the case with no forcing, the wavelength of the disturbance is the most unstable wave of the system.

Winant and Browand [77], describes flow field by three stages: small amplitude regime, followed by discrete vortices region, and the third region where the turbulent vortices are seen to interact by rolling around each other.

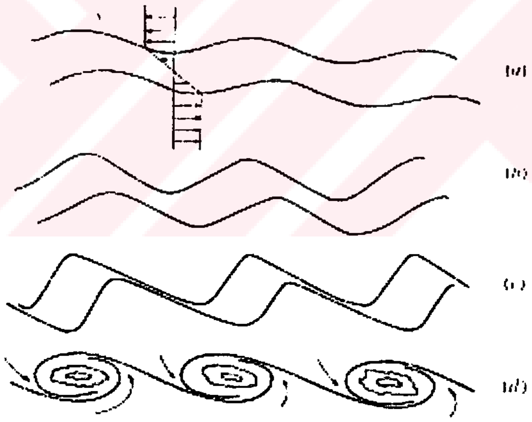

Figure 2.3 Formation of discrete vortex lumps [77].

According to Winant and Browand's mixing layer growth model, initial small amplitude wave distorts the boundaries of the region containing the vorticity. This vorticity-containing region induces vertical velocities which cause the perturbations to grow and to become discrete vortex lumps (Figure 2.3). The pairing process results from the mutual interaction of neighboring vortices to form a single larger vortex (Figure 2.4). These interactions depend on imperfections in the vortex spacing and strength.

The mixing region grow is governed by vortex pairing (or merging) process. Jets spread initially (in the potential core region or initial region) via the same mechanism as the mixing layer. Several vortex interactions (merging) occur between the nozzle exit and the end of the potential core. After each merging, vortex size increases and vortex passage frequency drops by a factor of two. Consequently jet spreads out.

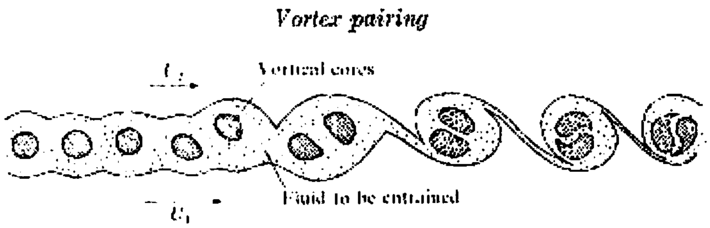

Figure 2.4 Vortex pairing model [77].

Jet spreading rates given by several authors has many discrepancies. It is known that, initial shear layer conditions (laminar or turbulent shear layer) can alter the spreading rate. Gutmark and Ho [78], discovered that spatially coherent background perturbations has also affected the initial instability frequency, hence the spreading rate.

The growth of small disturbances in a shear layer has been studied by Mihalke [79] and Stuart[80]. Mihalke calculated spatial growth of small perturbations by superimposing small disturbances in to Helmoltz vorticity equation. He found that, the most amplified frequency f_0 was identified by a constant Strouhal number in a band of unstable frequencies (Figure 2.5).

$$St_0 = \frac{f_0 \theta_0}{U_0} = 0.017 \qquad (2.30)$$

where θ_0 is initial momentum thickness and U_0 is jet exit velocity.

Nevertheless, the Strouhal number based on the initial instability frequency, measured by many researchers has varied between 0.013 and 0.023 [78]. These discrepancies are attributed to spatially coherent background disturbances by Gutmark and Ho [78]. A spatially coherent background perturbation (acoustical or vortical) can affect the instability of initial shear layer, alter the frequency prevailing waves and therefore change merging locations.

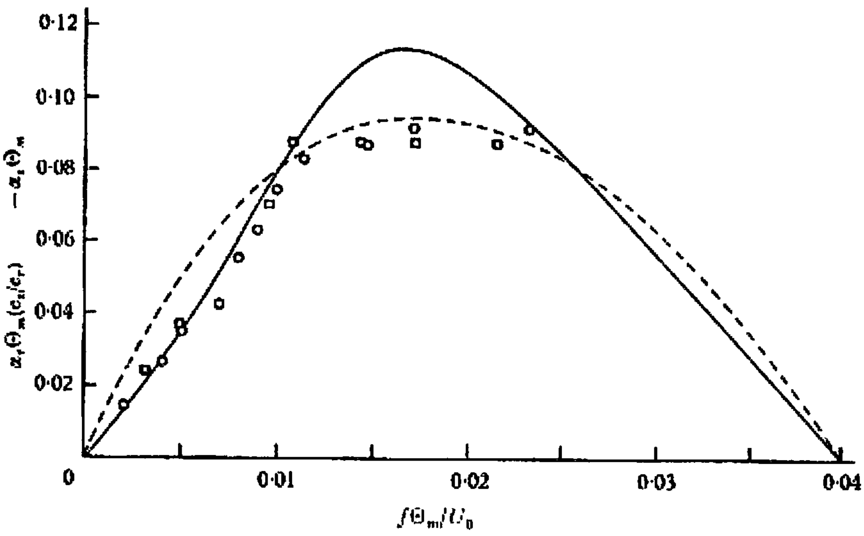

Figure 2.5 Spatial growth rates measured in the free boundary layer of an axisymmetric jet [79].

After Mihalke's linearized disturbance equation, Stuart developed a non-linear disturbance theory including exact solution of two-dimensional steady, inviscid, incompressible mixing layer solution (based on the hyperbolic tangent velocity profile). Stuart's solution represents a spatially periodic mixing layer consisting of a single row of vortical structures. Velocity field of Stuart solution is given by;

$$u = 1 + R\frac{\sinh y}{\cosh y + \alpha\cos(x - t)} \tag{2.31}$$

$$v = R + \frac{\alpha\sin(x - t)}{\cosh y + \alpha\cos(x - t)} \tag{2.32}$$

where,

$$R = \frac{u_1 - u_2}{u_1 + u_2} \tag{2.33}$$

u_1 and u_2 are mean velocities of and α is vorticity concentration parameter.

A vortex pairing model has been developed by Winant [77]. The mixing layer is considered to be a double row of Stuart vortices. The rows are vertically offset by $\varepsilon\lambda$. λ is the horizontal distance between vortices. He found that the mixing layer growth rate is a function of ε, α and $\Delta u/u$:

$$\gamma = (\Delta u / u) f(\varepsilon, \alpha) \tag{2.34}$$

Vortex merging process produces a pressure disturbance which will propagate upstream and force the shear layer. This feedback mechanism was investigated by Laufer and Markewitz [81].

In a developing shear layer the subharmonic perturbations can be provided by the induced field of the downstream (already paired) vortices. A vortex interaction occurring at $x=x_p$, creates an induced flow field perturbing vortices generated at the trailing edge of the nozzle. The perturbed vortices interact with their neighboring vortices at $x=x_p$ to form larger vortices (Figure 2.6). Disturbance signal, generated by the interaction, propagates with speed of sound through the nozzle exit. According to Laufer[80] the feed-back equation;

$$\frac{x_p}{V_c} + \frac{x_p}{a} = \frac{N}{f_p} \tag{2.35}$$

or

$$\frac{f_p D}{V_j}\left(\frac{x_p}{D}\right)\left(\frac{V_j}{V_c} + \frac{V_j}{a}\right) = N \tag{2.36}$$

where V_c and V_j are vortex convection and jet exit velocities, a is the speed of sound, N is an integer and f_p is the frequency after merging.

Gutmark and Ho[78], suggested that the merging location could be predicted by neglecting the second term in equation (2.35) as $a \gg V_c$ in a low subsonic flow.

$$f_p x_p / V_c = N \tag{2.37}$$

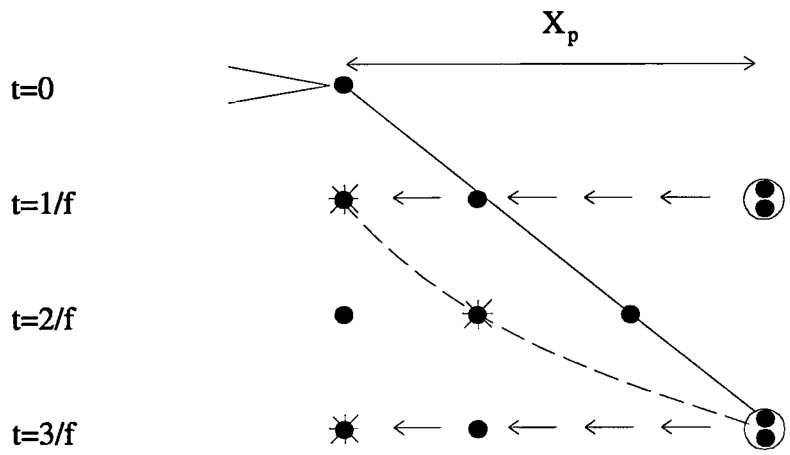

Fig 2.6 Sub-harmonic feedback [81].

and

$$f_p = f_o / 2^p \tag{2.38}$$

where f_0 is the initial instability frequency. Hence,

$$x_p = 2^p \frac{NV_c}{f_0} \tag{2.39}$$

Vortex merging process occurs several times along the potential core region. The last merging appears at the end of the potential core where a preferred frequency, corresponding to the passage frequency of vortical structures can be detected. Strouhal number based on the jet nozzle height (for rectangular jets) or the nozzle diameter (for circular jets) corresponding to this frequency is called "preferred mode" of the jet. Drubka's experiments show that Reynolds number has no effect on the preferred mode of turbulent jet [78]. However, preferred modes given by different authors are scattered in a wide frequency range as can be seen in Figure 2.7.

Pairing of vortex rings is the primary mechanism responsible for the production of jet noise [77]. Large number of studies are concentrated on the aeroacoustics of jet flows [82,83].

Pioneering studies on aeroacoustics has been realized by Lighthill. He concluded from his analysis that the far field radiation of a jet noise is caused by a string of quadruple sound sources along the jet stream. Lighthill showed that the radiated acoustic power in the far field should vary as the eighth power of the jet velocity,

$$\pi_{rad} \propto \rho_c^2 \ell_c^2 V_j^8 / (\rho_0 c_0^5) \tag{2.38}$$

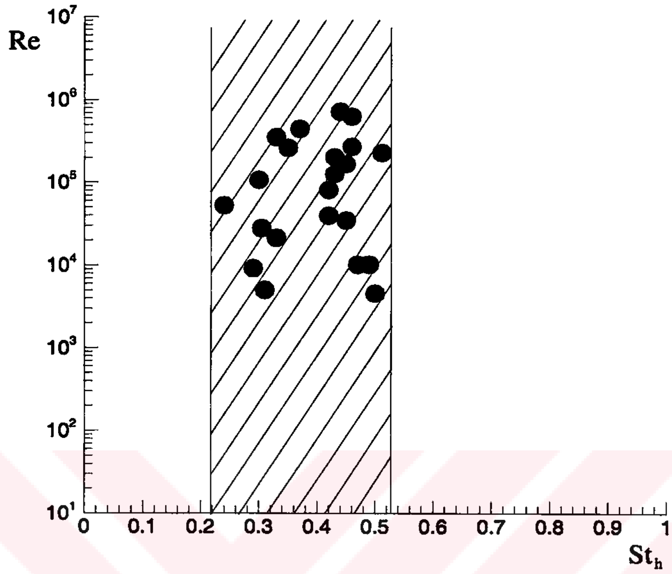

Figure 2.7 The preferred mode of different jet facilities [78].

where ρ_c is the characteristic jet density, V_j is the characteristic jet velocity, ρ_0 is the ambient density, ℓ_c is a characteristic dimension, c_0 is the ambient speed of sound. This equation is known as eight power law of Lighthill for sound radiation in subsonic flows. After Lighthill's theory, Proudman dedicated the radiated noise power per unit volume of turbulence, for isotropic turbulence

$$p_s = \alpha \rho_0 u^8 / c_0^5 L \tag{2.39}$$

where α is the Proudman constant and L is the integral scale of turbulence. Lilley [82] re-evaluated the Proudman constant for weak compressible isotropic turbulence. Tam [83] introduced that the large turbulent structures are important direct noise sources of supersonic jets as well as subsonic jets, hence to predict the noise radiated by the large structures numerically, statistical description of these structures in the form of stochastic instability wave model is necessary. Many authors have been used stochastic approach to solve the problem. But recent studies could not predict accurately the characteristics of jet noise.

2.4 Non-Circular Jets

Jets issuing from non-circular nozzles, as rectangular, elliptic, square, etc. are subject of many studies as passive control mechanism of the jet flow [16-30]. Non-circular nozzles have been used by many investigators for improving jet mixing process. It is known that the elliptic jets are capable of entraining large amounts of surrounding fluid by the axis switching phenomenon [16].

Hussain and Husain [17, 18], examined the vortex structure, switching process and vortex pairing phenomenon in elliptic jets. Elliptic jets provide a capability to control turbulence via both passive and active means. Consider the motion of an elliptic vortical structure. As the major axis side shrinks, it brings in ambient fluid toward the jet centerline and simultaneously, jet fluid is carried outward on the minor axis side as the side moves outwards. The elliptic structures thus as pumping devices to mix ambient and core fluids [17]. The locations and number of switchovers are strongly dependent on the initial conditions and the aspect ratio. Studies of Hussain and Husain reveals that the switching of axes, similar to elliptic jets also occurs in other non-circular jets.

Experimental results of Quinn [16] show the structure of the flow field development by means of mean streamwise velocity contours for sharp-edged elliptical jet (of aspect ratio 5) (Fig 2.8). After two switches of the major and minor axis, jet attains an axisymmetric shape at about 30 equivalent diameters downstream of the jet exit plane.

Quinn's study [21] on low aspect ratio contoured rectangular nozzle (of aspect ratio 10.8), points out that the mean streamwise velocity field changes from a rectangular to an oval and finally to an approximately circular shape at about twenty equivalent nozzle diameter downstream of the nozzle exit plane.

Sforza, Steigner and Trentacosta [23], investigated the mean flow properties of incompressible turbulent jets, emanating from three-dimensional orifices (rectangular, elliptical, triangular) of different geometric eccentricities. They characterize the flow by three distinct regions: Potential core region, characteristic decay region where the axis velocity decay is dependent upon orifice configuration and axisymmetric type decay region where the axis velocity decay is same as the axisymmetric jet velocity decay, i.e., $U_m \propto x^{-1}$, and profiles in both symmetry plane are similar. The extent of potential core region and characteristic decay region were both dependent upon the orifice geometry. They explained this result as the influence of lateral extent of mixing originating at the boundaries of the orifice.

Krothapalli, Baganoff and Karamcheti [22], describe the flow field of a single rectangular jet by using the decay of the square of the axial mean velocity (Figure 2.9). The slope of the curve characterizes the presence of three distinct regions. These regions are potential core region, two dimensional type region and axisymmetric type region. Two dimensional type region of Krothapalli et al. [22] consist of the characteristic region of Trentacoste et al. [23]. The conflict between two flow definition probably comes from the high aspect ratio effect which is forcing the flow to approach to two dimensional jet.

Trentacoste and Sforza's results [24], indicate that the major axis half width ($z_{1/2}$) decreases initially, where as the minor axis half width ($y_{1/2}$) grows; and crossovers at a point corresponding to the onset of axisymmetric decay. After this point half widths grow similarly but at different rates, and further downstream tends to approach each other. Velocity distributions in yz plane (vertical plane to jet axis) show also that isovels were initially elliptic with major axis aligned with major axis of the orifice. At the streamwise location corresponding to the onset of axisymmetric decay region they become nearly circular. As x increases further, isovels become elliptical again, however, the major axis is rotated 90°, and then becomes circular further downstream.

Many researchers [19, 24-27, 54], are reported saddle shaped velocity distributions in the major axis direction.

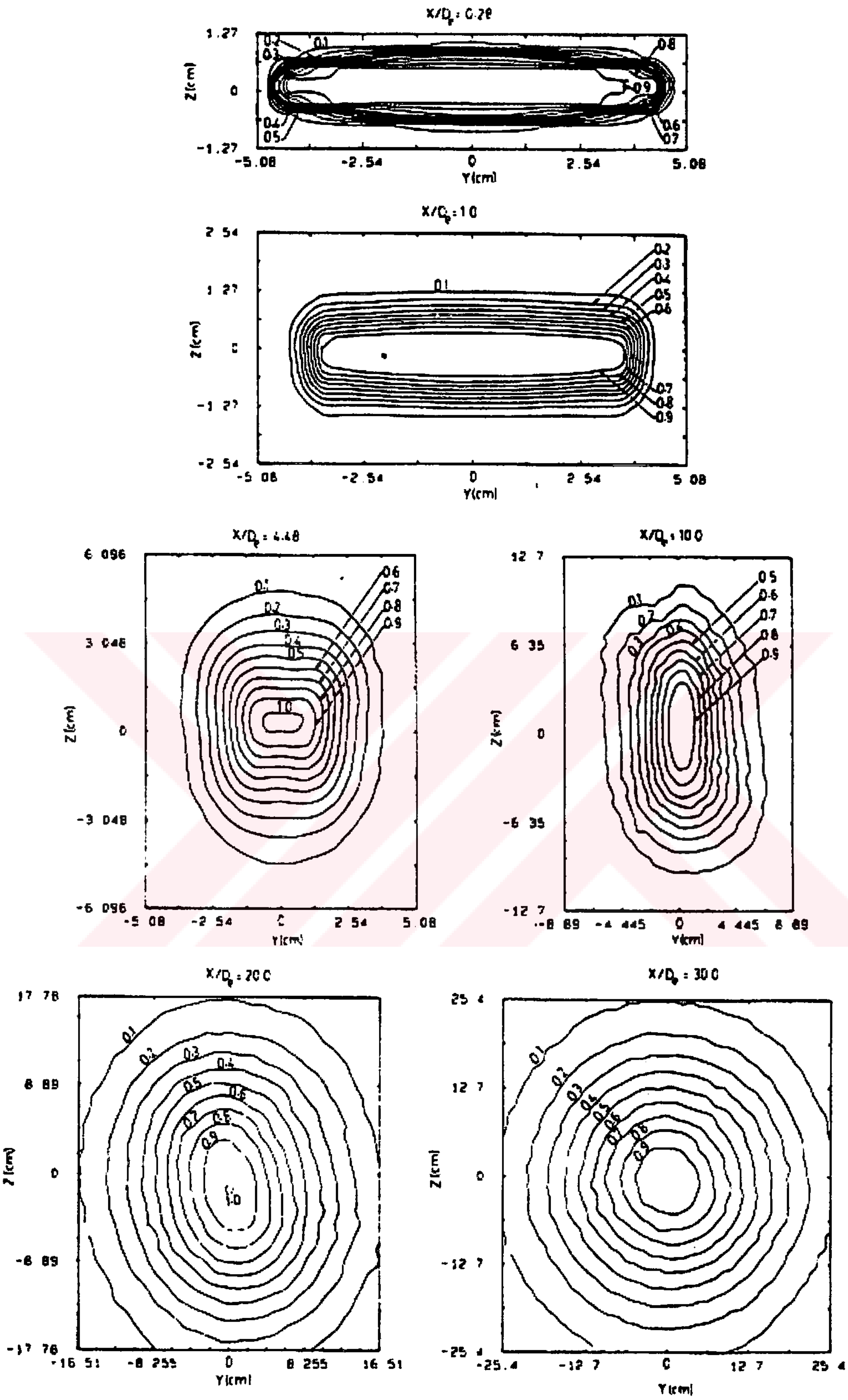

Figure 2.8 Non-dimensional velocity contours at different downstream positions of an elliptical jet[16]

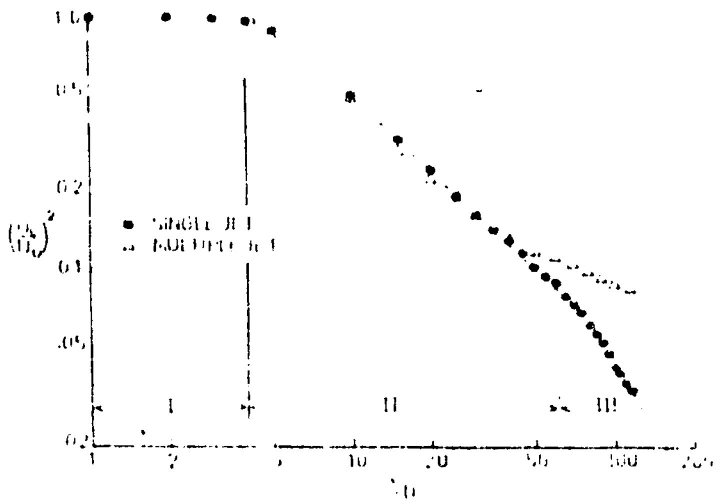

Figure 2.9 The decay of the axial mean velocity along the center-line of the rectangular jet [22].

Sfeir [25], investigated jet mount effects on three-dimensional rectangular jets. The influence of the condition of the jet exit decreases with x, whereas three-dimensional effects increase with x. The saddle back shaped velocity profiles have been observed. Saddle back shaped velocity profiles are more pronounced in flows from sharp-edged slots.

Quinn, Pollard and Marsters's experiments [26], clarify that these mean streamwise velocity off-center peaks, moves towards the jet centerline with downstream distance and disappears after the shear layer growing in the xz plane, merge on the jet centerline.

The peak of mean velocity corresponds to the minimum turbulence intensity. As the peak moves to the jet axis and affects the mixing region near the jet axis, it may cause a dip in turbulence intensity distribution. Tsuchiya, Horikoshi and Sato [27] postulated that the saddle-backed profile might be due to the formation of a region where the mixing is retarded as compared with the surrounding region.

From the measurements of Krothapalli et al. [22], it is deduced that the mean velocity and shear stress of a rectangular jet, show similarity about 30 widths downstream from the nozzle exit. Similar results are obtained by Sfeir [25]. For x less than 60 D, the profiles of axial mean velocity of a rectangular jet exhibit a saddle shape, while the profiles in axisymetric type region, approach the similarity profile of an axisymetric jet.

In the Reynolds number range between 1000 and 7000 the various flow properties of the jet are dependent upon the jet Reynolds number [28]. However, the size and the number of the large scale eddies of turbulence is unaffected by the jet Reynolds number. As the Reynolds number increases turbulent flow structure develops into a self-preserving state faster and therefore the Reynolds number dependence becomes less significant.

2.5 Twin Jets

Two parallel jets, issuing from nearby nozzles, into still surrounding is called, in the literature, "twin jets" or "dual jets"[63,65].

The entrainment of surrounding fluid from the jet boundaries causes a subatmospheric region between jets. Because of the depressurized region, jet trajectories deflect towards each other. Finally two jets converge and merge together to form a single jet (Figure 2.10).

The effect whereby a jet whose initial axis does not intersect a solid surface can nevertheless attach itself to the surface is called by Metral and Zerner the "Chilowsky effect" [88]. As is explained by Bradshaw, this phenomena has been called by many authors "Coanda effect" which is essentially the tendency of a fluid jet, initially tangential to a curved surface, to remain attached to the surface. Coanda, made experiments on plane jets near a solid wall made of straight segments increasingly diverging. The jet was progressively attaching to each segment. Two effects were noted: The pressure near the wall was less than that of the surroundings and thus for given upstream conditions the mass flow from the slot was increased. Secondly, the quantity of flow entrained by the jet from the surrounding fluid was increased.

These effects were applied by Coanda to produce a nozzle with high trust augmentation and to increase the maximum lift coefficient of a wing. At this point, it is necessary to note that for each of the cases mentioned above (Coanda and

Chilowsky flow) the streamline curvature effect is surprisingly important on the flow structure. Wall jet flow on a convex surface grows more rapidly than the wall jet on a plane wall. And a deflected jet by an subatmospheric pressure region spreads faster than a free jet.

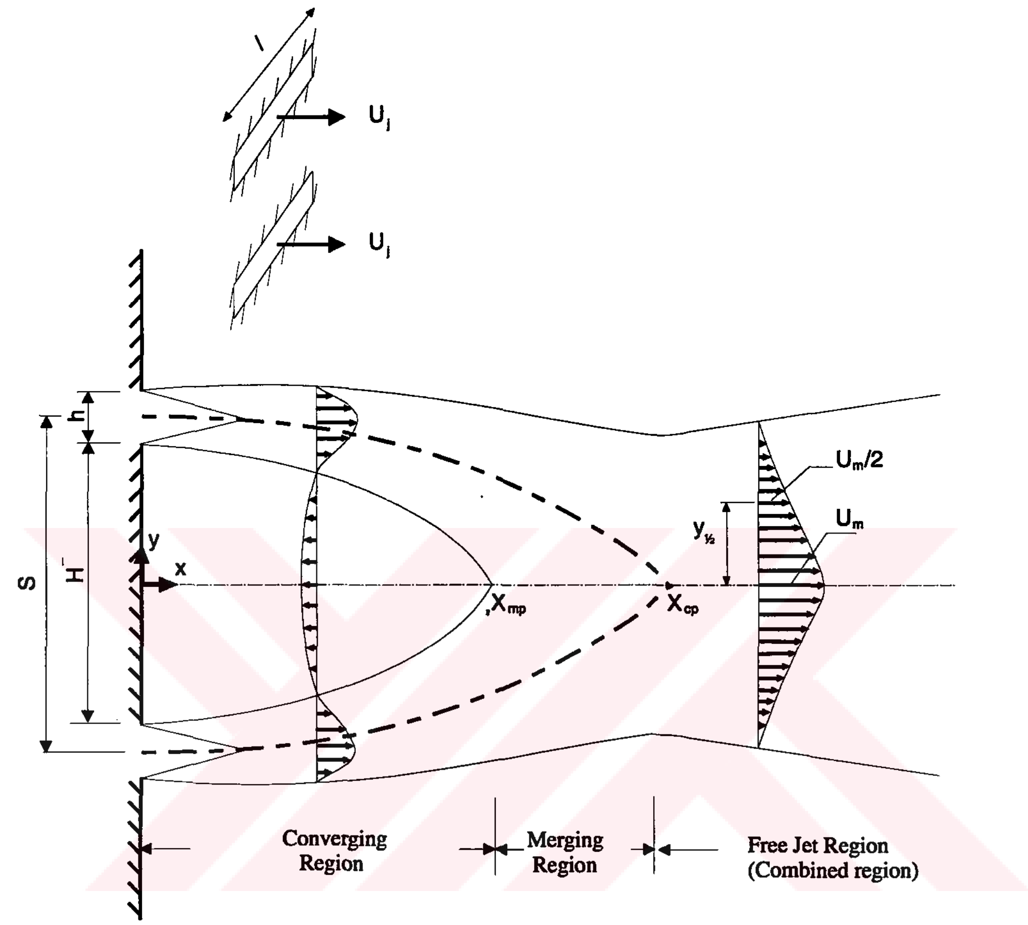

Figure 2.10 Schematic of twin jet flow structure

Surface curvature is used in many applications in order to deviate the jet flow. Lepretre and Portier [89], investigated experimentally jet deviation devices for orientation of jet trust vector on a fighter. Plane and curved wall jets are investigated by many researchers [90-95]. The imposition of longitudinal curvature on a two dimensional turbulent mixing layer produces increases in the spreading rate [96].

Twin and offset jet flows have several common features. A general offset jet pattern is depicted in Figure 2.11. The jet is confined by a wall placed parallel to the jet discharge axis with a gap H. Due to the depresurized region between the jet and the wall, jet deflects towards the wall and attach on it at the impingement point X_{ip}. After impingement, inner part of the flow deflects upstream (in to recirculation region) while the outer part tends downstream and forms a wall jet. There have been many researches on wall attaching offset jets [31-38]. Twin and offset jet flow characteristics are compared and significant similarity was recognized in this study.

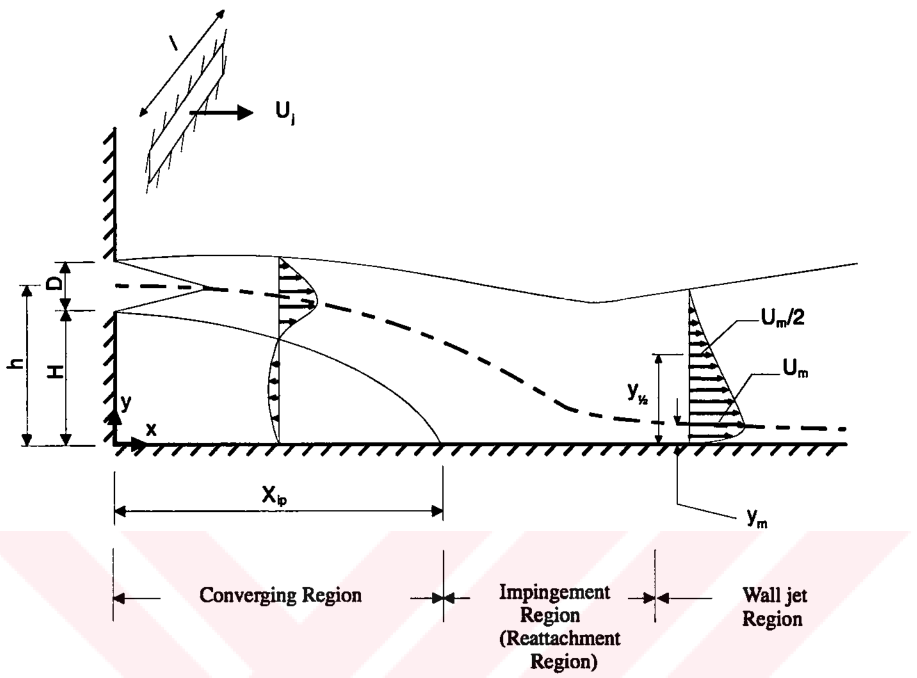

Figure 2.11 Schematic of offset jet flow

The flow field generated by two plane jets has been investigated by many researchers [60-64, 66-74]. These studies can be classified in two groups as ventilated and unventileted twin jets. In the case of ventilated jets a secondary flow has been entrained between two jets issuing from freestanding nozzles (Figure 2.12). This kind of flow structures has been investigated by Marsters [71] and Elbanna et al.[69]. Such configurations may be useful for STOL/VTOL applications.

The aim of this study is to investigate flow structure of incompressible unventilated twin jets. In this case, the secondary flow between nozzles is no more exists since jets emanated from slot nozzles on a solid wall (Figure 2.13).

Twin jets have many technological applications such as burners in combustion systems, boilers, injection and carburetor systems and fluidics. In spite of its importance, limited number of study has been realized on this subject as would be seen the following literature critics.

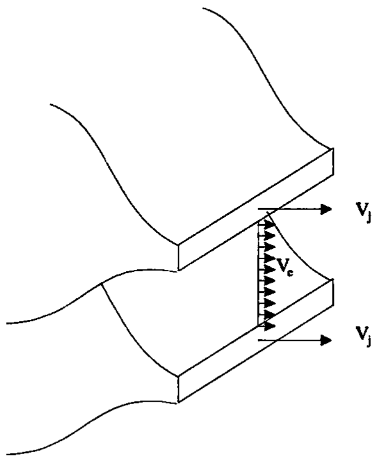

Figure 2.12 Ventilated twin jet configuration

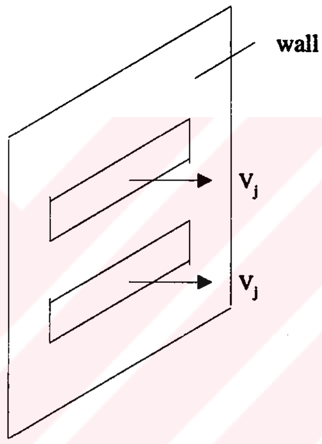

Figure 2.13 Unventilated twin jet configuration

Previous studies on twin jets treat, in the majority, two dimensional plane parallel jets (Table 2.1). To assure two dimensionality, high aspect ratio nozzles and side plates have been used by many researchers as can be seen in Table 2.1.

Twin jet flow field is characterized by three distinct regions. These regions are converging region, merging region and combined region. The schematic of the flow field is given by Figure 2.10. Two converging jets, deflected by the subatmospheric region between them, approach the plane of symmetry with increasing distance x from the nozzle exit. At the end of the converging region, jets merge at X_{mp}. The merging point is determined by the stagnation point where the mean velocity is zero in the symmetry axis x. The axial mean velocities have positive direction downstream of the merging point and negative direction upstream of the merging point. The velocity on the symmetry axis increases from zero at the merging point until it reaches a maximum value, just upstream of the point where two jets join to form a single jet. After this point (X_{cp}), jet behaves like a single jet.

Table 2.1 Previous studies on two dimensional plane parallel jets.

Authors	Aspect ratio	Side wall	Re_h	Nozzle spacing (S/h)	Measurement Technique
C.S. Wang, Lin Sheu (1993) [63]	90	x	8700	15	split film
Tanaka (1974) [61]	80-60	x	4290~8750	20	hot-wire
Tanaka (1970) [60]	80-60	x	4290~8750	8.5~26.3	hot-wire
Murai, Taga Akagawa (1976) [66]	20.61	x	3250~18100	4.1~30.9	hot-wire, pressure probes
Elbanna Sabbagh (1987) [70]	89	x	16600	27.64	hot-wire
Lin Sheu (1990) [62]	90	x	9000	30-40	split film
Lin Sheu (1991) [64]	90	x	9000	30-35-40	split film
Marsters (1977) [71]	45	x	8600~19300	11	pitot-static tubes and hot-wire
Nasr, Lai (1997) [68]	24	x	8300-19300	4.25	LDA

Lin and Sheu [62], investigated flow field experimentally and found that the velocity profiles were self-preserved in both converging and combined regions. The jet spreads linearly in these regions. However, in the merging region, flow shows more complex behaviors due to strong interference between two jets. Lin and Sheu's experiments point out that the structure of the flow field varies little with variances in nozzle spacing (Figure 2.14).

Lin and Sheu [64], studied with various nozzle spacing and found that twin jet flows have almost same normalized trajectories of maximum velocity. Nozzle spacing ratio

S/h were varied from 30 to 40. Normalized values of merging and combining point by nozzle spacing S (X_{mp}/S and X_{cp}/S), are found constant at various nozzle spacing.

Tanaka [60,61] studied the effect of the distance between two nozzles on the interference region of dual jets. According to his results, the relation between the position of the merging point, nozzle width (h) and the nozzle spacing (S) can be expressed as follows;

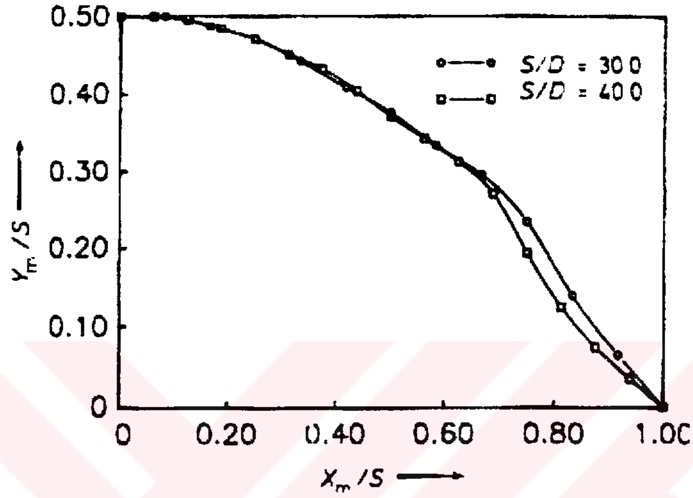

Figure 2.14 Jet spacing effect on the trajectory of maximum axial velocity [62]

$X_{mp}/h = 5.06(S/h)^{0.27}$ S/h < 16

$X_{mp}/h = 0.667(S/h)$ S/h >16

Similar empirical results are reported by several authors. Unfortunately, it is difficult to compare experimental results obtained by different authors since the initial conditions of the experiments vary considerably.

Previous studies were mainly focused on large nozzle spacing ratios (S/h). There is a lack of documentation on the whole flow field of parallel jets with small nozzle spacing ratio. The unique study with small spacing ratio belongs to Nasr and Lai [68].Other studies listed in Table 2.1 were focused on large spacing ratios.

In the present study, experiments were carried out with small nozzle spacing ratios, to represent an experimental source data containing whole flow field characteristics without any change in the initial conditions as nozzle exit turbulence level, nozzle lip conditions etc.

In practical cases jet is limited to a given jet height. The ratio of nozzle height to nozzle width is called "aspect ratio". For high aspect ratios, jets behave like quasi-two-dimensional.

Besides two dimensional plane parallel jet studies, a few information is available in the literature on multijet configurations of non-circular jets [55-57, 65], but not on the interaction two parallel rectangular jets.

Krothapalli, Baganoff and Karamcheti[56],studied the flow from a series of equally spaced rectangular nozzles. Measurements are carried out on a single rectangular free jet in a multiple jet configuration. They deduced from the comparison of multiple jet results, that far downstream the flow field appeared as if it is emerging from a single two dimensional slot with the width of the slot being the long dimension of a single lobe. Their further studies [59],on confined multiple jets, indicated that the flow field was slightly affected by the presence of confining plates, placed symmetrically perpendicular to the long dimension of the nozzle.

Raghunathan and Reid [55] investigated different multijet configurations. Multiple axisymmetric nozzles were equally spaced around a circle with a constant radius from the axis of central nozzle. Pressure difference between the settling chamber and the ambient, and the total exit area were kept constant during the experiments. They have investigated not only velocity but also noise characteristics of the flow and found a substantial reduction in noise level by increasing the number of the jets without significant reduction in the momentum of the jet.

Moustafa and Rathakrishnan's experiments [57] attempt to identify the advantage of multijets and non-circular jets. They have used four circular nozzles in square configuration and compared with single, twin and triple jet configurations and found that the nozzle configuration influences velocity decay and jet growth. They have observed axis switching which can be considered as a distinct advantage of multiple configuration and showed that the nozzle configuration plays a vital role in mixing process.

2.6 Jet Impingement

Nature of the wall flow produced by single or twin normal jet impingement has been investigated by many authors [39-54]. Most of these investigations deals with the flow field of the jet in a crossflow. Turbulent jets, impinging on a flat surface through a low velocity crossflow are typical in a vertical/short take off and landing aircraft which is lifting off and landing with zero or small forward momentum.

Multiple jet impingement is of particular interest areas in drying and cooling devices. Impingement drying is a common industrial operation involving the drying of divers products such as papers, textiles, peat pots, by impingement of hot air jets issuing from rows of plane nozzles.

The impingement of a downward directed jet on the surface results in the formation of a wall jet which flows radially from the impinging point along the surface. In the case of multiple jet impingement, the collision of wall jets originates a fountain of upwash flow (Figure 2.15). Improved knowledge of impinging flow is necessary to avoid these effects.

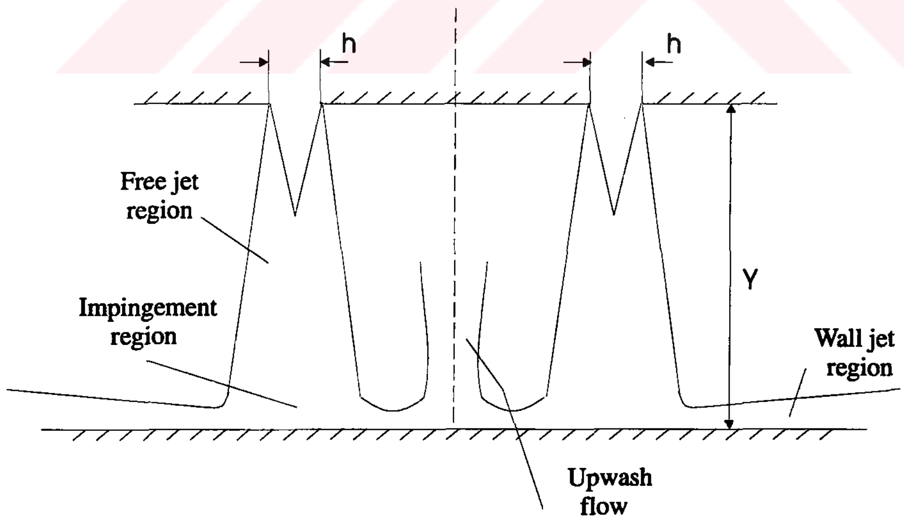

Figure 2.15 Twin jet impingement

A free jet impacting on a wall contains three distinct region: Free jet region which is unaffected by the impact, the impingement region where the jet deflects towards the direction of its final state and wall jet region in which flow is parallel to the wall and behaves like a wall jet.

The performance of dual-jet configurations has received little attention in the literature. Schetz et al.[45] studied surface pressures generated by the impingement of dual jets on a flat plate in crossflow. For the side by side jets, they have noticed significant enhanced flow velocity (thus reduced surface pressures) between the jets due to the channeling of the flow.

Barata [43, 44] gives a detailed analysis of complex flow field beneath multiple jets through a low velocity crossflow.

Elbanna and Sabbagh [46] investigated impingement of two plane ventilated jets of unequal strength on a normal plane surface.

Miller and Wilson [47] analyzed wall jet velocities for cases of single normal and twin normal jet impingement up to 70 jet diameters from impingement. They have noticed that the twin jet flows are dominated by a reinforced region on the symmetry plane that produces both thicker and more energetic wall jets. Peak reinforcement line velocities can be of the order of three times those of the single jet. Simultaneously, the remote region behaves quite differently to a single normal jet flow with substantial weakening of the wall jets.

Recent studies on three-dimensional twin jet impingement concern about circular jets. Although there exists little information on two dimensional plane dual jet impingement, there is a lack of information on rectangular twin jets and its impingement on a flat surface. Objective of the present study is to make a contribution to the existent rectangular jet studies.

3. EXPERIMENTAL METHOD

3.1 Introduction

In this chapter, experimental setup and measurement techniques used for investigation of twin jet flow field are presented. The experiments were carried out in Trisonik Laboratory of Istanbul Technical University.

3.2 Apparatus

Experiments are carried out in a blowing down open type wind tunnel which provides a jet flow from a rectangular nozzle (Figure 3.1). The wind tunnel comprises a fan which draws air from the atmosphere and delivers it along a pipe to a settling chamber which is located above the nozzle. A valve in the pipe is used to regulate the discharge from the fan. The contraction ratio of the nozzle is equal to 10.5. The honeycombs at the entrance of settling chamber are used to reduce the turbulence intensity. Air jet velocity provided by the jet facility can be varied between 3 m/s and 32 m/s.

The flow facility is transformed to a twin jet facility after some modifications. An 520mm x 470mm aluminum rectangular plate is mounted on the nozzle exit to obtain a submerged jet. Plate dimensions are large enough to prevent flow entrainment from the upper side (Figure 3.1). A separating body is inserted in to the nozzle as sketched in Figure 3.2 so that the jet facility produce two parallel rectangular jets.

Five separating bodies of different thickness from 10mm to 40mm was used. Dimensions of all twin jet configurations used in this study are listed in Table 3.1.

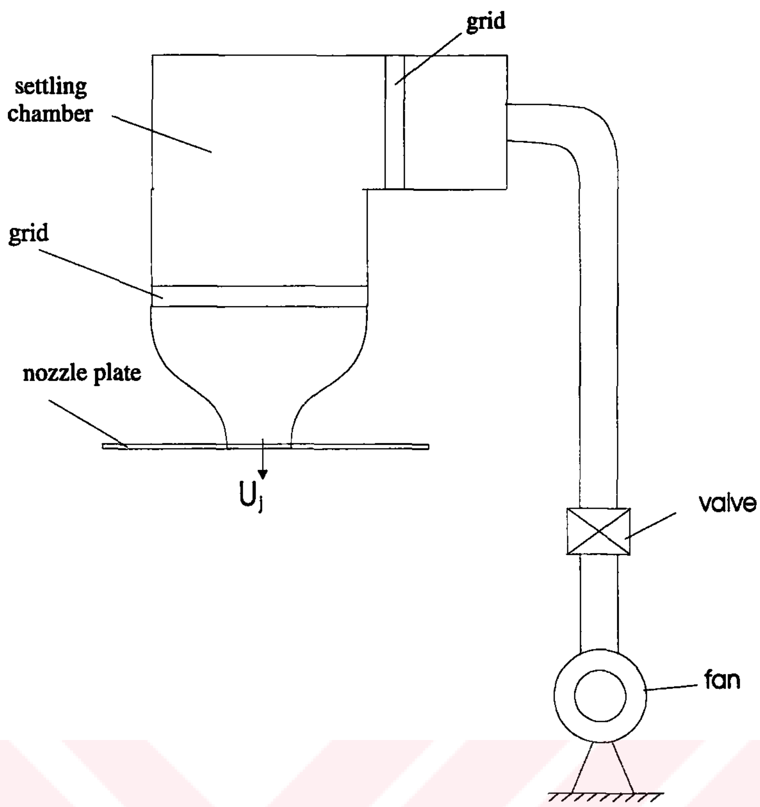

Figure 3.1 Schematic diagram of the jet facility

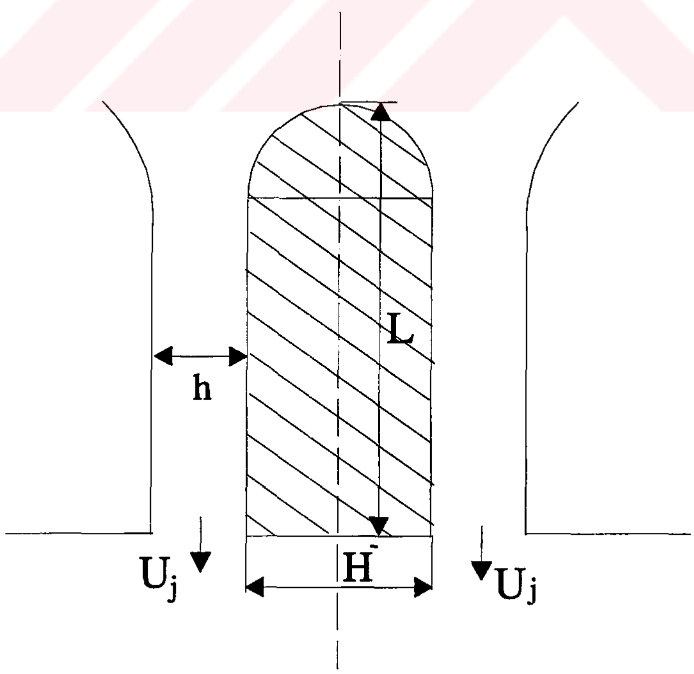

Figure 3.2 Schematic diagram of the nozzle exit arrangement for twin jet flow

The turbulence intensity of each slot at the jet exit was 0.8% for the exit velocity of 30m/s. Momentum thickness of the shear layer at nozzle exit plane was ~0.11 and the shape factor was 2.6-2.7. Detailed velocity and turbulence characteristics of jet exit plane are given in Chapter 4.

Table 3.1 Twin jet configurations

Jet exit high (h) mm	**H^*** mm	**Jet spacing ($S=H^*+h$)** mm
5	40	45
7.5	35	42.5
10	30	40
15	20	35
20	10	30

In the second part of twin jet experiments a cylindrical solid body is placed between jets as sketched in Figure 3.3.

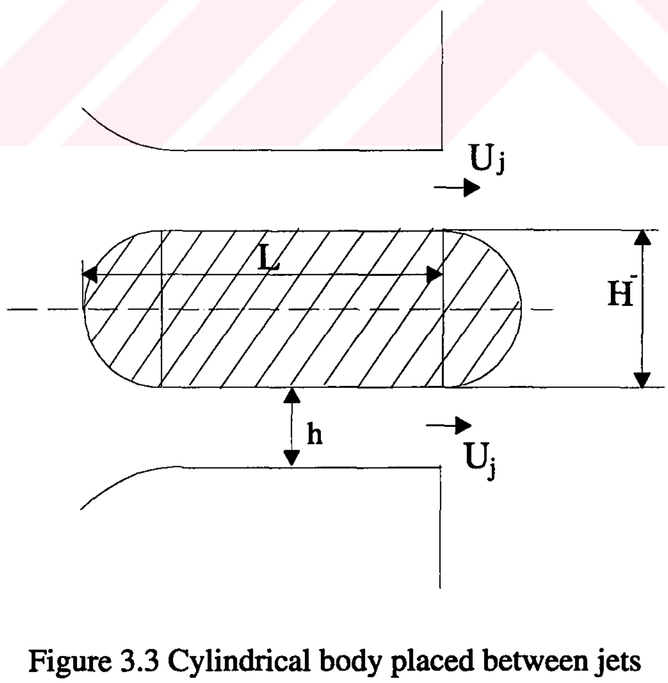

Figure 3.3 Cylindrical body placed between jets

3.3 Instrumentation

Flow field of twin jet is investigated by using qualitative and the quantitative experimental techniques. Smoke and surface oil flow techniques were used to visualize the flow pattern. Mean velocity and turbulence profiles were obtained by using constant temperature hot wire anemometer (CTA).

3.3.1 Flow Visualization Techniques

3.3.1.1 Smoke Visualization

The word "smoke" is used in a very broad sense in flow visualization techniques and includes a variety of smokelike materials such as vapors, fumes and mists. The smoke used must be generated in a safe manner and must posses the necessary light scattering qualities so that it can be readily photographed. Smoke particles should be small enough to follow the flow pattern and large enough to scatter a sufficient amount of light [75].

The oils are most commonly used to produce smoke. Since it would be safer to produce smoke by vaporizing rather than combustion; the oils requiring the lowest temperatures for vaporization are preferred. Low flammability is also an important property. A vapor of an oil mixture is used in present study.

Smoke is injected from a fine perforated tube mounted close to jet exit plane of the nozzle and aligned with the symmetry axis of the long dimension of the nozzle (Figure 3.4). Details of the smoke generator are given by Acar [54]. Flow is visualized by means of a light source of 2000W. Flow pattern becomes visible in illuminated plane. Experiments are recorded by a Sony CCD camera.

3.3.1.2 Surface Oil Flow Technique

This technique is used for visualization of jet flow impingement on a wall. Flow pattern on the wall is determined by surface oil technique.

The surface is coated with a mixture of gasoline, motor oil and carbon dust. The mixture is applied homogeneously on the surface. After being subjected to the steady flow during a time period, the pigments (carbon particles) gives the information of the direction of the flow, lines of separation and reattachment.

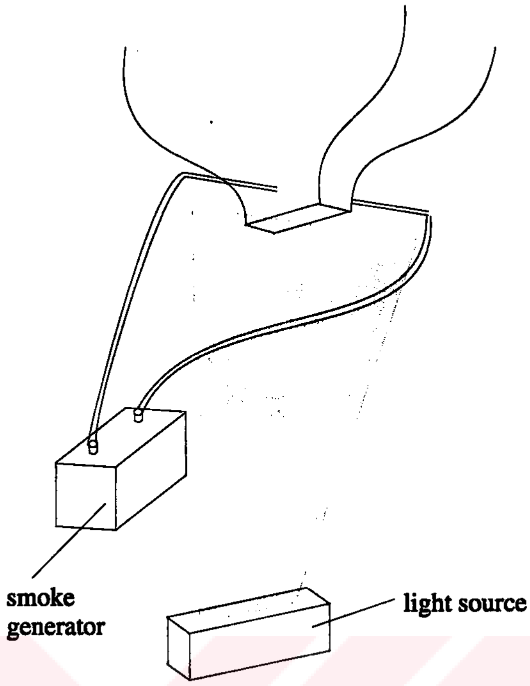

Figure 3.4 Smoke visualization arrangement

3.3.2 Hot-wire Technique

Hot wire anemometer is one of the principal research tools for most of complex turbulent flow studies.

Hot wire anemometer is basically a thermal transducer. The information of velocity, temperature, concentration or phase changes can be provided by an heated element (wire or film) placed in a fluid flow. Technique is based on convective heat transfer from the heated element. As the flow conditions vary, the heat transfer from the filament varies. The variation of the resistance of heated element due to the temperature variations is monitored by electronic methods which gives signals related to the variations in flow velocity or temperature [97]. To measure the velocity, the heated element is placed in a feedback of circuit which tends to maintain the wire at constant temperature (CTA). The output voltage of feedback unit which compensates temperature changes is related with the flow velocity.

Frequency response of HWA is definitely superior then the other experimental techniques. Measurements to several hundred KHz are quite easily obtained [75]. Hot wire results are very repeatable, so accuracy is high. The noise level is very low. Measuring volume of hot wire is very small. Besides all these advantages, it appears limited to low turbulence intensities [75].

3.3.2.1 Calibration of Hot-wire Probe

Jet flow facility was used for hot-wire probe calibration. Probe was placed at the jet exit plane. Reference velocity was determined from the pressure drop across the nozzle. The pressure difference between the settling chamber (P_0) and the jet exit plane (p_s) was measured by means of a micro-manometer which is connected to pressure tabs. The flow velocity is evaluated from Bernoulli equation.

The relation between velocity and voltage output of HWA is often assumed to be of the form,

$$E^2 = A + BU^n \tag{3.1}$$

according to King's law.

A polynomial equation is introduced for inverse process, $U=F^{-1}(E)$.

$$U = A + BE + CE^2 + DE^3 + \ldots \tag{3.2}$$

This method was tested by Bruun up to tenth degree. In order to achieve a good accuracy, it is necessary to use either a full forth order polynomial or a third order polynomial in E^2. Expressing the velocity U in a polynomial form of E has computational advantages.

3.3.2.2 Uncertainty Analysis

For moderate/high turbulence intensity flows some errors occurs in velocity and turbulence measurements employing HWA. The effective velocity measured by a single hot wire in three dimensional flow may be expressed as,

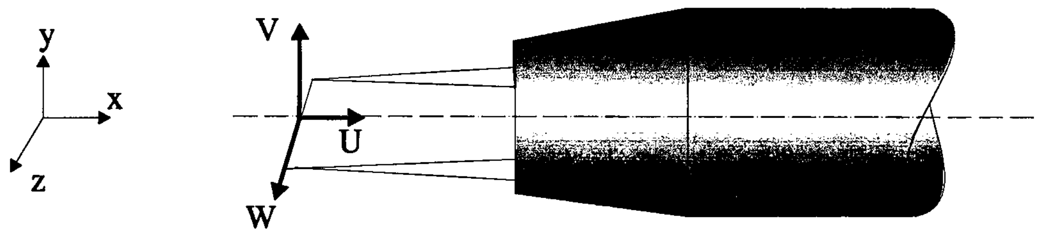

Figure 3.5 Wire oriented coordinate system

$$V_e^2 = U^2 + k^2V^2 + h^2W^2 \tag{3.3}$$

where

$$U = \overline{U} + u$$
$$V = \overline{V} + v$$
$$W = \overline{W} + w$$

considering the probe axis is oriented parallel to the flow direction ($\overline{V} = 0, \overline{W} = 0$) as seen in Figure 3.5 and neglecting terms containing k^2 since $k^2 << h^2$, the measured velocity and turbulence may be obtained by the series expansion method

$$\overline{U}_m = \overline{U}\left(1 + \frac{1}{2}h^2\frac{\overline{w^2}}{\overline{U}^2}\right) \tag{3.4}$$

$$\overline{u_m^2} = \overline{u^2}\left(1 + h^2R_{uw^2}Tu\right) \tag{3.5}$$

where

$$Tu = \frac{\left(\overline{u^2}\right)^{1/2}}{\overline{U}} \quad , \quad R_{uw^2} = \frac{\overline{uw^2}}{\left(\overline{u^2}\right)^{3/2}} \tag{3.6}$$

Acrivlellis [98], proposes that evaluation in terms of $\overline{V_e^2}$, would reduce the error since no series expansion required in this method. A related numerical error analysis for $V_e(t)$ has been carried out by Swaminathan et al. [99]. In their analysis the hot-wire was exposed to a random turbulent flow. They have presented exact error and the error calculated from Equation 3.4 for mean velocity.

Retaining same assumptions the expression (3.3) becomes

$$\overline{V_e^{\,2}} = \overline{U^2} + \overline{u^2} + h^2\overline{w^2} \qquad (3.7)$$

The mean velocity is evaluated from conventional series expansion and fluctuating terms related to $\overline{V_e^{\,2}}$ and $\overline{V_e}$ can be expressed as,

$$\overline{v_e^2} = \overline{V_e^2} - \overline{V_e}^{\,2} \qquad (3.8)$$

using (3.3), (3.7) and (3.8) the equation for $\overline{u_m^2}$ can be expressed as,

$$\overline{u_m^{\,2}} = \overline{u^2}\left[1 + O(4)\right] \qquad (3.9)$$

Figure 3.6 shows exact and second order correction factors for mean velocity versus turbulent intensity.

3.4 Experimental Procedure

All velocity and turbulence data were obtained using a DISA 55D01 type CTA main unit. Voltage output of main unit is filtered by DISA 55D35 filter. 55P01 and 55P15 type single wire sensors with a diameter of 5μm and an active length of 1.25 mm were used. The hot wire signal was digitized using a DAS 20 A/D 12 bit converter. During the experiments, probe location was controlled by a DANTEC three directional (linear motion along three axis x,y,z and rotation around z axis) traverse mechanism. The accuracy of linear motion was ± 0.016 mm. Both probe traversing and data acquisition processes were controlled by a PC. A software application named as "AcqWIRE" written for CTA systems was used for probe calibration, data acquisition and processing, and instrument control. Schematic diagram of the experimental rig is given in Figure 3.7.

A micro-manometer, an interface unit, a PCL718 A/D converter, and a PC are used to measure jet exit velocity. Manometer was measuring the pressure difference between the static pressure at the exit plane and the total pressure at the settling chamber.

Probe calibration is performed placing the probe at the origin of exit plane. Output voltage of anemometer versus velocity was measured and stored. This procedure was repeated before each set of measurements.

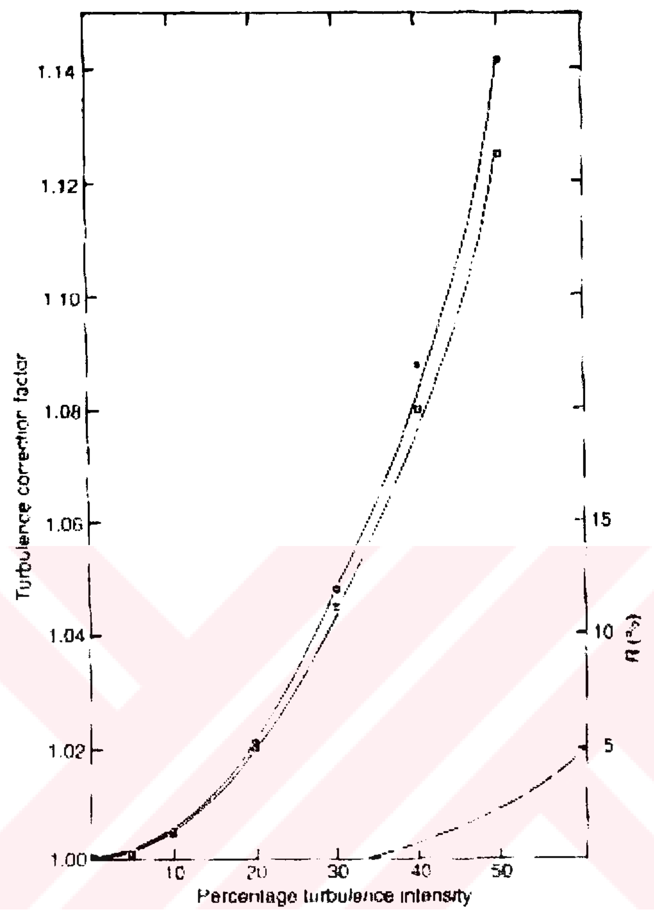

Figure 3.6 The variation of the turbulence correction factor for the mean velocity with the turbulence intensity (⊙ exact correction,⊡second order correction)[99]

A set of experiments consists of successive measurements along y or z-axis, at a constant x distance from jet exit plane.

For hot-wire measurements sampling rate was set at 0.5 KHz and sampling time was about ~8s. for each measurement point.

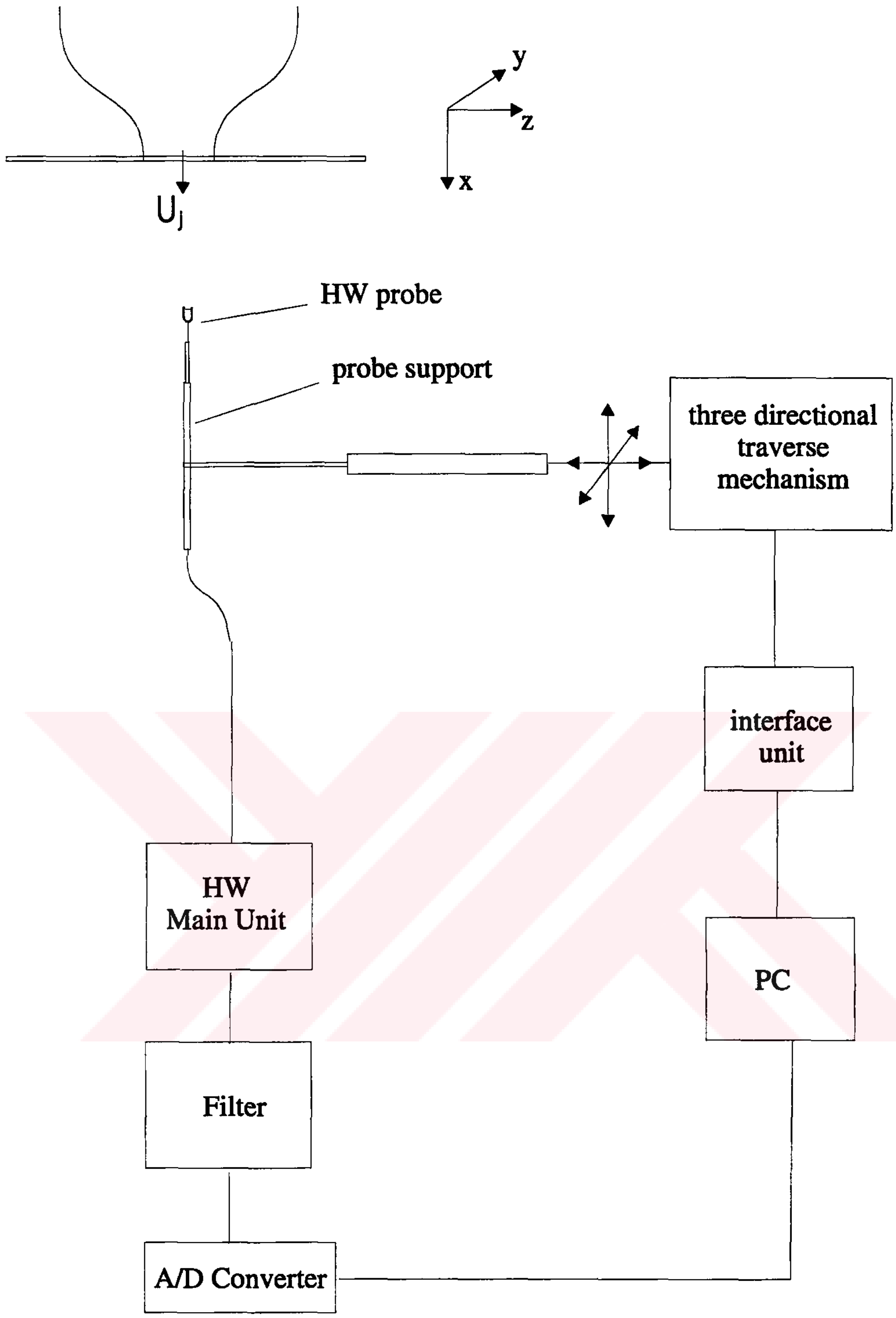

Figure 3.7 Schematic diagram of the experimental rig.

Spectral measurements have been performed by using hot-wire probe in mixing region of the twin jet. Successive time series measurements are done by controlling the probe position with Dantec traversing mechanism. The analog signal was filtered by a low pass filter at the Nyquist frequency. The data acquisition rate was 10000 or

20000 data per second depending on the amplified frequency that would be measured. Each record consists of 16384 samples.

Acquired data has been processed by using "Acqwire" software program. This program calculates spectra of the acquired data records via Finite Fourier Transforms. Detailed explanations on the calculation technique is given in Appendix A. Consider a record $x_k(t)$ from stationary random process for a finite time interval. Auto Spectral density function can be expressed as;

$$S_T(f) = \frac{|F_T(f)|^2}{T} \tag{3.10}$$

where

$$F_T(f) = \frac{T}{N}\sum_{r=1}^{N} U(n)e^{-2\pi kr/N} \qquad k=0,1,\ldots,N/2 \tag{3.11}$$

The pressure distribution on the wall where the twin jet impinged normally is measured by means of the pressure tabs of 1mm inner diameter on the surface. The pressure tab locations are sketched in Figure 3.8. Half plane pressure distributions are measured by turning the plate around y-axis. Pressure difference between the surface static pressure and the ambient pressure was measured by a micro-manometer of 1000 mm-H_2O maximum pressure range and ±1% accuracy. The micro-manometer output voltage is digitized by a PCL-718 A/D converter and data is stored on a PC. Experimental setup is illustrated in Figure 3.9.

Pressure data is acquired by a computer program which takes the average of the data from time series. Sampling time was about 4 s. for each measurement.

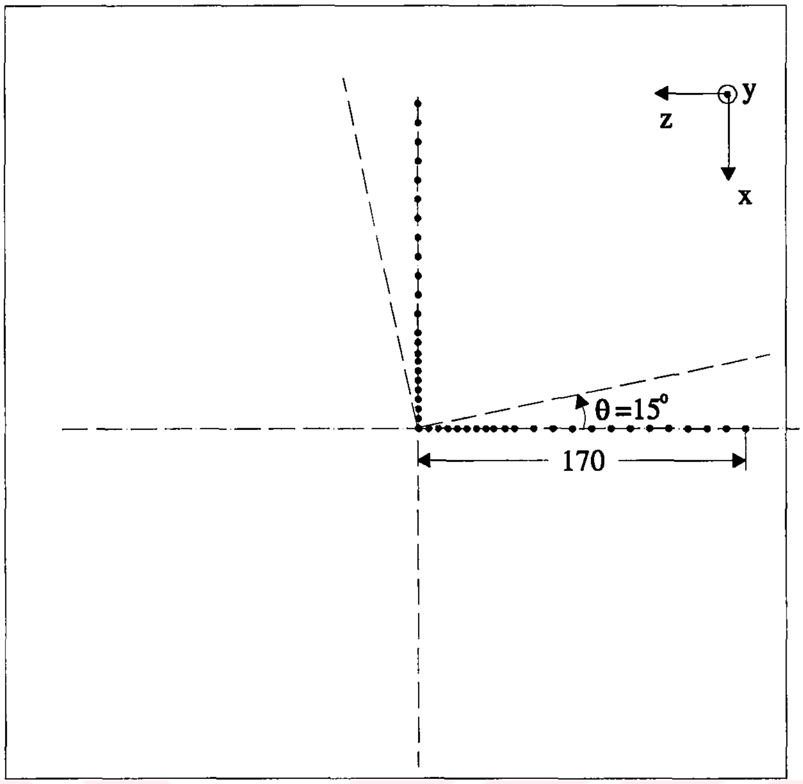

Figure 3.8 Pressure tabs on the impingement surface.

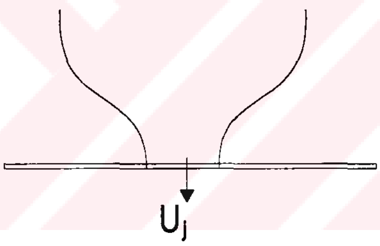

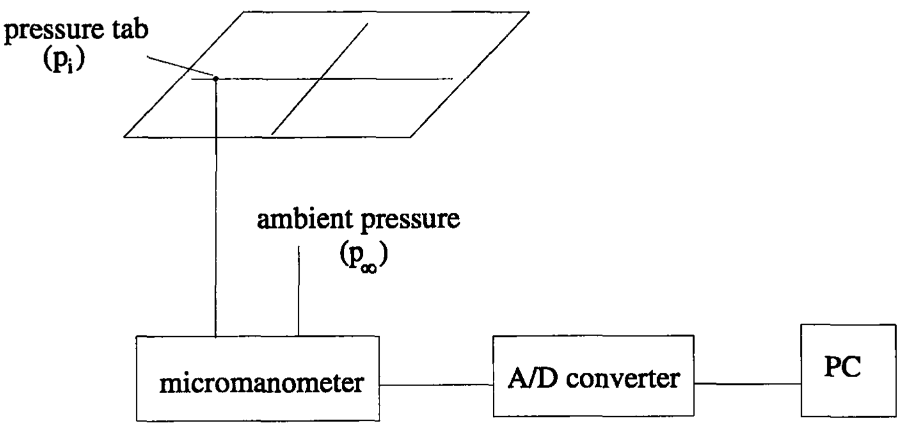

Figure 3.9 Experimental setup for surface pressure measurements of impinging twin jet configuration.

4. RESULTS AND DISCUSSION

4.1 Introduction

Experimental results are presented in this chapter. The initial conditions of jet facility are presented in the first step. Then the Reynolds similarity of twin jet flow is investigated for a particular twin jet configuration. Twin jet experiments are given in two parts. The objective of the first part is to investigate flow characteristics of five different twin jet configuration. The second part of measurements aims to examine curvature effects on twin jets. For this reason a half cylinder of diameter H^* is placed between the jets. The last part of this study is reserved for the twin jet impingement.

4.2 Initial Conditions

For a given set of boundary conditions the mean and turbulence characteristics of the initial boundary layer as well as the Reynolds number determine the evaluation of the jet flow [13]. When the initial flow is turbulent the decay rate of centerline mean velocity is higher but spreading rate is lower comparing with the initially laminar case [13]. The effects of upstream conditions on jet evaluation were investigated by Hussain and Clark [13] and Tsuchiya et al. [27].

Mean velocity distribution at the exit plane of the nozzle is given in Figure 4.1. The exit velocity profiles of all investigated jets are almost uniform along the y axis. The turbulence intensity distribution at the nozzle exit section are also uniform and have a constant value of about 0.8% along the uniform velocity region. Mean exit velocity for each twin jet configuration is retained constant, Uj=30m/s, during the experiments.

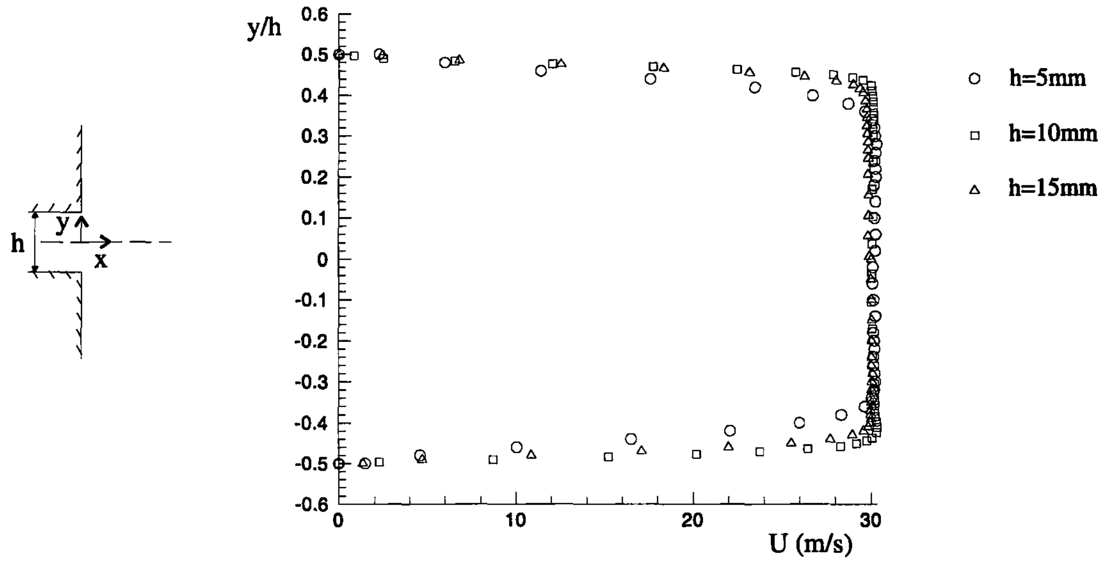

Figure 4.1 Velocity profiles at the exit plane.

Figure 4.2.a shows inner and outer boundary layer velocity profiles at exit plane for different jet configurations. Initial boundary layers are plotted in non-dimensional form and agreed well with the Blasius laminar profile.

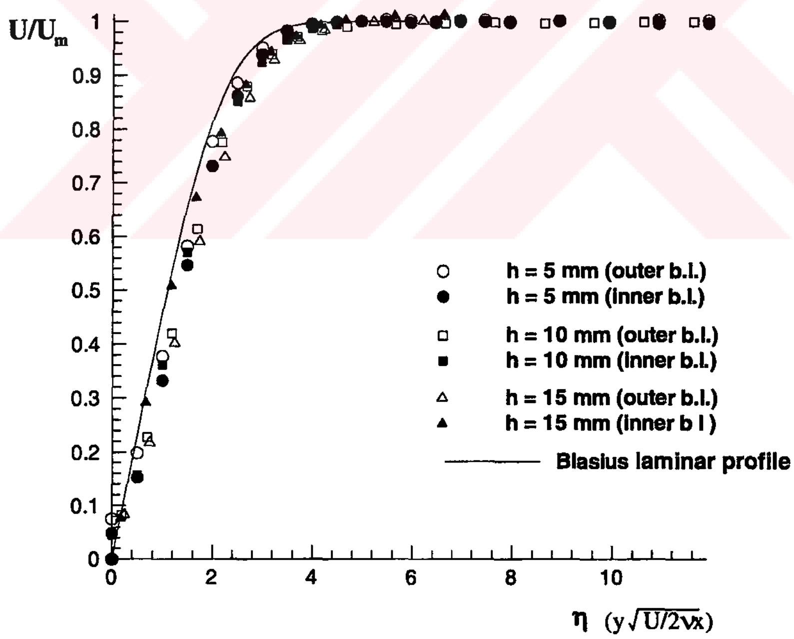

Figure 4.2.a Initial boundary layer profiles

Turbulence intensity profiles in boundary layer is given in Figure 4.2.b. Peak values of rms velocity fluctuations in the initial boundary layer are located at η~2. Boundary layer thickness δ, displacement thickness δ^* and momentum thickness θ

are calculated and listed in Table 4.1. The values of shape factor H are approximately equal to that of Blasius profile.

Even though the initial boundary layer is laminar, due to inflection in velocity profile the flow in the mixing layer is highly unstable and quickly becomes turbulent, and according measurements of Liepmann and Laufer, transition occurs at a distance $7 \times 10^4 \nu/U$ from the exit [93].

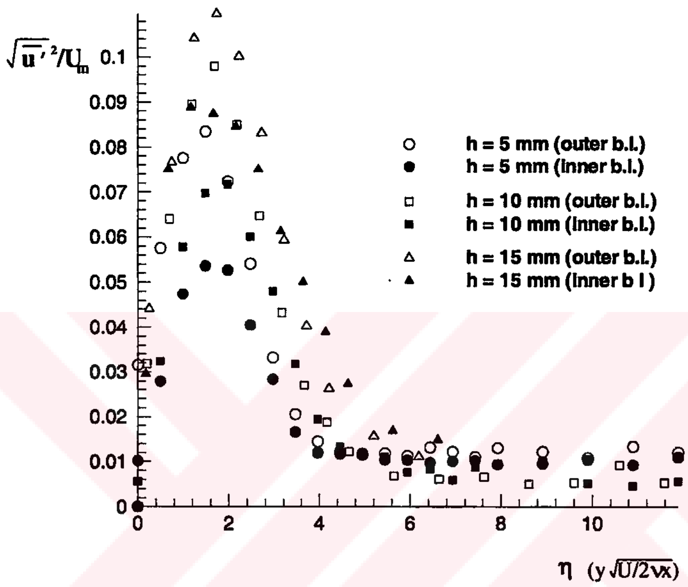

Figure 4.2.b Turbulence intensity distribution in the initial boundary layer

Table 4.1 Initial boundary layer characteristics

V_j m/s	h mm	Re_h	δ mm	δ^* mm	θ mm	$H=\delta^*/\theta$
30	5	10067	1.05	0.2714682	0.1051991	2.58052
30	10	20135	1.5	0.3047623	0.1144645	2.662505
30	15	30201	1.8	0.3280437	0.119901	2.73595

The spectral distribution of the velocity fluctuations inside the boundary layer were obtained by placing the probe very near the nozzle lip. The spectral analyzes did not show any dominant frequencies for any case. A power spectra inside the initial boundary layer of 15 mm high nozzle is presented in Figure 4.3. This measurement demonstrates the absence of facility dependent perturbations. Gutmark and Ho's study[78], demonstrates that spatially coherent background perturbations has affected whole flow field by changing initial instability frequency, hence the spreading rate.

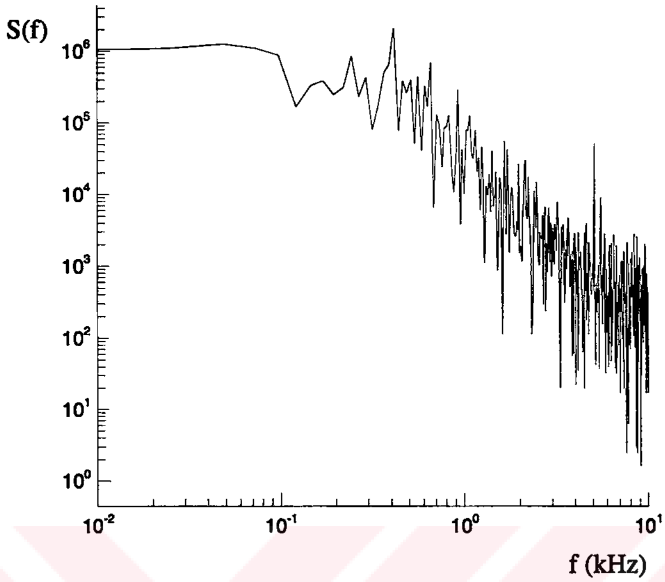

Figure 4.3 Power spectra inside the boundary layer

4.3 Reynolds Similarity of Twin Jets

The mean velocity and turbulence profiles of a twin jet for the Reynolds numbers based on nozzle high of 13422, 26845 and 40268 are measured at different x/h stations. Different Reynolds numbers are obtained by changing jet exit velocity of 20 mm high twin jet configuration from 10 to 30 m/s. Jet spacing S was 30 mm. The velocity is normalized with respect to the maximum velocity (U_m) and the y coordinate is normalized with respect to jet half with $y_{1/2}$.

Mean velocity profiles are given in Figure 4.4. Non-dimensional velocity profiles are agreed well with each other. Since merging point is located very close to nozzle exit for this case, profiles in Figure 4.4 does not contain reverse flow characteristics.

Merging process of twin jet can easily be seen from the figure. The recirculation region terminates at the merging point and the two individual jets continue to merge until at the combined point where the velocity on the axis of symmetry becomes

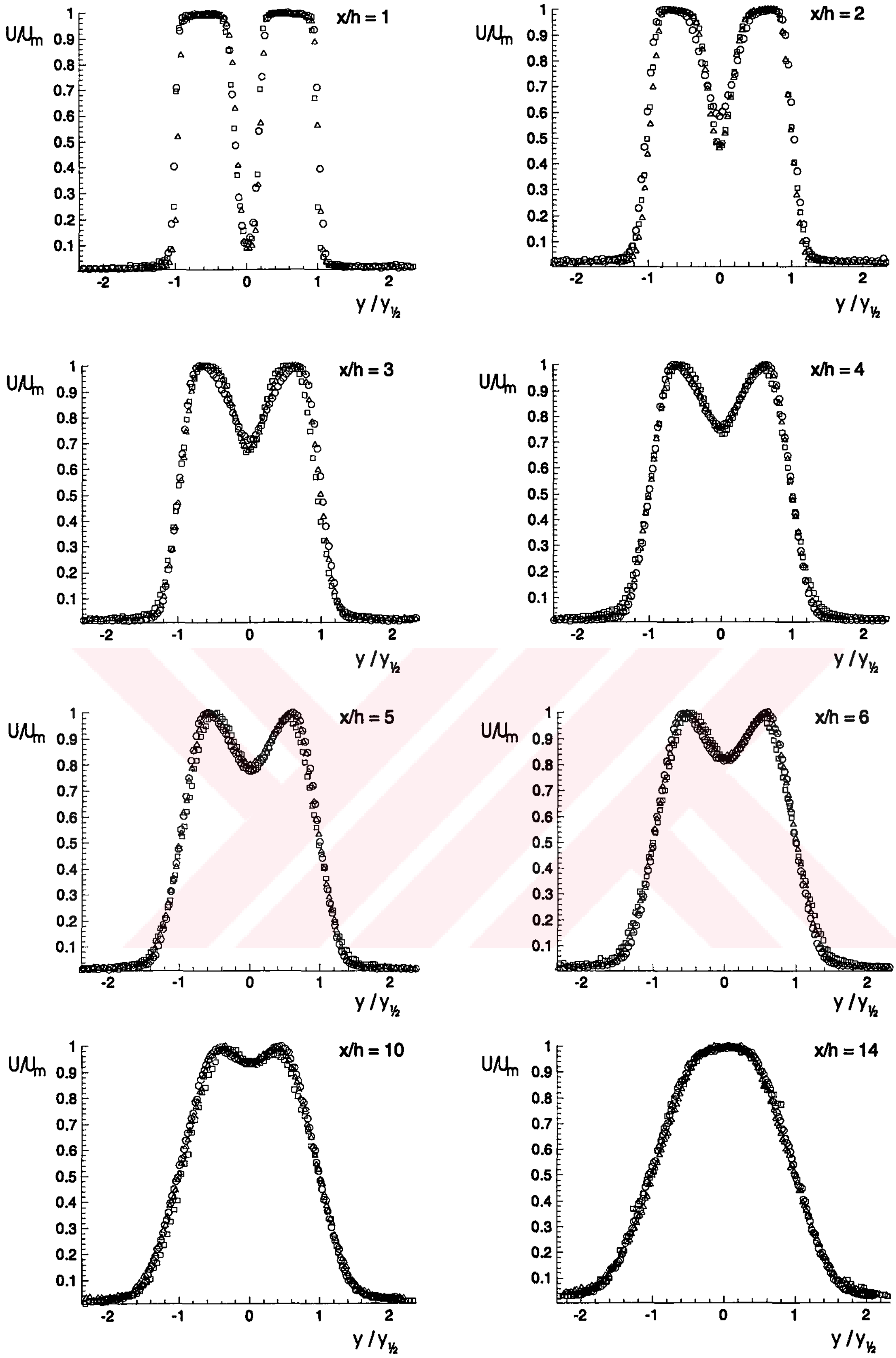

Figure 4.4 Mean velocity profiles for Reynolds numbers of □13422, △26845 and ○40268

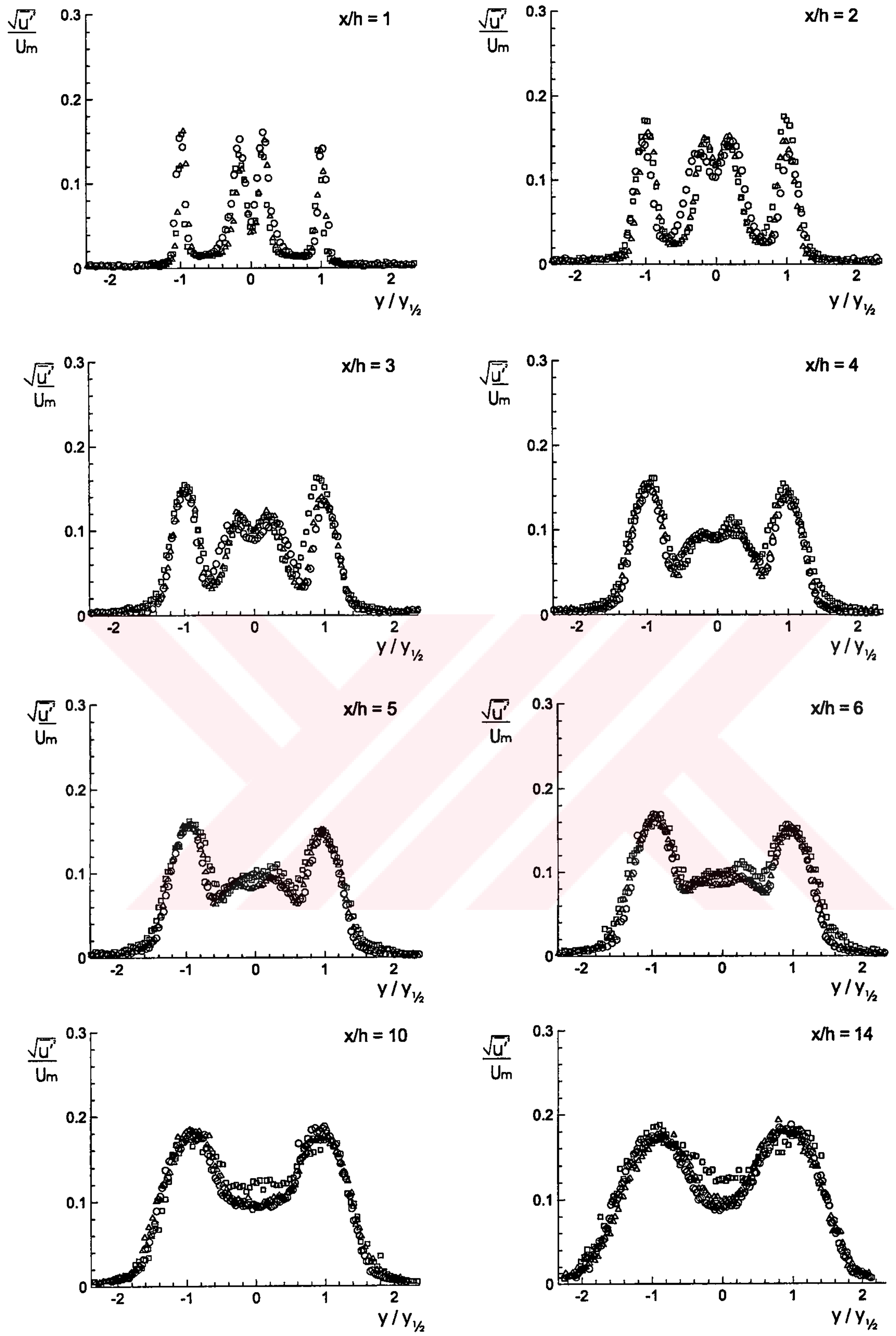

Figure 4.5 Turbulence intensity profiles for Reynolds numbers of 13422, 26845 and 40268

maximum. Combined point is located very near to x/h=12 station for each case. After this point, flow resemble a single jet and reaches self-similarity.

Figure 4.5 display the development of turbulence intensity profiles. Maximum peak values in inner and outer shear layers are in good agreement.

Velocity profiles in single jet region are plotted on same axis in order to demonstrate self-similarity of the flow (Figure 4.6-4.8). Non-dimensional velocity profiles agree with the theoretical curve of Gortler. This result indicates that the flow in combined region is approached to a fully developed single jet flow. For downstream locations greater than 12h, turbulence intensity profiles exhibit saddle back shape as shown in Figures 4.9-4.11. The appearance of a saddle shape profile in a jet usually indicates the end of the potential core[56]. Krothapalli et all.[56], concludes these in such a way that the multiple jet flow field appears as though it is emerging from a single slot and defines a pseudo-potential core which ends at combined point.

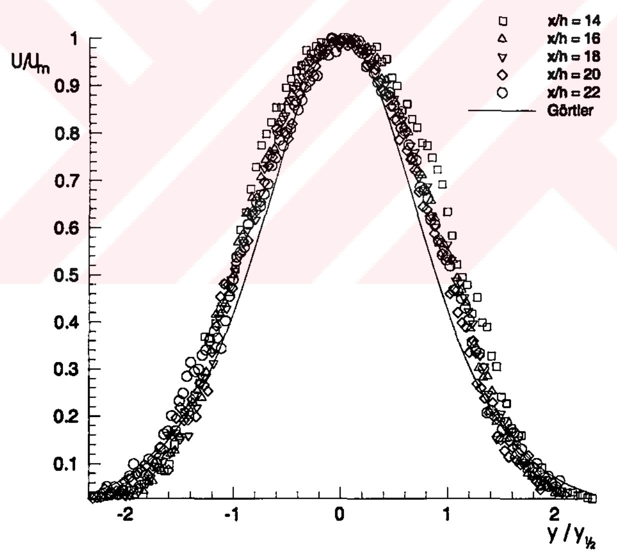

Figure 4.6 Self-similarity profiles for Re_h=13422 case.

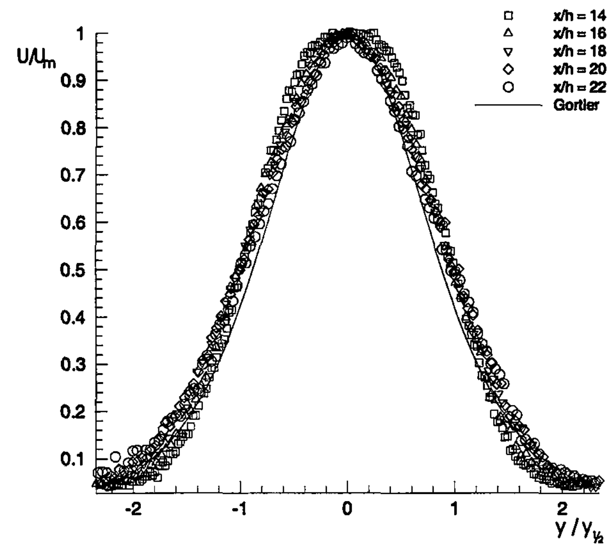

Figure 4.7 Self-similarity profile for Re_h=26845 case.

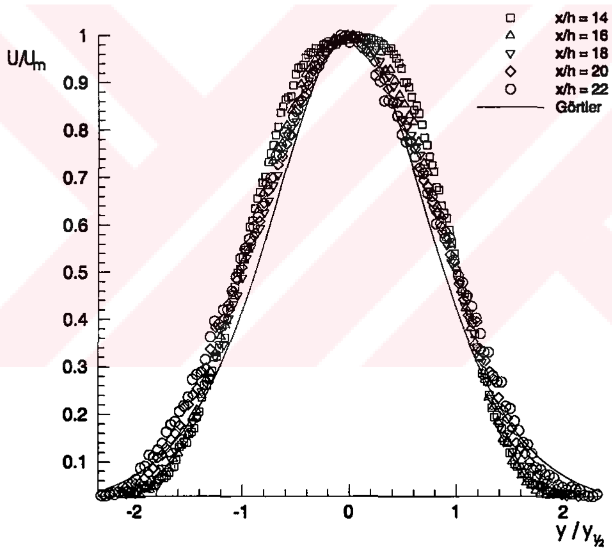

Figure 4.8 Self-similarity profile for Re_h=40268 case.

As a result, the distributions of mean velocity and turbulence intensity, indicate that they are virtually independent of the Reynolds number in the range 13422-40468. Similar results were reported by Nasr and Lai [68], and Tanaka[61]. Self similar velocity and turbulence profiles were obtained downstream of combined point.

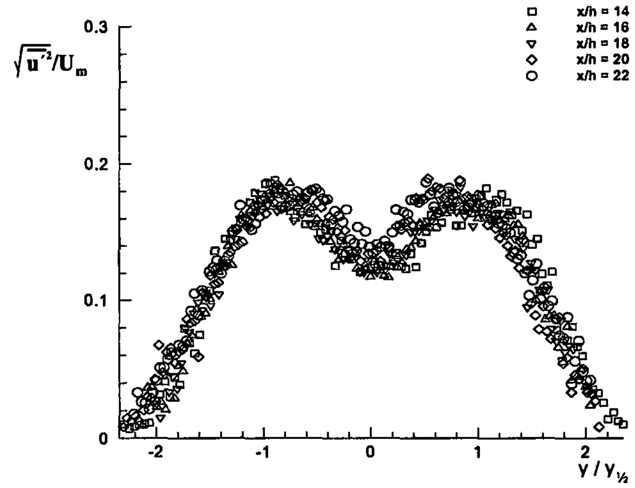

Figure 4.9 Turbulence intensity profiles in single jet region of Re_h=13422 case.

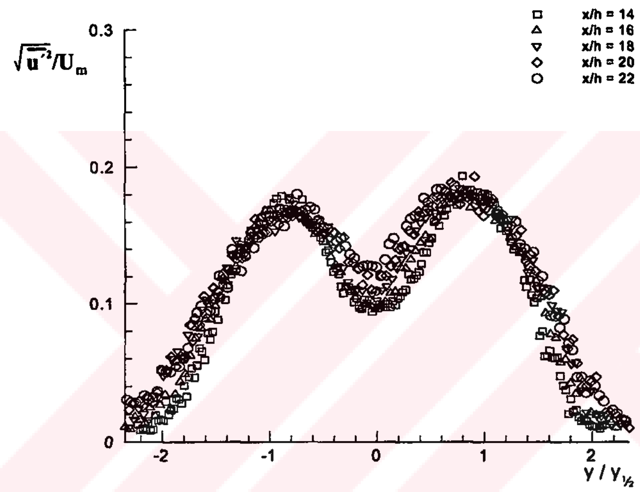

Figure 4.10 Turbulence intensity profiles in single jet region of Re_h=26845 case.

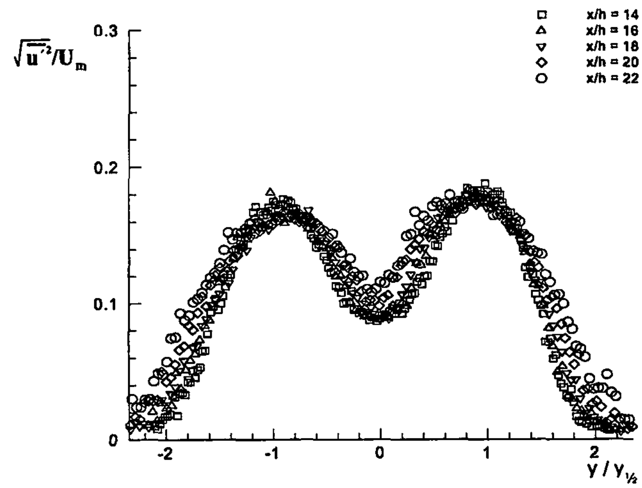

Figure 4.11 Turbulence intensity profiles in single jet region of Re_h=46268 case.

4.4 TWIN JET FLOW

Five different twin rectangular jet configurations are investigated in this part. These configurations are described in Chapter 3. The coordinate system used in this part originates in exit plane at the mid point of two jets as sketched in Figure 4.12.

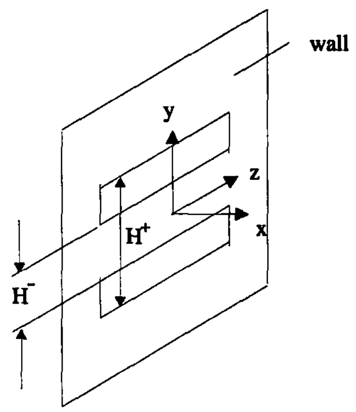

Figure 4.12 Cartesian coordinate system for twin jets

Some photographs of smoke visualization are presented in Figure 4.13. These visualizations are in xy plane. Small photographs in Figure 4.13 are obtained by psychedelic color transformation of original photos. It is observed from flow visualization experiments that the parallel rectangular jets issuing from adjacent slots, which are separated in the lateral direction by a distance H^-, deflect towards the symmetry plane. The deflection results in merging of two jets. The position of merging point where the velocity on symmetry axis is zero can be observed from the photographs. Downstream from the merging point, flow continues to merging process up to combined point where the flow has a single jet form.

As is evident from Reynolds similarity experiments, Reynolds number has no effect on flow characteristics in the Reynolds number range studied. Jet exit velocity is maintained constant (V_j=30m/s) according to this result.

4.4.1 Mean Velocity and Turbulence Intensity Distributions

Hot-wire experiments for each configuration in xy plane are presented in Appendix B. The velocity is normalized with respect to maximum velocity U_m and y coordinate

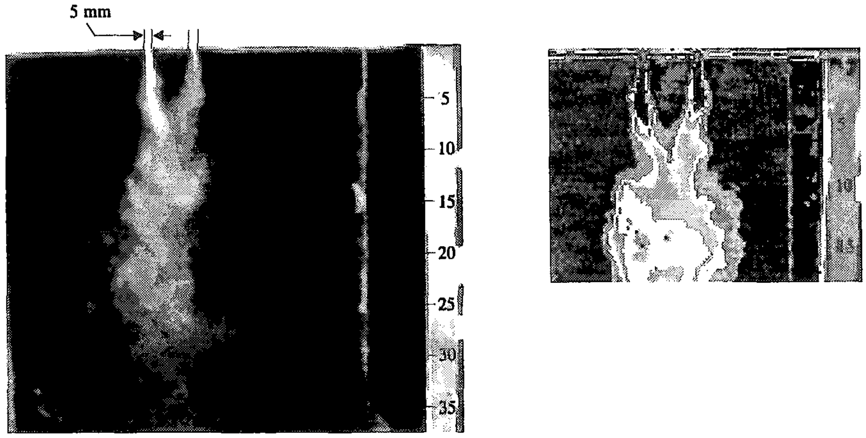

(a)

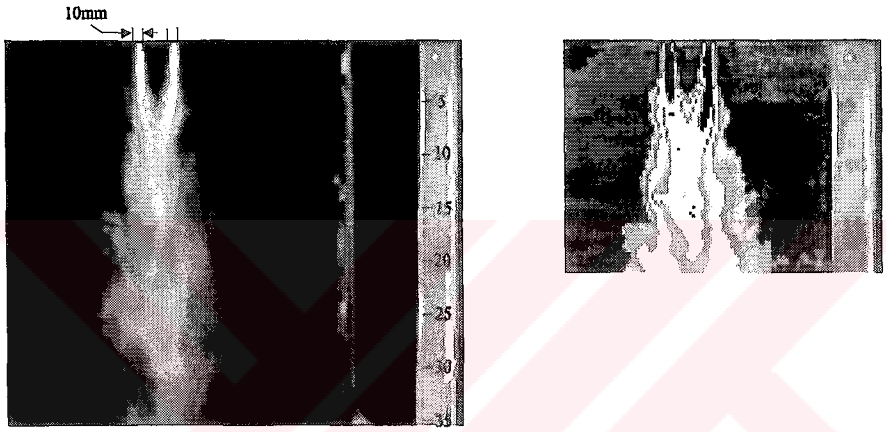

(b)

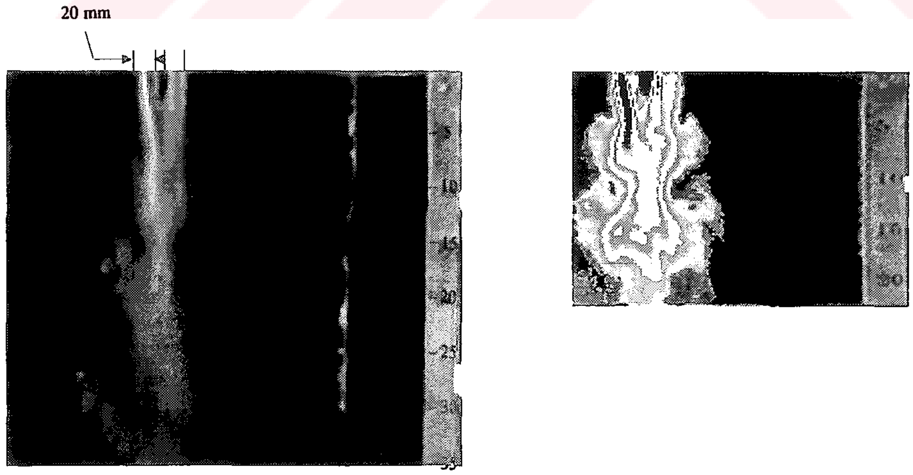

(c)

Figure 4.13 Smoke visualization of twin jet flow in xy plane. a) h=5mm, b) h=10mm, c) h=20mm is normalized with respect to nozzle spacing S. x distance is normalized with nozzle high h, as usual in recent studies. Beside x/h axis, a second axis x/H^+ is introduced in order to demonstrate that the flow development characteristics (as merging point, combined point etc.) are similar with respect to constant normalized distance x/H^+.

For the comparison of results, selected velocity and turbulence profiles of twin jets at different x/H^+ stations are plotted in Figure 4.14 and 4.15. Velocity is normalized with maximum velocity and y distance with jet half width $y_{1/2}$. Normalization with jet half width, was applied only to velocity profiles in combined region of twin jet by several investigators [60-62, 64, 73]. In this study, whole flow field is presented in the form of U/U_m versus $y/y_{1/2}$, since velocity profiles exhibit a high degree of similarity.

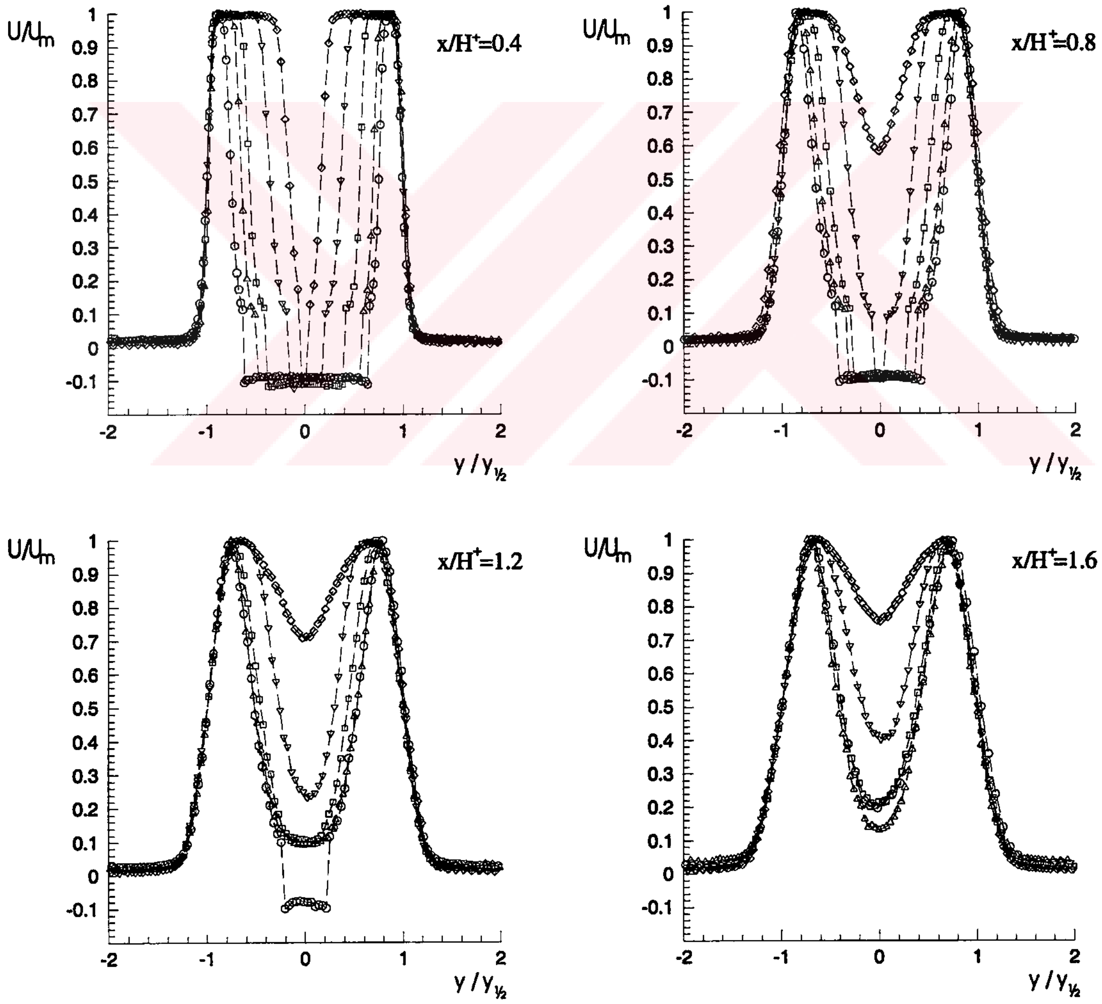

Figure 4.14.a Non-dimensional velocity profiles in converging region of twin jets, ○ $h/H^+=0.1$, △ $h//H^+=0.15$, □ $h/H^+=0.2$, ▽ $h/H^+=0.3$, ◇ $h/H^+=0.4$

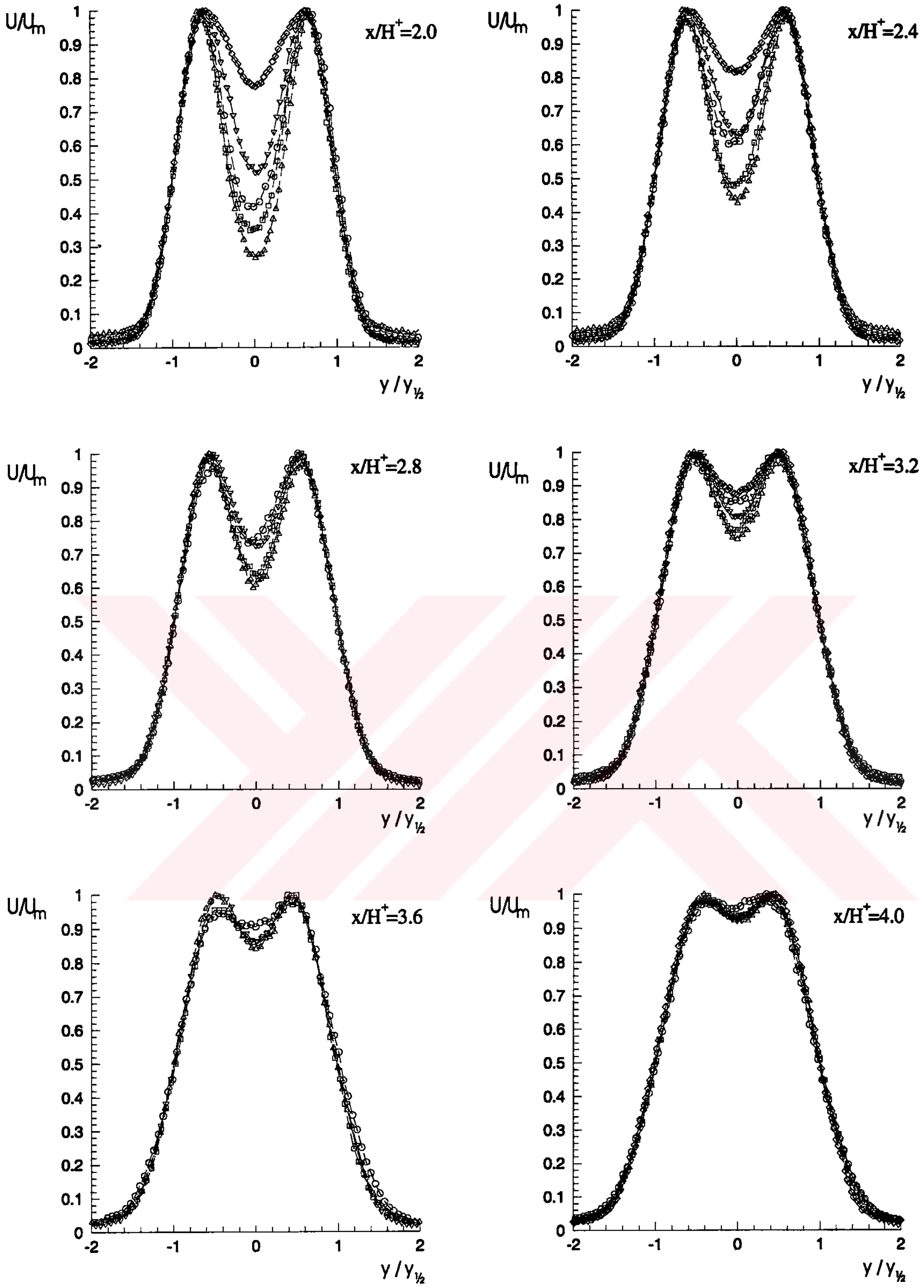

Figure 4.14.b Non-dimensional velocity profiles in merging region of twin jets

○ $h/H^{+}=0.1$, △ $h//H^{+}=0.15$, □ $h/H^{+}=0.2$, ▽ $h/H^{+}=0.3$, ◇ $h/H^{+}=0.4$

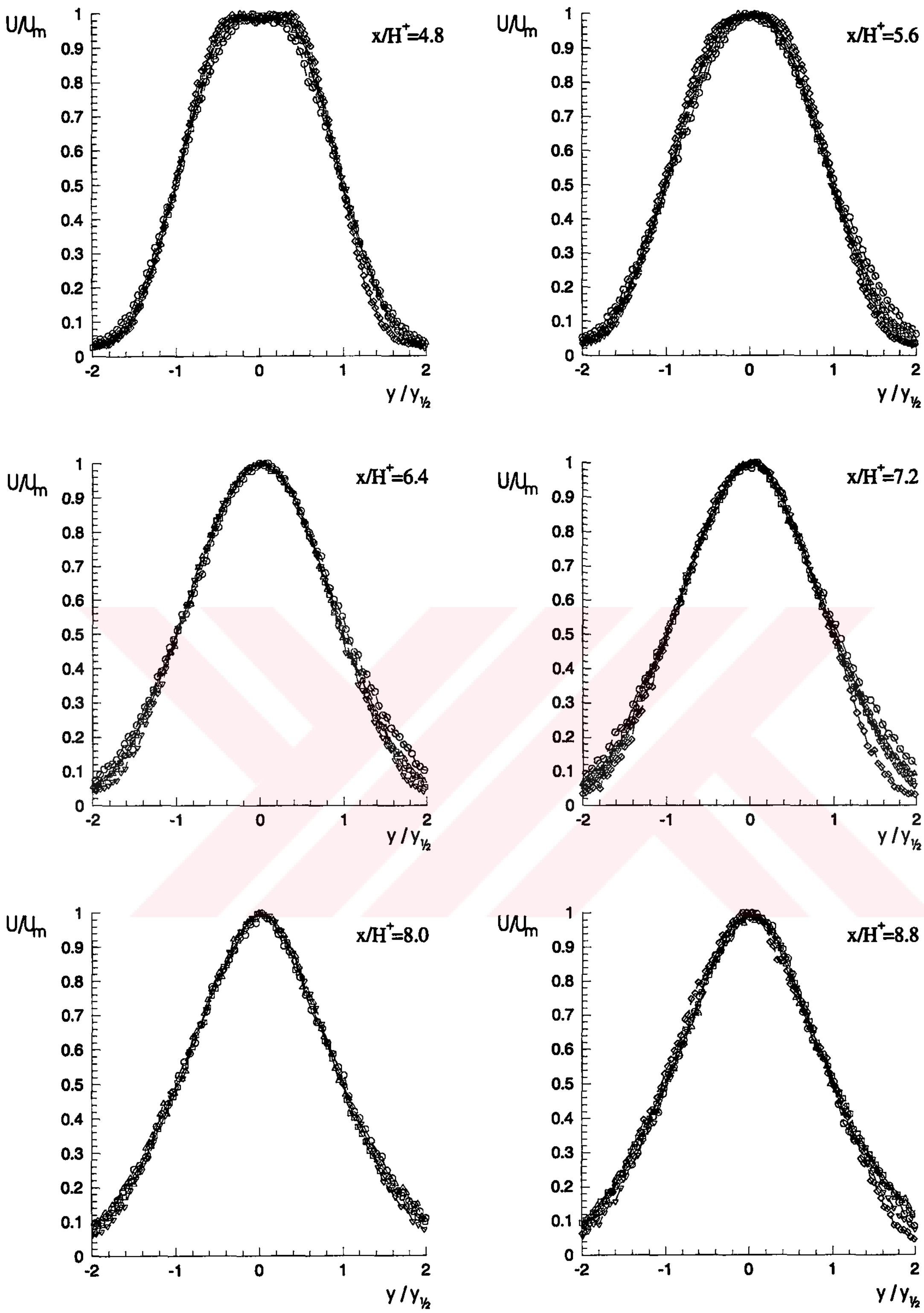

Figure 4.14.c Non-dimensional velocity profiles in combined region of twin jets, ○ $h/H^{+}=0.1$, △ $h//H^{+}=0.15$, □ $h/H^{+}=0.2$, ▽ $h/H^{+}=0.3$, ◇ $h/H^{+}=0.4$

In Figure 4.14.a non-dimensional velocity profiles are presented near the jet exit region where converging process can be observed. As can be seen from the figure the outer shear layer exhibit similarity while the inner shear layer differs one from other. Therefore, the length of the recirculation region changes depending on the distance between two jet H^{+}. The lower nozzle spacing gives the shorter merging point. Downstream from the merging point, similarity of profiles spreads to whole flow field with increasing x distance as is obvious from the Figure 14.4.b. Thus, the flow in the merging region would approach to similarity with increasing downstream distance. In combined region (Figure 4.14.c) all jet configurations approach to single jet flow and reach the self similarity as mentioned in part 4.3.

Corresponding turbulent intensity profiles of twin jets are given in Fig 4.15.a-c.The turbulence intensity distributions exhibit two peaks in the inner and outer shear layers

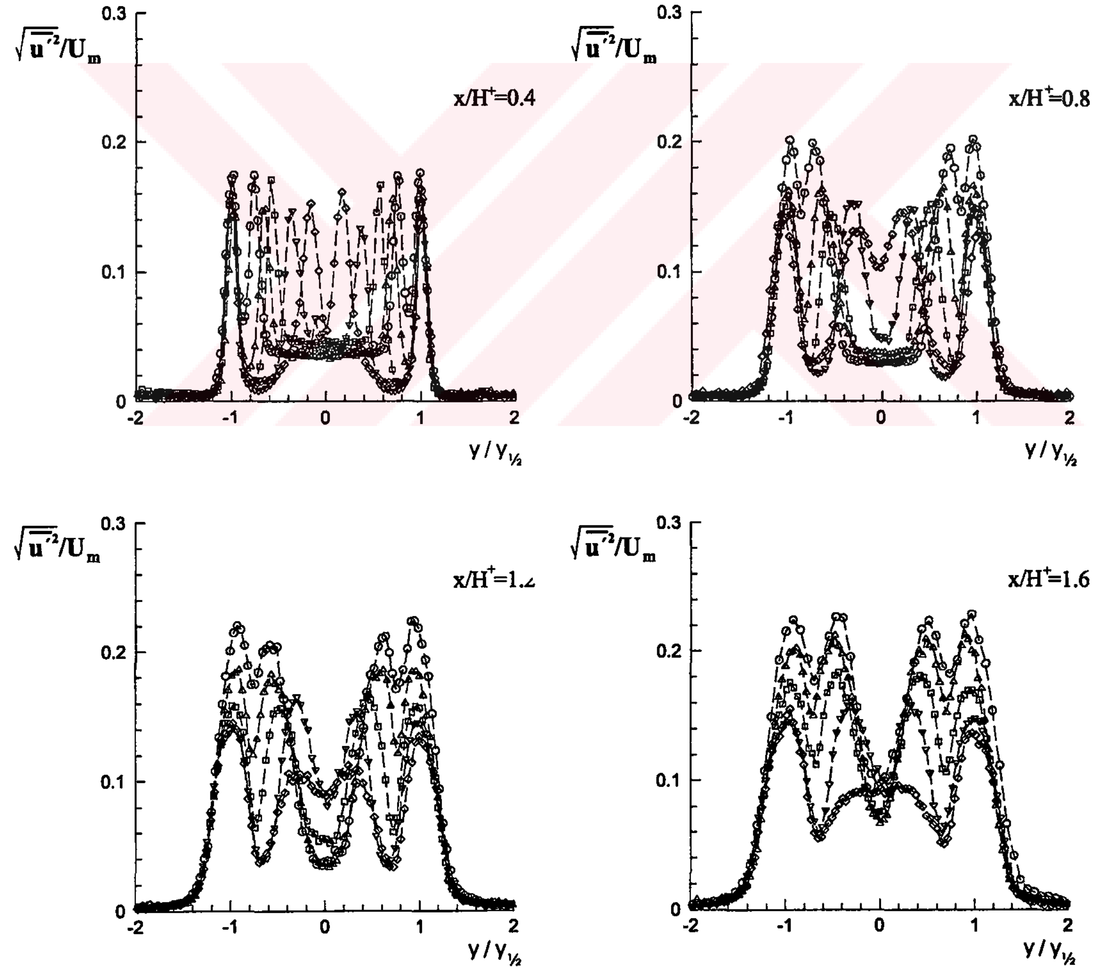

Figure 4.15.c Turbulence intensity profiles in converging region of twin jets, ○ h/H^{+}=0.1, △ h/H^{+}=0.15, □ h/H^{+}=0.2, ▽ h/H^{+}=0.3, ◇ h/H^{+}=0.4.

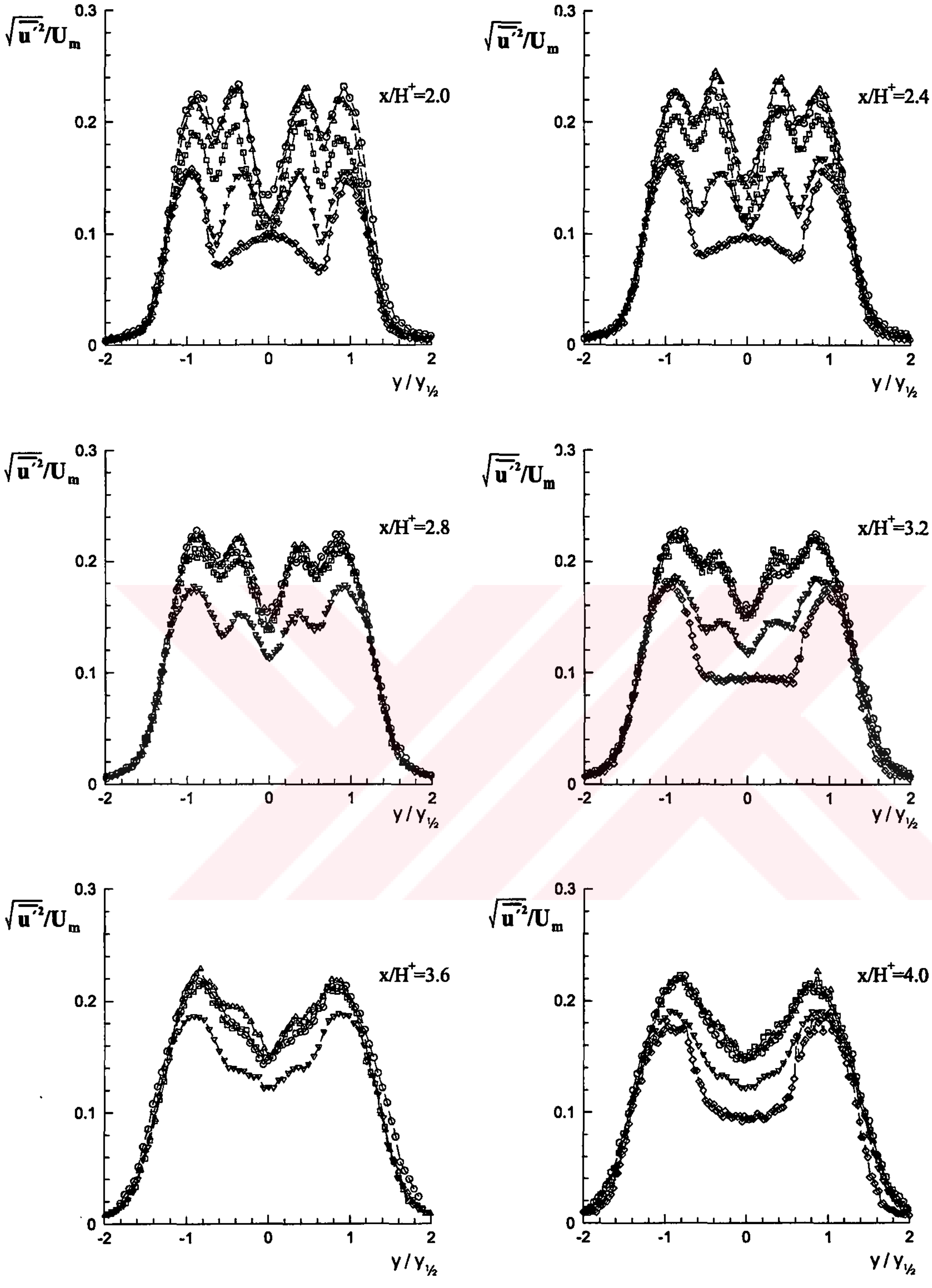

Figure 4.15.b Turbulence intensity profiles in merging region of twin jets, ○ $h/H^+=0.1$, △ $h/H^+=0.15$, □ $h/H^+=0.2$, ▽ $h/H^+=0.3$, ◇ $h/H^+=0.4$.

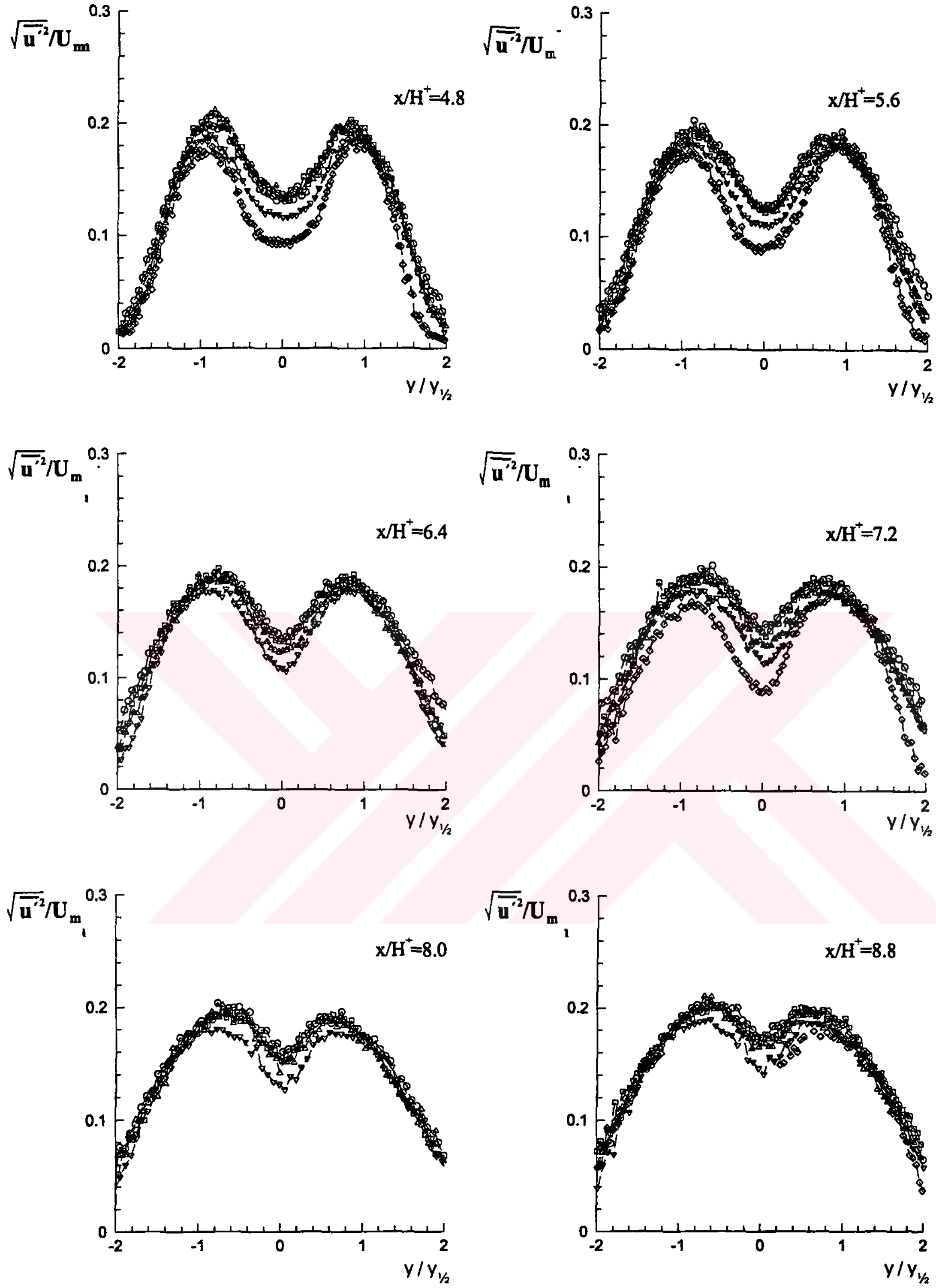

Figure 4.15.c Turbulence intensity profiles in combined region of twin jets, ○ $h/H^{+}=0.1$, △ $h/H^{+}=0.15$, □ $h/H^{+}=0.2$, ▽ $h/H^{+}=0.3$, ◇ $h/H^{+}=0.4$.

layers upstream of the merging point (Figure 4.15.a).The peak value has a higher magnitude in the outer shear layer than that in the inner shear layer. It means that the turbulence intensity in the outer shear layer is less constrained by the recirculating flow and the merging process. Peaks in the outer shear layer are located at same $y/y_{1/2}$ positions while second peak locations are scattered. Second peak locations in inner shear layer move along the y direction with increasing x/H^+ distance. Although maximum peak values in initial outer shear layers ($x/H^+=0.4$) are coincident, a differentiation in maximum peak values is observed with increasing downstream distance. Twin jet configuration with minimum nozzle width (h=5mm) gives lower turbulence intensity profiles while the maximum nozzle width (h=20mm) provides higher turbulence intensities.

After merging point, second peaks in turbulence intensity profiles are decreased in magnitude and then disappeared with increasing x distance (Figure 4.15.b). Saddle back shaped turbulence profiles indicate the appearance of single jet flow. But self-similarity of turbulence profiles in combined region (Figure 4.15.c) is retarded comparing with self similar velocity profiles.

The normalized mean velocity and turbulence intensity profiles in the central xz plane are shown in Figure 4.16 and 4.17 for various downstream locations. For x less than $4.8H^+$ the profiles exhibit a saddle shape as is reported by several authors for rectangular jets. After this station velocity profiles are identical to that of single jet flow. Profiles in this flow region are broader than that of a single jet at their corresponding locations.

Turbulence intensity profiles in xz plane exhibit higher values near the nozzle exit ($x/H^+=0.8$). In a short distance, maximum peak values in this region decrease to the expected values which are same as the values measured in xy plane. Secondary peaks, in turbulence profiles could not be observed clearly in xz plane measurements.

4.4.2 Jet spreading

In order to examine the growth rate of twin jets in xy and xz planes jet half widths are plotted against the downstream location x in Figure 4.18 and 4.19.

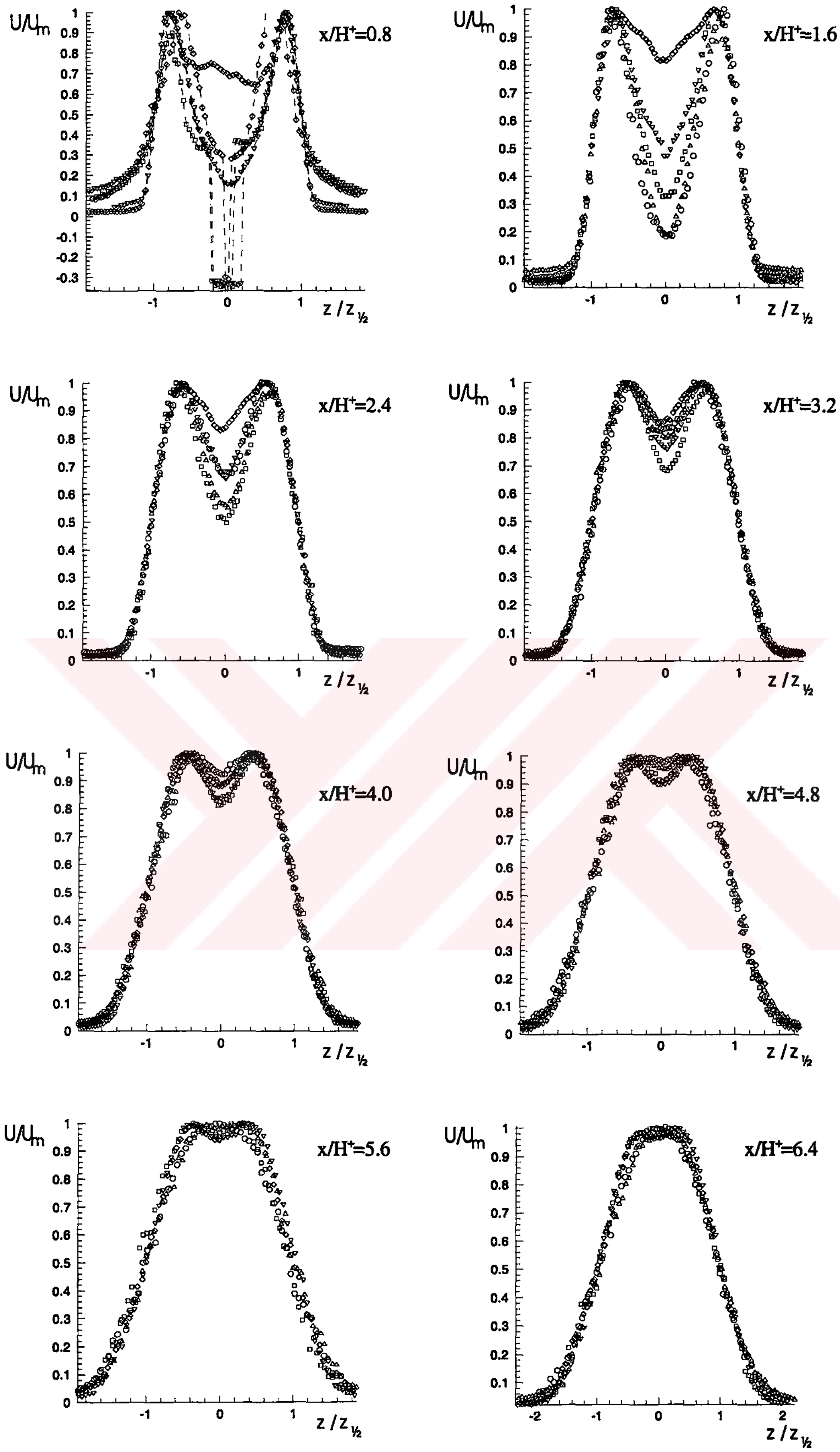

Figure 4.16 Non-dimensional velocity profiles in x-z plane, ○ $h/H^{+}=0.1$, △ $h//H^{+}=0.15$, □ $h/H^{+}=0.2$, ▽ $h/H^{+}=0.3$, ◇ $h/H^{+}=0.4$

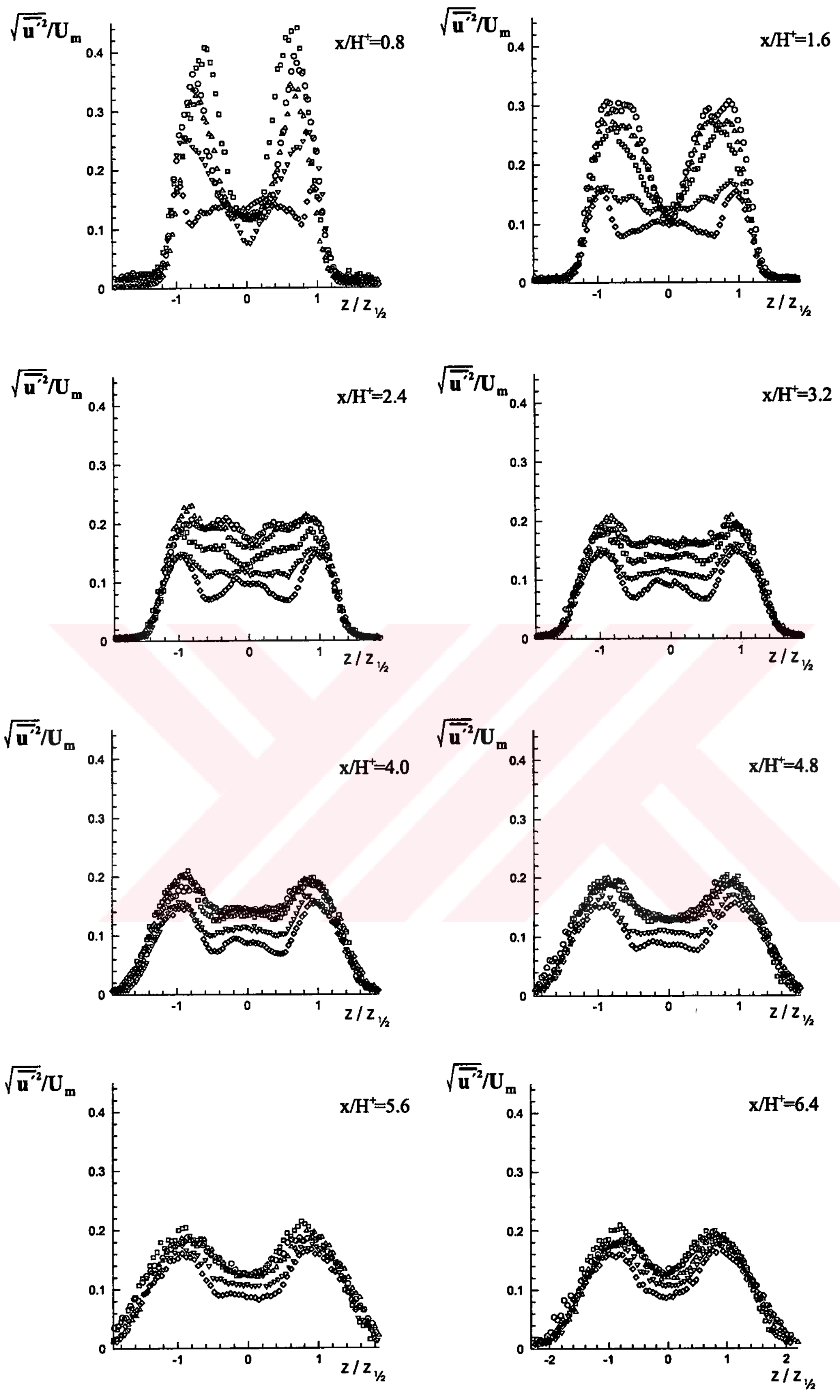

Figure 4.17 Non-dimensional turbulence intensity profiles in x-z plane, ○ $h/H^{+}=0.1$, △ $h/H^{+}=0.15$, □ $h/H^{+}=0.1$, ▽ $h/H^{+}=0.3$, ◇ $h/H^{+}=0.4$

It can be seen from the Figure 4.18 that boundaries of twin jets have similar spreading trends for all twin jet configurations. Jet half width values in both plane approaches to same value with increasing x distance. The crossover point is located outside of the measurement area.

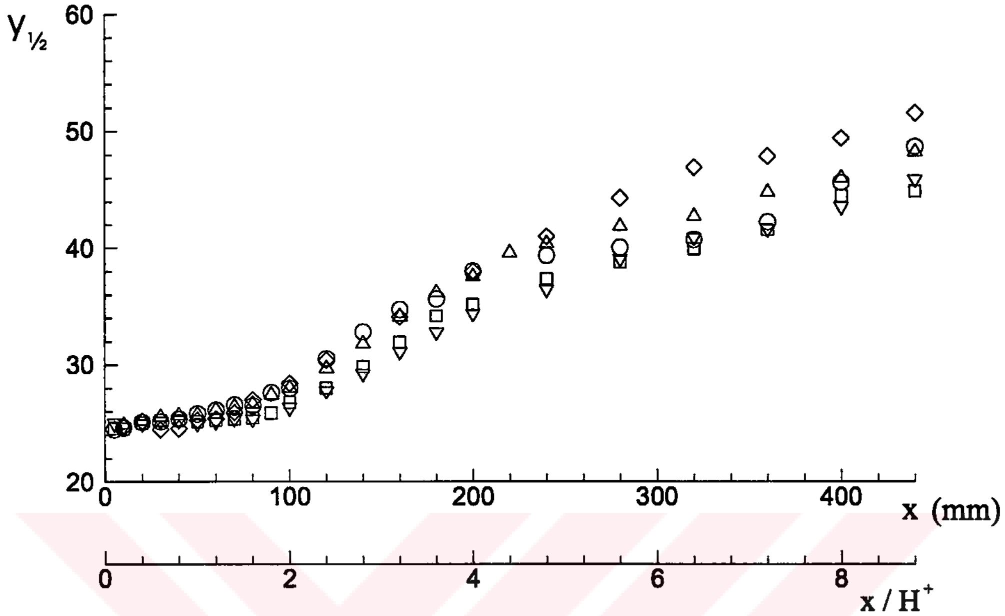

Figure 4.18 The growth of the twin jets with downstream distance in the x-y plane, ○ $h/H^+=0.1$, △ $h//H^+=0.15$, □ $h/H^+=0.2$, ▽ $h/H^+=0.3$, ◇ $h/H^+=0.4$

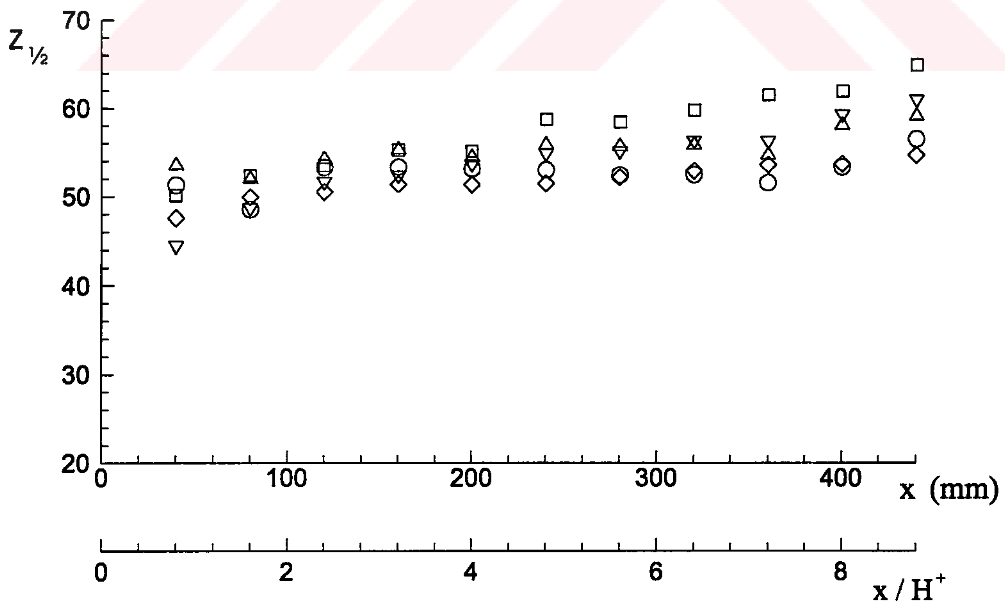

Figure 4.19 The growth of the twin jets with downstream distance in the x-z plane, ○ $h/H^+=0.1$, △ $h//H^+=0.15$, □ $h/H^+=0.2$, ▽ $h/H^+=0.3$, ◇ $h/H^+=0.4$

Jet growth rate is related with the maximum velocity decay rate of the jet. Faster decay in the maximum velocity implies higher jet spreading. Figure 4.20 shows the decays of the square of the non-dimensional maximum velocity with downstream distance. The flow field may be classified as potential core region, characteristic region and axisymmetric region. Characteristic region of jets extends up to $x/H^+ \approx 4\text{-}5$. Maximum velocity decay rate in the characteristic region is provided by the jet discharging from 5mm high nozzle. As long as the jet nozzle high increase the maximum velocity decay rate decreases.

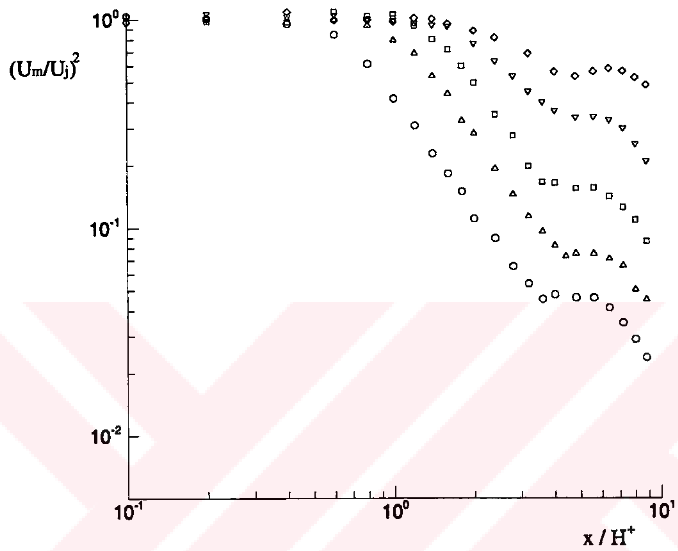

Figure 4.20 Decay of maximum velocity with downstream distances ○ $h/H^+=0.1$, △ $h//H^+=0.15$, □ $h/H^+=0.2$, ▽ $h/H^+=0.3$, ◇ $h/H^+=0.4$

The variation of the centerline velocity along the x axis, is presented in Figure 4.21. Negative velocity region indicates the recirculation region between two jets. The length of the recirculation region which is surrounded by two jets is important in practice. The extension point of recirculation region where the mean velocity is zero can be deduced from the figure. Downstream from the merging point non-dimensional centerline velocity U_c/U_j increases up to a maximum value at the combined point.

Distribution of the normalized turbulence intensity along the x axis is shown in Figure 4.22. Turbulence intensity increases with x position to a maximum near the merging point. After the merging point turbulence intensity increases again in

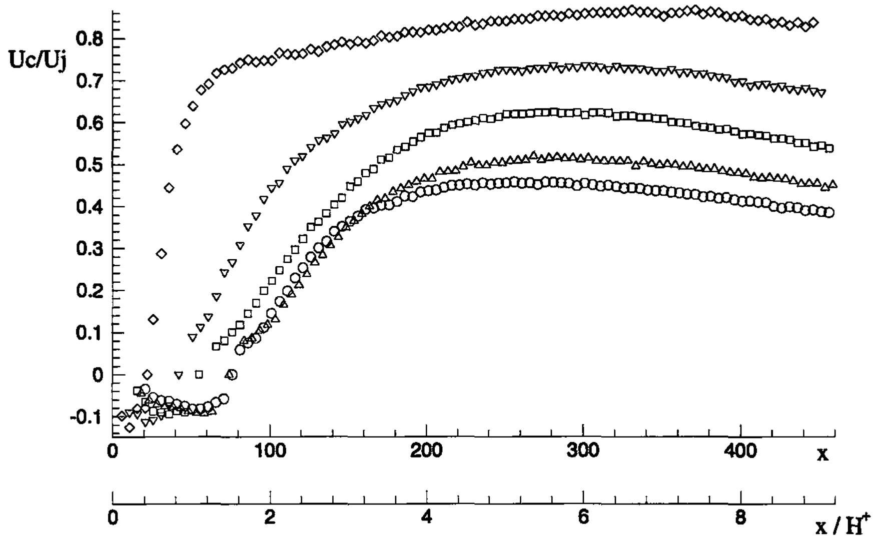

Figure 4.21 Variation of centerline velocity ○ $h/H^+=0.1$, △ $h//H^+=0.15$, □ $h/H^+=0.2$, ▽ $h/H^+=0.3$, ◇ $h/H^+=0.4$

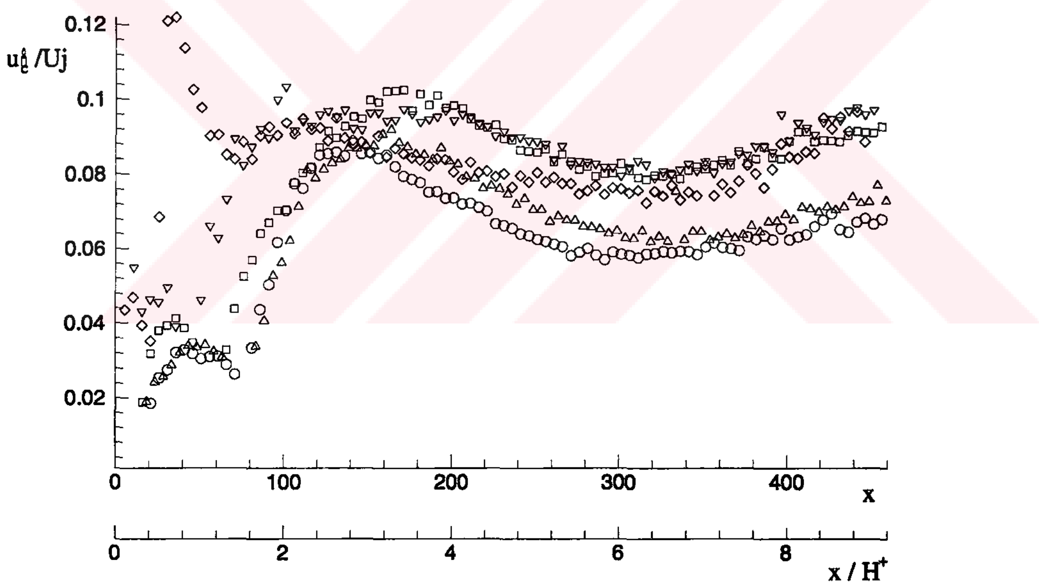

Figure 4.22 Turbulence intensities along the jet centerline ○ $h/H^+=0.1$, △ $h//H^+=0.15$, □ $h/H^+=0.2$, ▽ $h/H^+=0.3$, ◇ $h/H^+=0.4$

Figure 4.23 shows the relation between merging point X_{mp} and the nozzle spacing S. It is found that in the range $S/H^+<0.9$, the relationship between S/H^+ and X_{mp}/H^+ is linear while the relationship between S/h and X_{mp}/h, in the same domain is expressed with a power law. The position of the merging point is as follows;

$$X_{mp} / H^{+} = 3.948 S / H^{+} - 1.98$$
$$X_{mp} / h = 0.71004 (S / h)^{1.45036} \quad (4.1)$$

The position of combined point, determined from the Figure 4.21 is presented in Figure 4.24. The relation between combined point position X_{cp}/h, and jet spacing is linear;

$$X_{cp} / h = 4(S / h) + 9.62 \quad (4.2)$$

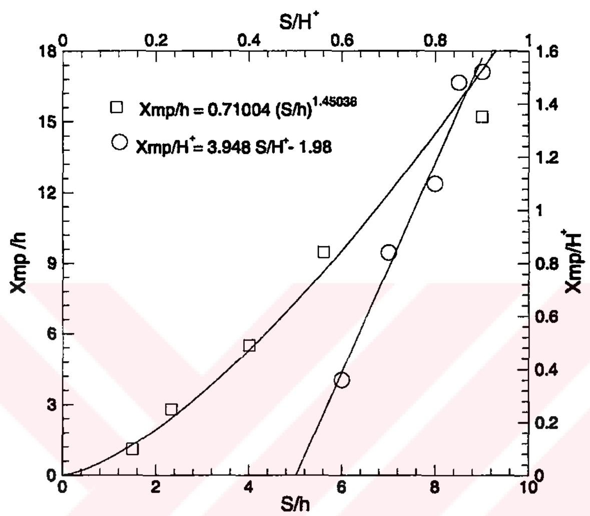

Figure 4.23 Position of merging point

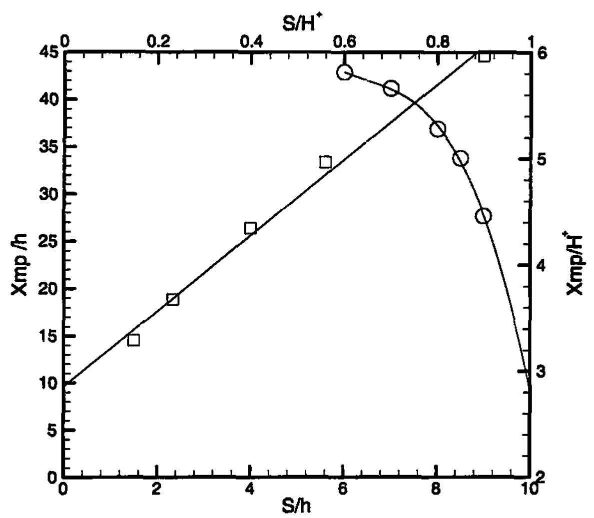

Figure 4.24 Position of combined point

As is mentioned in Chapter 2, the unique study on the interaction of plane parallel jets with small spacing ratio belongs to Nasr and Lai [68]. Two identical two dimensional jets, issuing from 10mm height nozzles were separated by 4.25 nozzle height (H^{+}=52.5mm) The effect of side plates was also investigated in this study. Side plates were placed horizontally at the top and sides of the nozzles in order to enhance the two-dimensional behavior of the flow. Experimental results of Nasr and Lai [68], are compared with the present results.

The variation of the normalized mean velocities on the x-axis (centerline velocity) is compared with the results of Nasr and Lai in Figure 4.25. When side plates are installed jets converges faster. In the absence of the side plates significant entrainment through the top and bottom sides of the jets, results in longer converging region. When the aspect ratio of the nozzles is not high enough, dominated three dimensional effects causes less curving of individual jet axis towards x-axis.

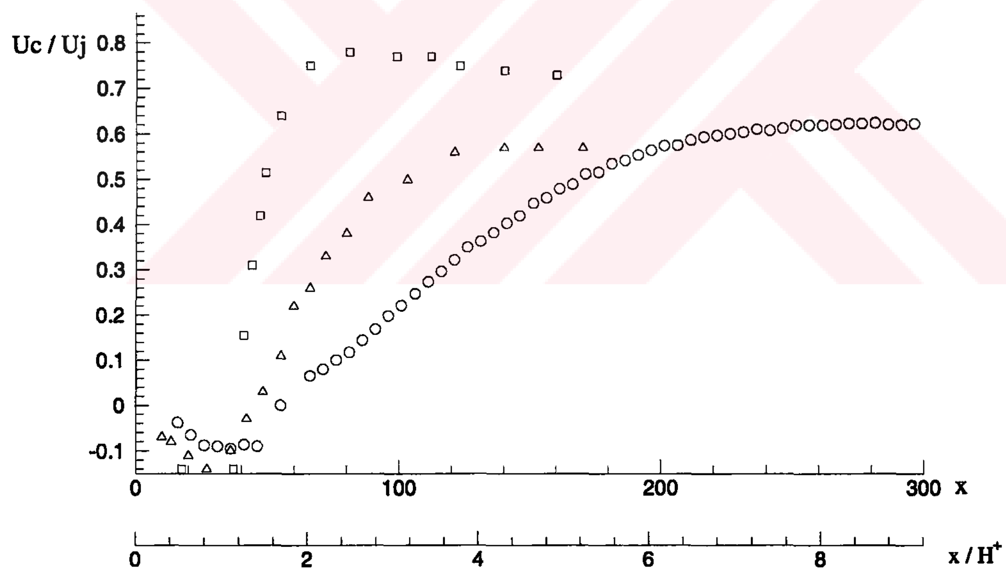

Figure 4.25 Variation of centerline velocity , ○ h=5mm, △ two-dimensional twin jet[68], □ two-dimensional twin jets with side wall[68]

Mean velocity profiles at the similar flow development stages are compared in Figure 4.26.a,b and c. Although the normalized distance consisting to the flow development stages are different, the shape of the velocity profiles at the same stages are similar.

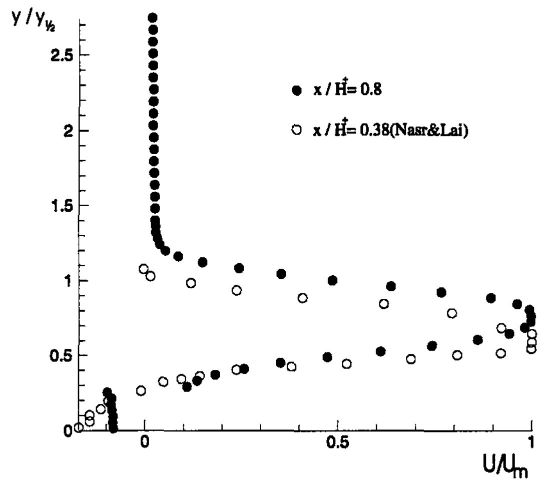

Figure 4.26.a Comparison of velocity profiles near the merging point

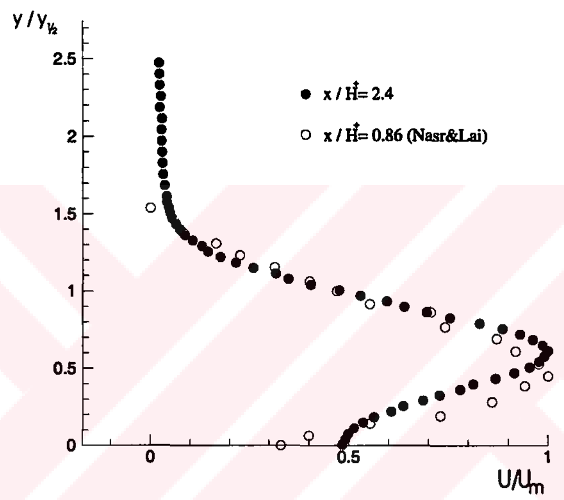

Figure 4.26.b Comparison of velocity profiles in merging region.

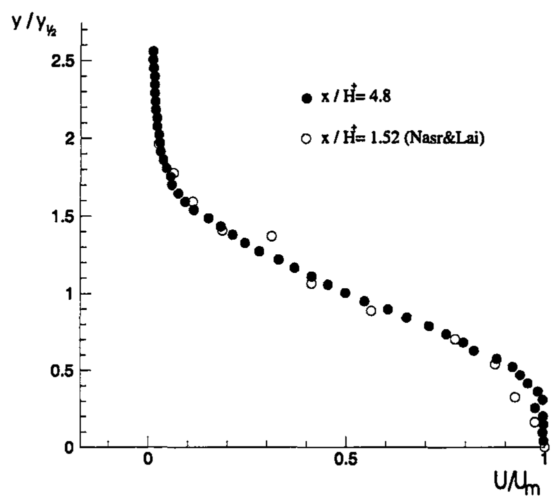

Figure 4.26.b Comparison of velocity profiles in combined region

4.4.3 Preferred Modes

Spectral measurements for five different jet exit height of twin jet configurations have been performed at constant exit velocity. Probe is moved through the mixing layer step by step until it reaches constant passage frequency. At each step, peak values of the recorded spectrum are plotted against the probe position for 10 mm high twin jet case in Figure 4.27. Similar results are obtained for all twin jet configurations. The frequency variation shows a staging behavior with downstream distance. The initial peak frequency is halved twice with increasing downstream location. These stages correspond to two successive pairing process.

Vortex merging positions and number of vortex interactions can easily be detected from the figure. The lowest frequency which has been detected near the end of the potential core is preferred mode of the jet. Termination of vortex pairing usually indicates the end of the potential core of a single jet. A vortex pairing process would terminate when the mixing layer is confined [77].

Strouhal number St_θ based on the mixing layer momentum thickness is obtained for the initial frequencies near the nozzle exit. The axial location and Strouhal numbers of initial vortex formations are listed in Table 4.2. In the present study, the most amplified frequency was measured inside the shear layer at a distance of x/H^+=0.2-0.3 from the nozzle.

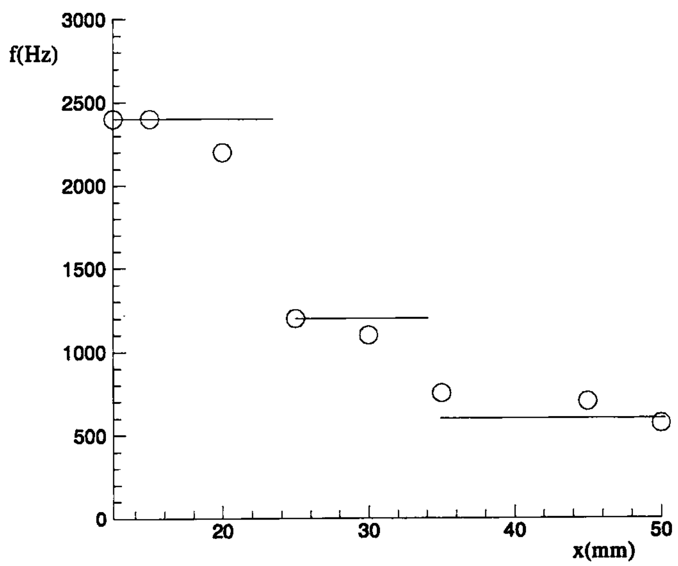

Figure 4.27 Variation of the most amplified frequency with the downstream distance

At the end of the potential core a preferred frequency corresponding to the passage frequency of the dominant vortical structures can be detected. Figure 4.28 shows a typical spectral distribution of velocity fluctuations near the end of the potential core. The most amplified frequency can easily be identified as the peak frequency in the spectrum. Consisting Strouhal numbers based on the jet exit high of preferred mode of jets are given in Table 4.2.

Table 4.2 The initial Strouhal number and preferred modes of twin jets

jet configuration	Re_h	St_θ ($=f_0\theta_0/U_j$)	St_h
h=5 mm	10067	0.012	0.245
h=7.5 mm	15100	0.011	0.185
h=10 mm	20135	0.0092	0.2
h=15 mm	30200	0.0119	0.2
h=20 mm	40270	0.0117	0.25

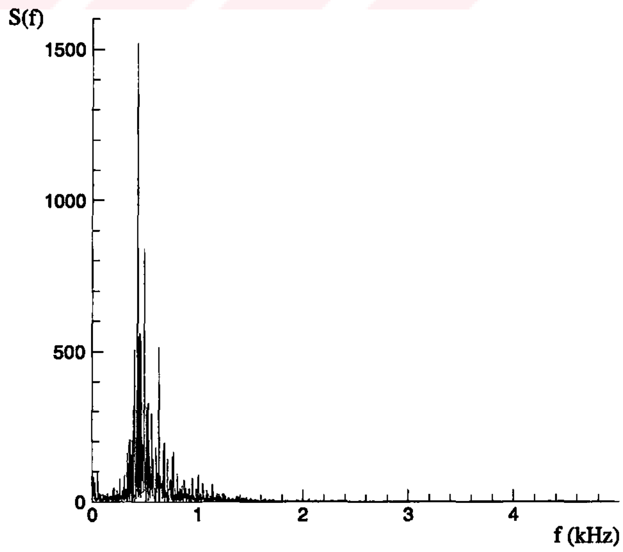

Figure 4.28 Spectral distribution near the end of the potential core.

4.5 Comparison of Flow Characteristics of Twin and Offset Jets

Twin jet and offset jet flow characteristics issuing from identical rectangular nozzles are compared in this study. The symmetry plane that exists between two parallel jets is replaced with a solid wall in order to obtain an offset jet. In this manner, identical initial conditions are provided for two flow structure. Schematic of offset jet flow was given in Figure 2.11.

Offset jet discharged from a 5mm high and 100mm long rectangular nozzle with mean streamwise velocity of 30m/s is investigated. The plate was made of 10mm Plexiglas and placed at a 22.5mm distance from the centerline of the nozzle exit, thus yielding an offset ratio of 4.5.

Spatial development of normalized velocity and turbulence intensity profiles are given in Appendix C. The air entrainment through the jet boundaries reduces jet pressure in the region between the jet and the wall. This sub atmospheric region forces the jet to deflect towards the wall and to attach on it. The reattachment point of the jet corresponds to the merging point of the twin jet. In the reattachment region the flow is subjected to strong interaction with the wall. Far downstream, flow forms a wall jet. The inner layer of the wall jet is similar to that of turbulent boundary layer, while the outer layer resembles of a free jet.

Velocity profiles of the offset jet are compared with that of the identical twin jet in Figure 4.29. In the recirculation region ($x/H^+=0.8$) velocity profiles agree well. Although the flow behaviors are similar, flow reversal occurs at a slightly downstream position for the offset jet. In the reattachment region (or merging region) ($x/H^+=1.6$-4.0) the offset jet is subjected to strong interactions with the wall. The wall effect retards the flow. Hence, twin jet merges slightly faster than the offset jet in merging region. The wall effect can be better observed from the turbulence intensity profiles (Figure 4.30). However, near the combined point, profiles of the two flow field are identical ($x/H^+=4.8$). At downstream positions, the flow in the free jet region of twin jet, having broader velocity profiles than that of offset jet, grows faster ($x/H^+=5.6$-6.4).

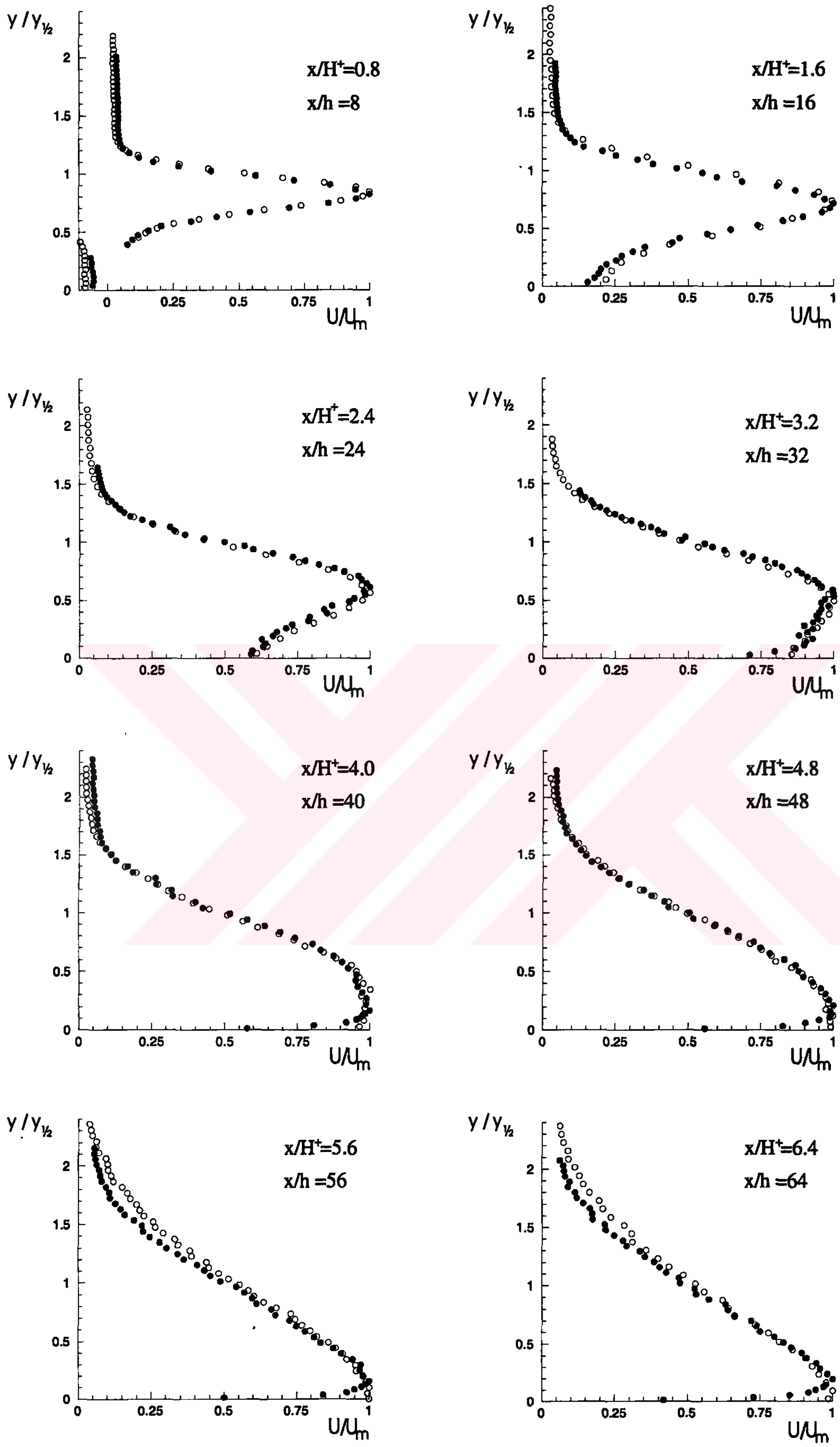

Figure 4.29 Velocity profiles of ○ twin jet and ● offset jet

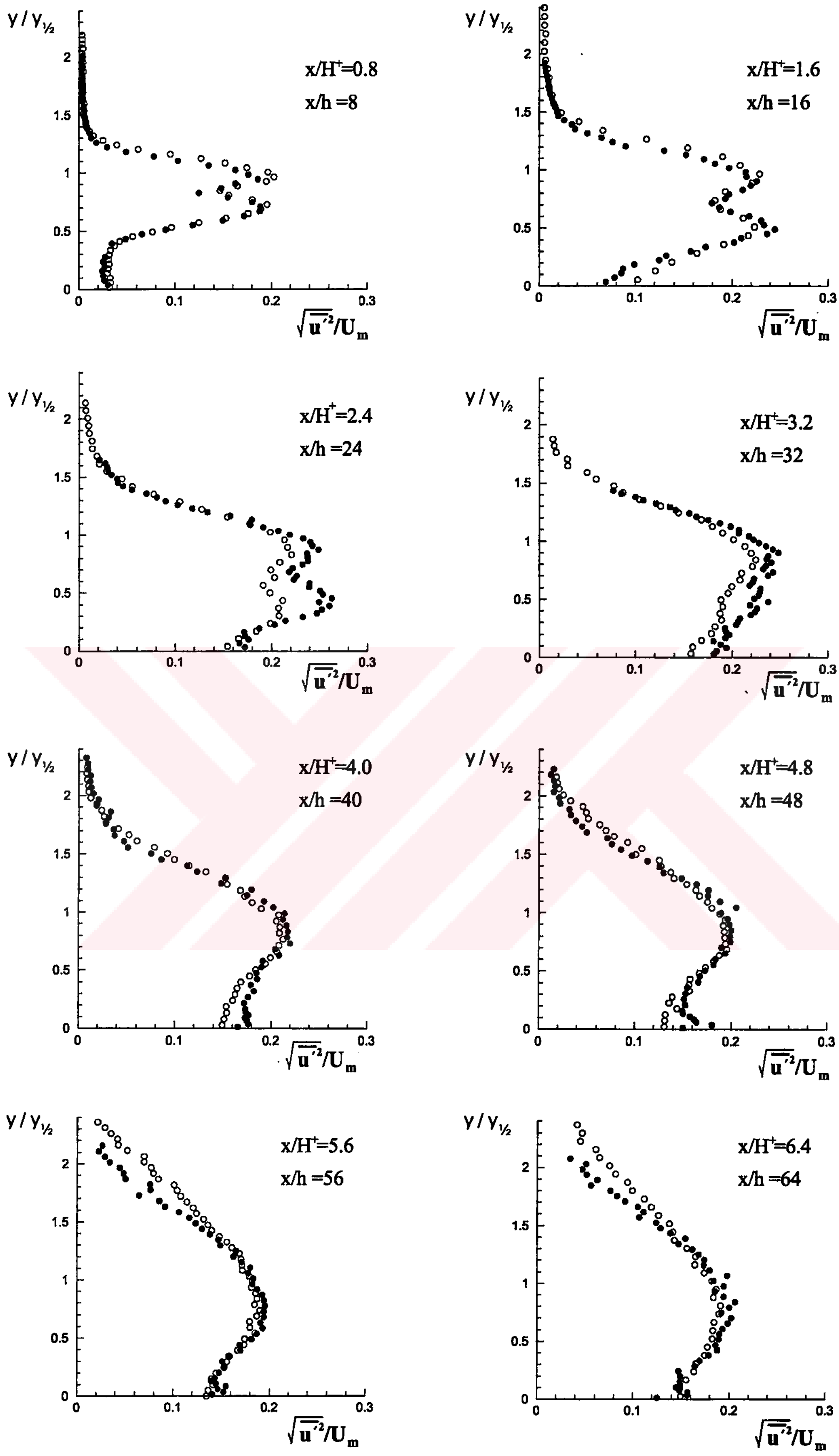

Figure 4.30 Turbulence intensity profiles of ○ twin jet and ● offset jet

Spreading rates of jets are plotted against the x distance from the nozzle exit plane, in Figure 4.31. Both twin and offset jet grow linearly with the downstream distance after combined point x/H^+~4.4. Additional momentum loses near wall region of the offset jet may cause lower spreading rates. The location of the virtual origin in the redeveloping free jet flow of the twin jet configuration, approaches to the nozzle exit plane.

The decay of the maximum velocity of the offset jet and twin jet are displayed in logarithmic scales in Figure 4.32. The maximum axial velocity before reattachment point decays nearly at the same rate. However, after the reattachment point smaller U_m/U_c values for offset jet flow are clearly seen. The maximum velocity decay after impingement region (or merging region), both in the wall jet region of the offset jet and in the free jet region of twin jet, give linear curves.

To investigate the existence of similarity at far downstream, the mean non-dimensional velocity profiles are compared in Figure 4.33. The profiles in the wall jet region becomes similar at downstream positions greater than $5.6H^+$(or 56h). Turbulence intensity profiles are also attained their self similarity at this downstream location (Figure 4.34). This result is similar to that of identical twin jet.

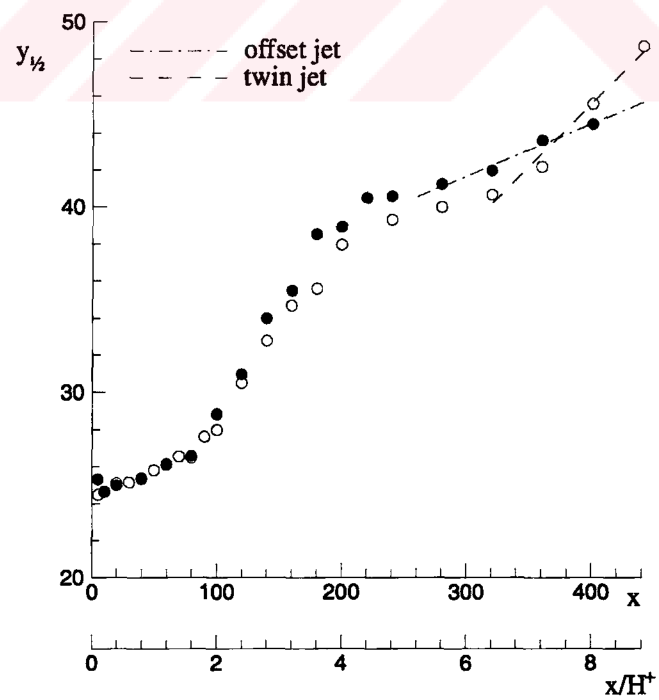

Figure 4.31 Spreading rates of the offset(●) and the twin jet(○)

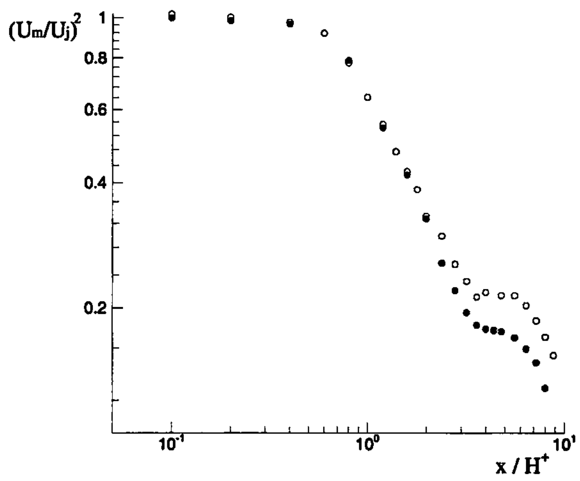

Figure 4.32 Maximum velocity decay of the offset jet(●) and the twin jet(○).

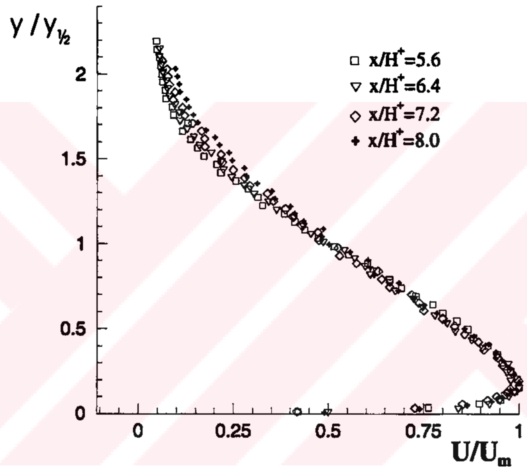

Figure 4.33 Non dimensional velocity profiles in wall jet region

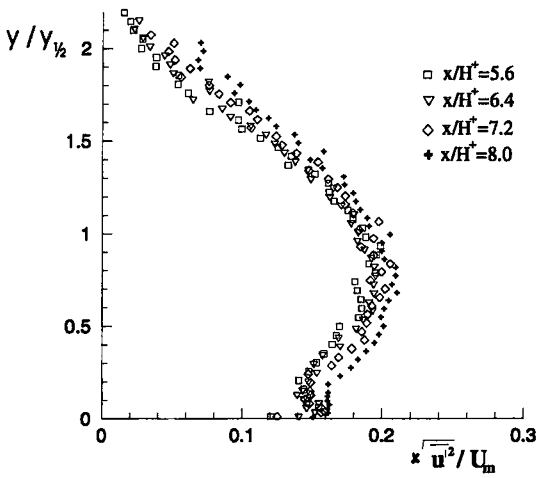

Figure 4.34 Turbulence intensity profiles in wall jet region

4.6 Convex Surface Between Jets at Exit

The turbulence is very sensitive to small amounts of curvature of mean streamlines. This, in turn, affects the development of the mean flow [100]. Turbulence may be nearly eliminated on highly convex surfaces, while on highly concave surface momentum transfer by quasi-steady longitudinal vortices dominates the ordinary turbulence processes [88].

In this part of the study, the effect of a cylindrical convex body placed between two jets on the flow development is investigated. A half cylinder is inserted between two slots as sketched in Figure 4.35 for all twin jet configurations.

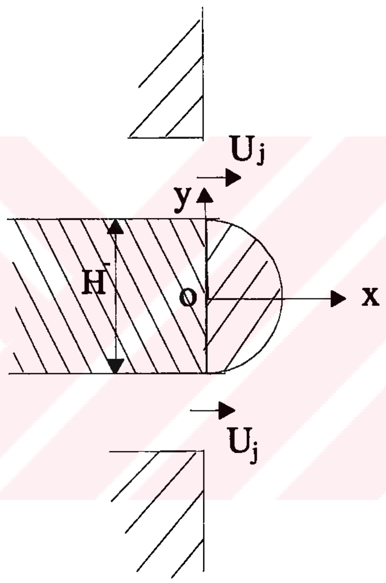

Figure 4.35 Nozzle exit configuration

Velocity and turbulence intensity profiles are compared with the previous twin jet measurements in order to examine the convex surface effects (Figure 4.36-4.40).

The surface curvature parameter is defined as the ratio of the jet width to the surface radius (R). The flow characteristics of the convex wall jets have been studied extensively by many researchers[89,90-92,95,96]. These studies represents the effects of mild convex curvature where the half width of the jet is much smaller than the surface radius. Surface curvature between twin jets may be classified as strong convex curvature in the present study. The jet spreads and the levels of Reynolds

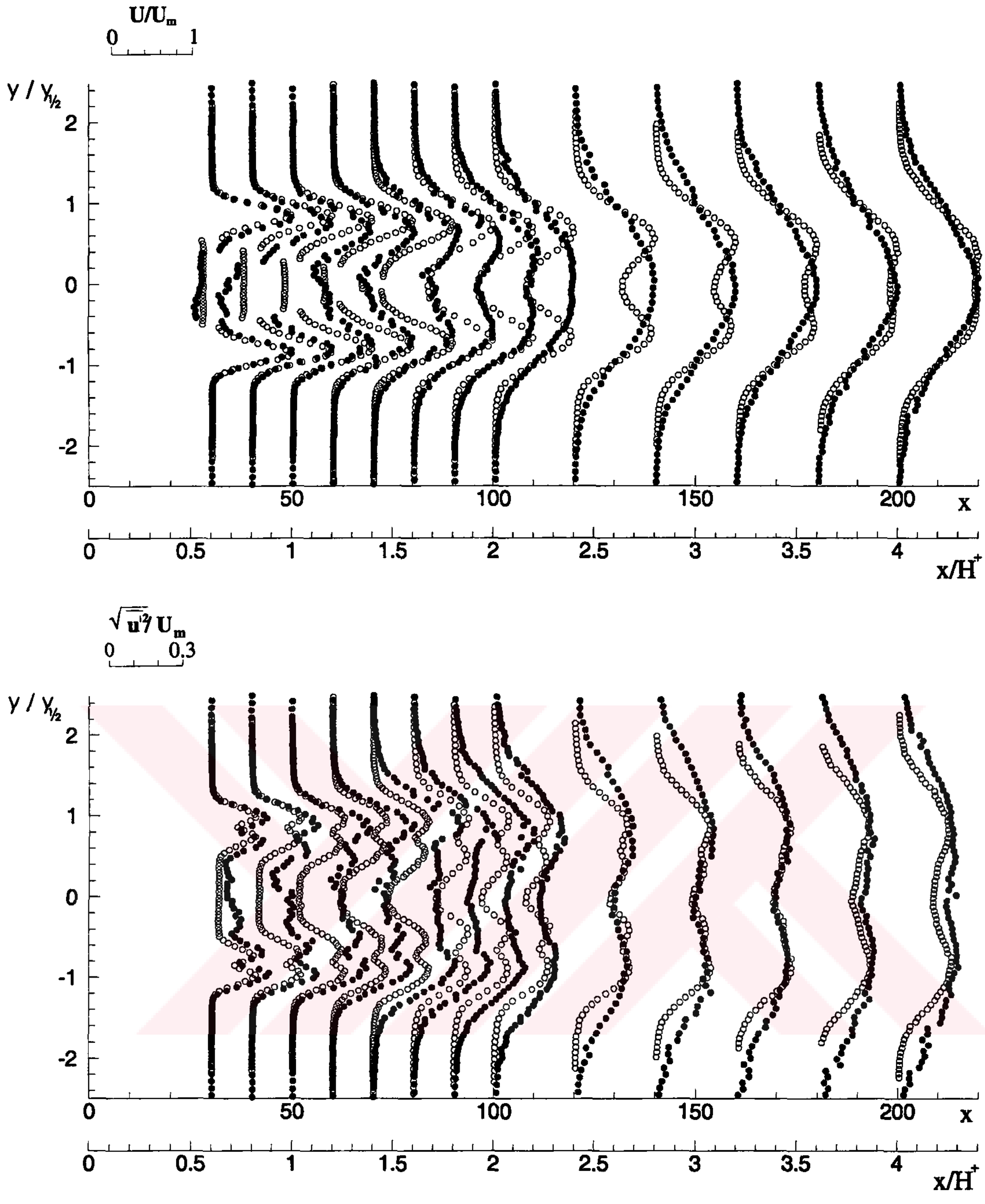

Figure 4.36 Comparison of the twin jet velocity and turbulence intensity profiles with (●) and without (○) the convex body between jets (for h=5 mm case).

stresses on strong convex wall increase significantly as the wall jets develop along the surfaces[101]. The convex surface effects can easily be observed from the Figure 4.36. The jets issued tangentially to the cylindrical surface, do not collide to the surface as a wall jet, but approach to it by the Coanda effect. At a certain distance from the nozzle exit they interact with each other and coalesce in to a single free jet. Figure 4.36 presents the profiles in downstream positions from the solid

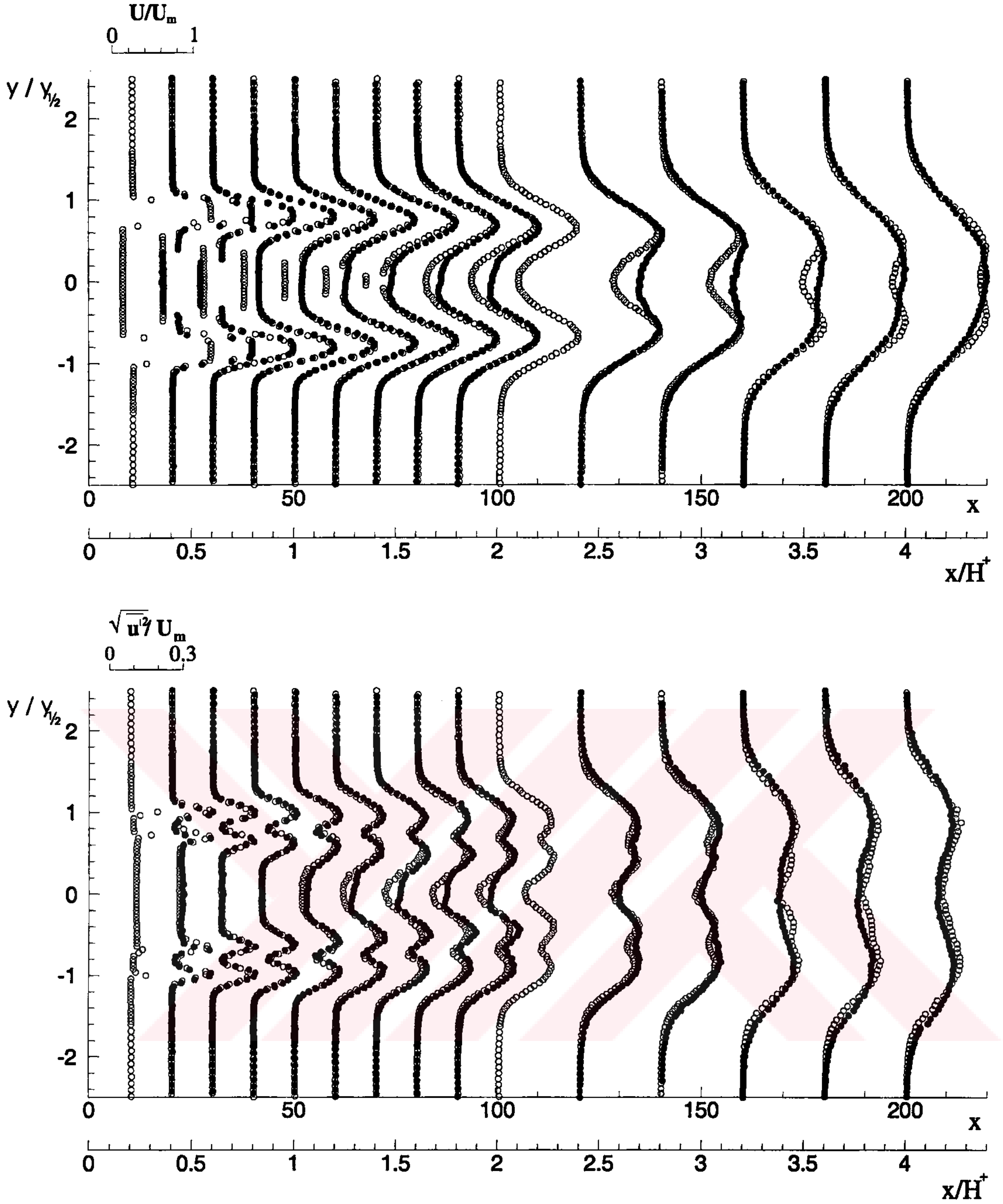

Figure 4.37 Comparison of the twin jet velocity and turbulence intensity profiles with(●) and without(○)the convex body between jets(for h=7.5 mm case)

surface. It is obvious that the existence of the convex surface make the recirculation region shorter. Thus merging point moves to upstream positions. Merging process of jets results in the coalescence of two jets at upstream positions from the combined point of twin jets (without convex surface) . Therefore, the effect of such a convex surface between two jets, can be explained as follows; A convex surface deflects the jets towards the symmetry axis more strongly and accelerates the flow development procedure.

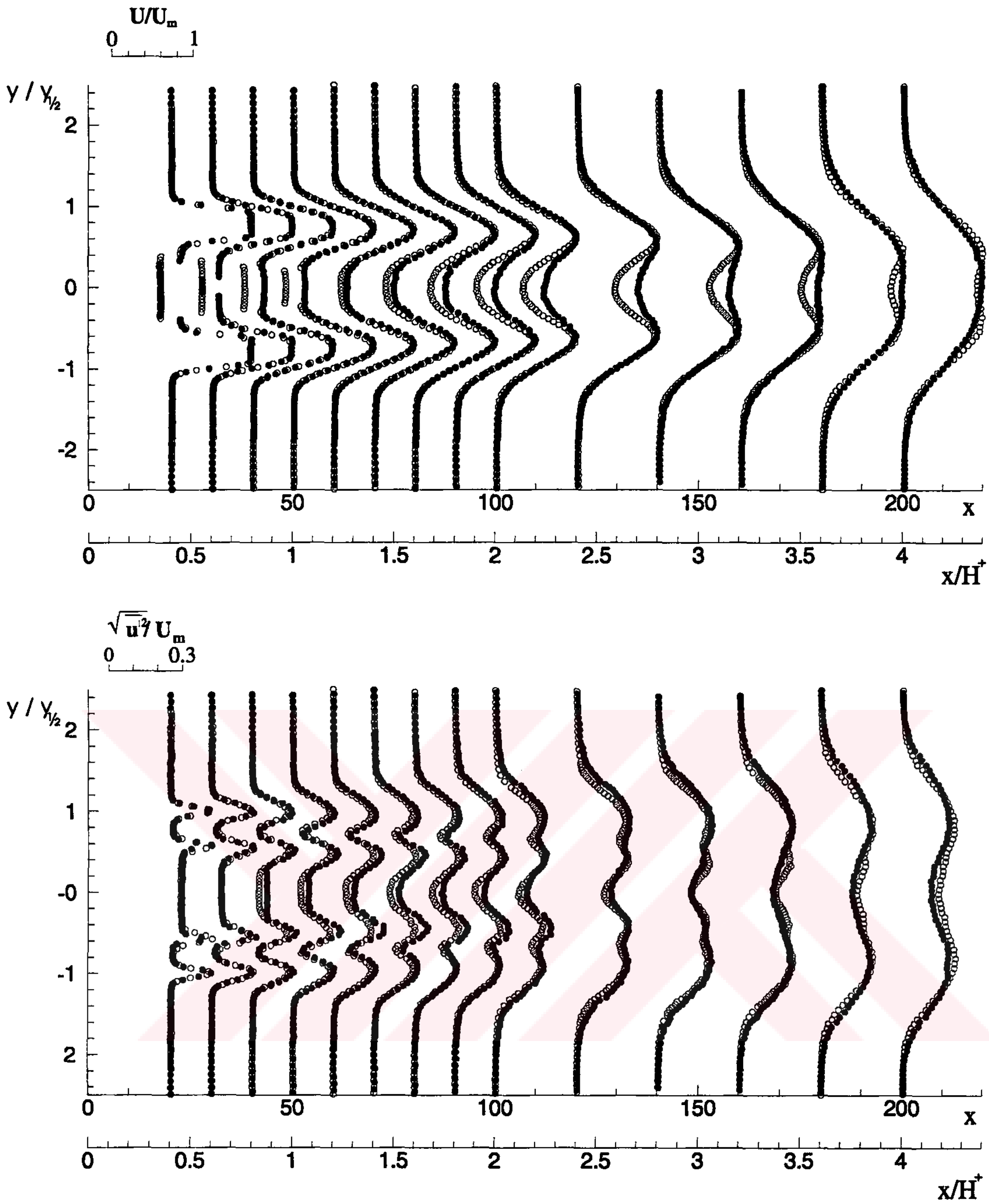

Figure 4.38 Comparison of the twin jet velocity and turbulence intensity profiles with (●) and without(○)the convex body between jets (for h=10 mm case).

Comparison of the turbulence intensity profiles of h=5mm case indicates higher values for twin jet with convex surface(TJCS) configuration. The appearance of saddle back shaped turbulence profiles indicating the single free jet flow, is clearly observed near the combined point of the TJCS, located about x/H$^+$~2.2.

The increasing surface curvature parameter does not give rise to stronger deflection

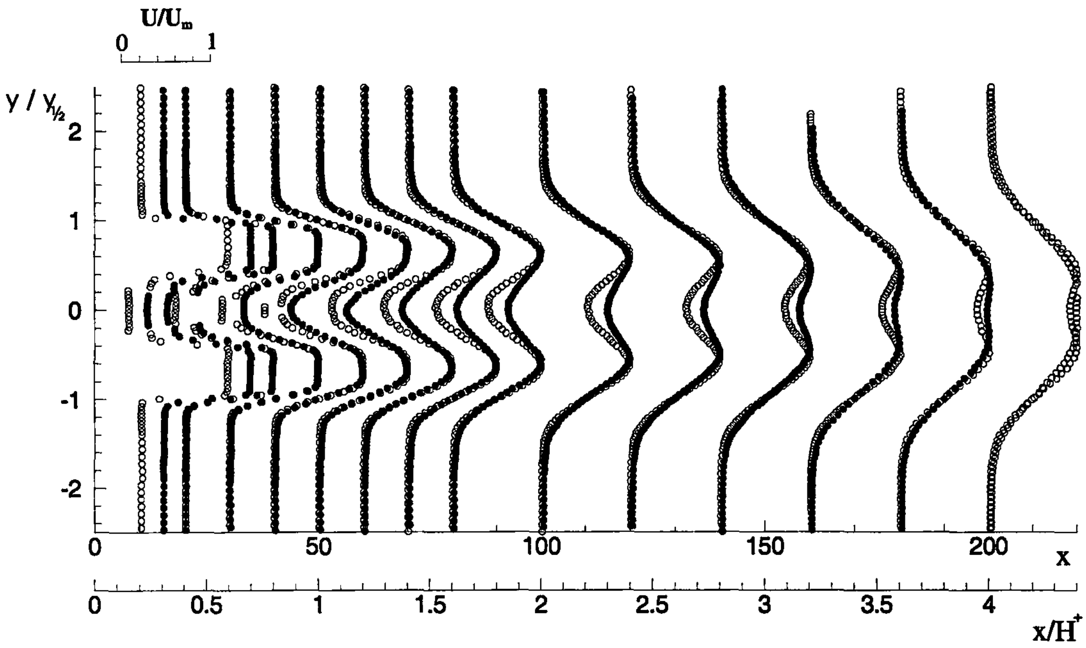

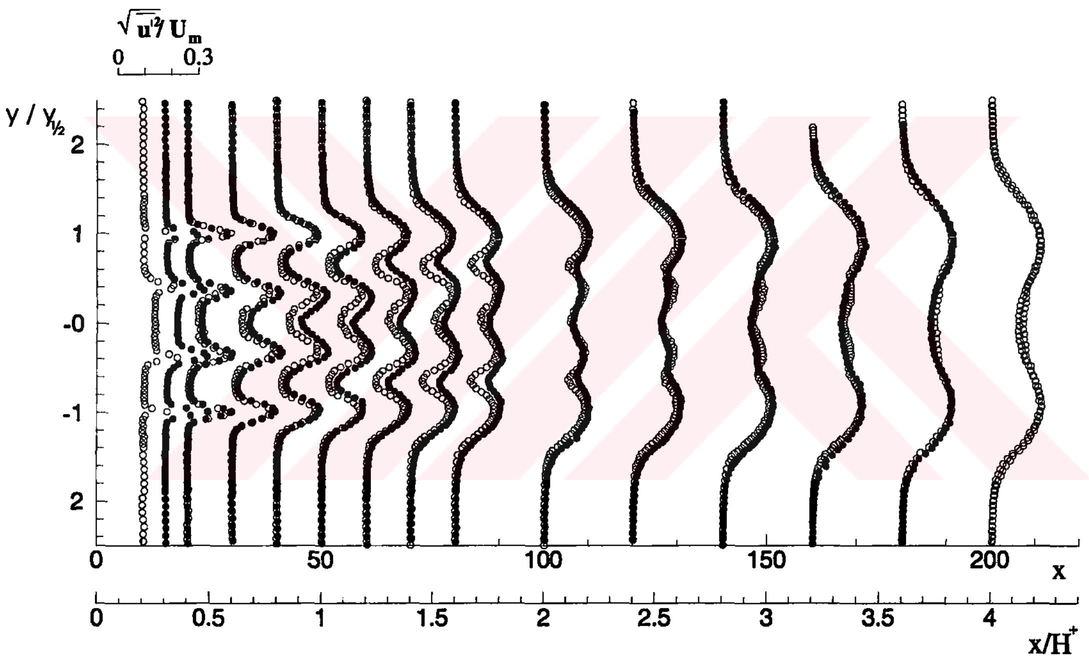

Figure 4.39 Comparison of the twin jet velocity and turbulence intensity profiles with(●) and without(○)the convex body between jets (for h=15mm case)

effects. Contrarily, for the highest curvature parameter flow structures seem to be unaffected. Flow structure is altered strongly by the highest curvature radius R=22.5mm. As the curvature radius diminishes, the influence of the surface curvature on the flow field is vanished.

To investigate the influence of the surface curvature on jet growth rates, jet half widths versus downstream positions are plotted in Figure 4.41. Even though the jet

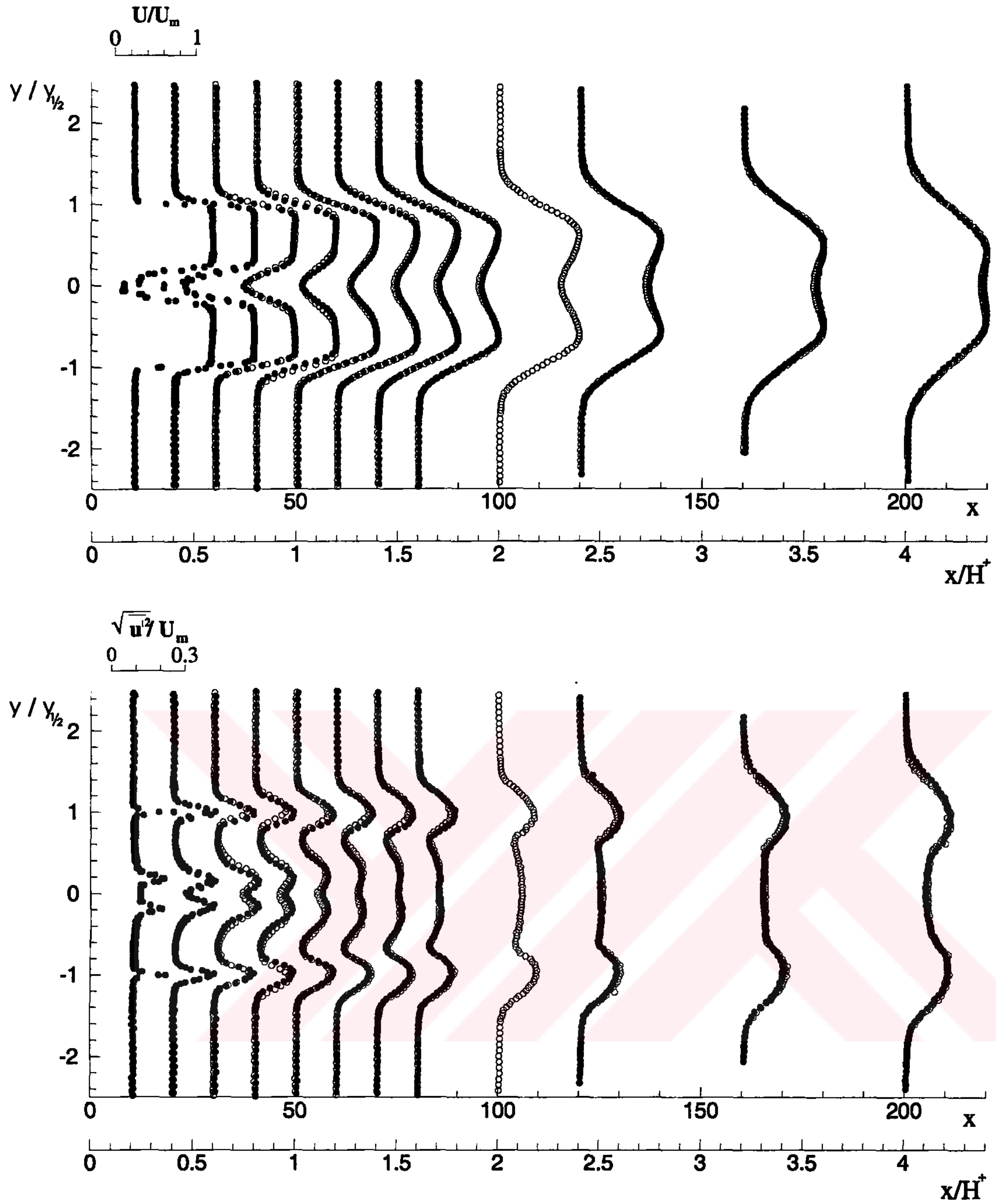

Figure 4.40 Comparison of the twin jet velocity and turbulence intensity profiles with(●) and without(○)the convex body between jets (for h=20 mm case).

half width values decreases in near field of the TJSC, after the combined point, in the single free jet region the TJSC flow grows faster especially for h=5, 7.5 and 10mm cases. As a consequence, the flow reaches higher half width values at far downstream positions. It should be noted that for all cases, jets grow linearly with the downstream distance after the combined point.

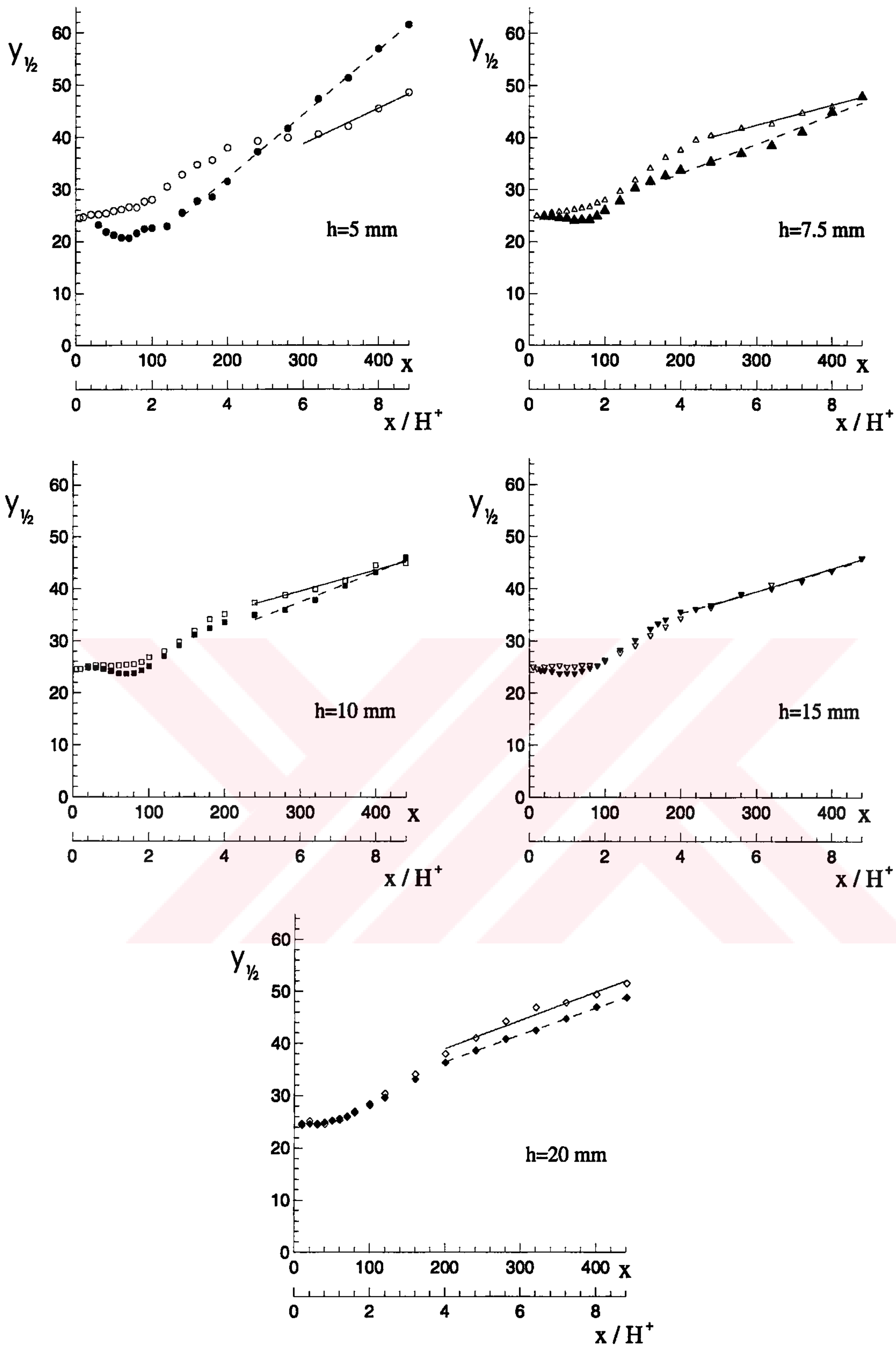

Figure 4.41 Jet spreading rates of twin jets with (●,▲,■,▼,◆) and without (○,△,□,▽,◇) convex surface

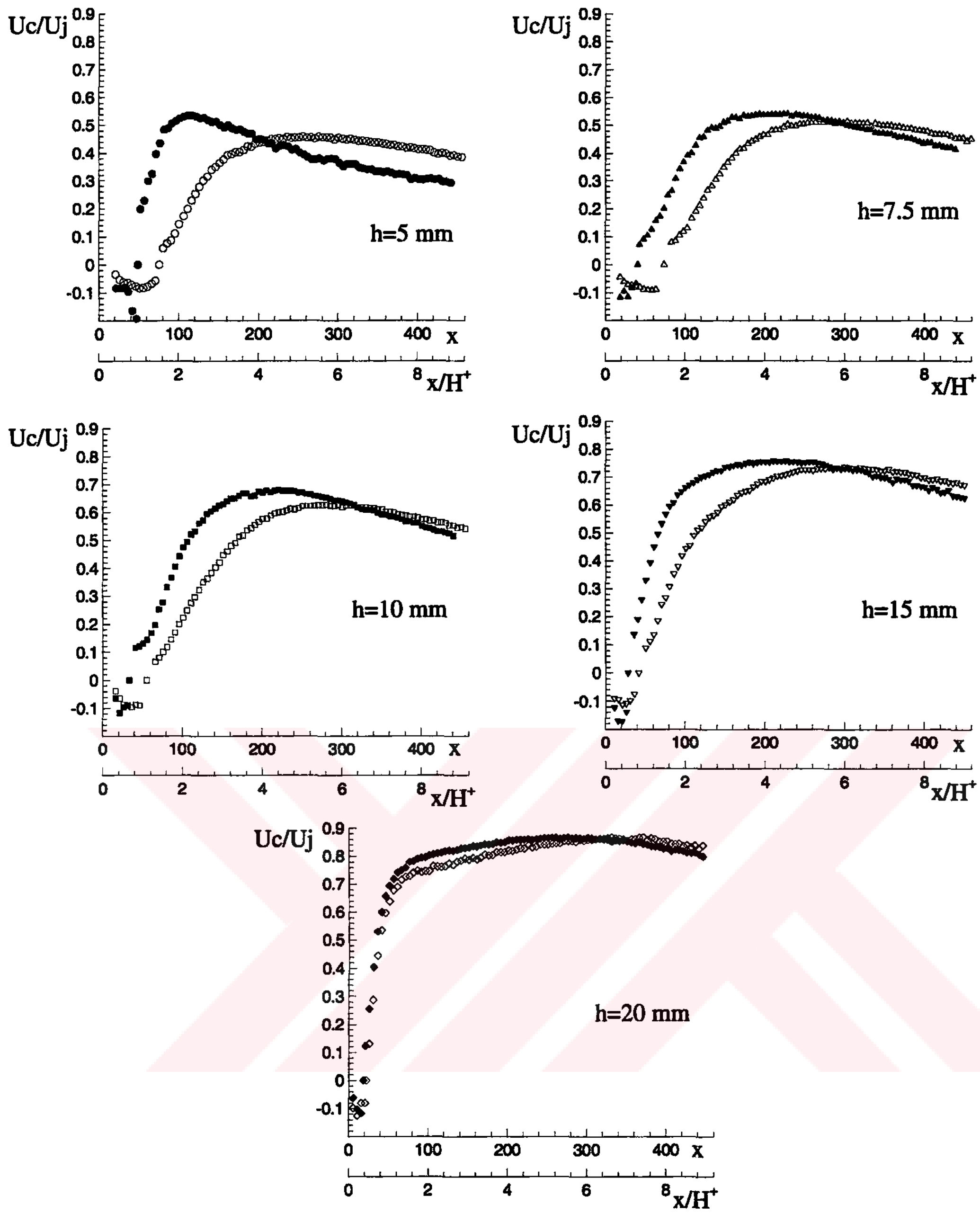

Figure 4.42 Jet centerline velocities of twin jets with (●,▲,■,▼,◆) and without (○,△,□,▽,◇) convex surface

The variation of centerline velocities are represented in Figure 4.42. The influence of the convex surface on the length of recirculation region can easily be noticed from the figure. Centerline velocity curves are shifted upstream by the convex surface effect. For that reason, the position of the maximum velocity which indicates combined point is also shifted. Furthermore, the maximum velocity on the symmetry axis is slightly increased. After the combined point centerline velocity decreases rapidly due to high spreading rates of the TJSC flow.

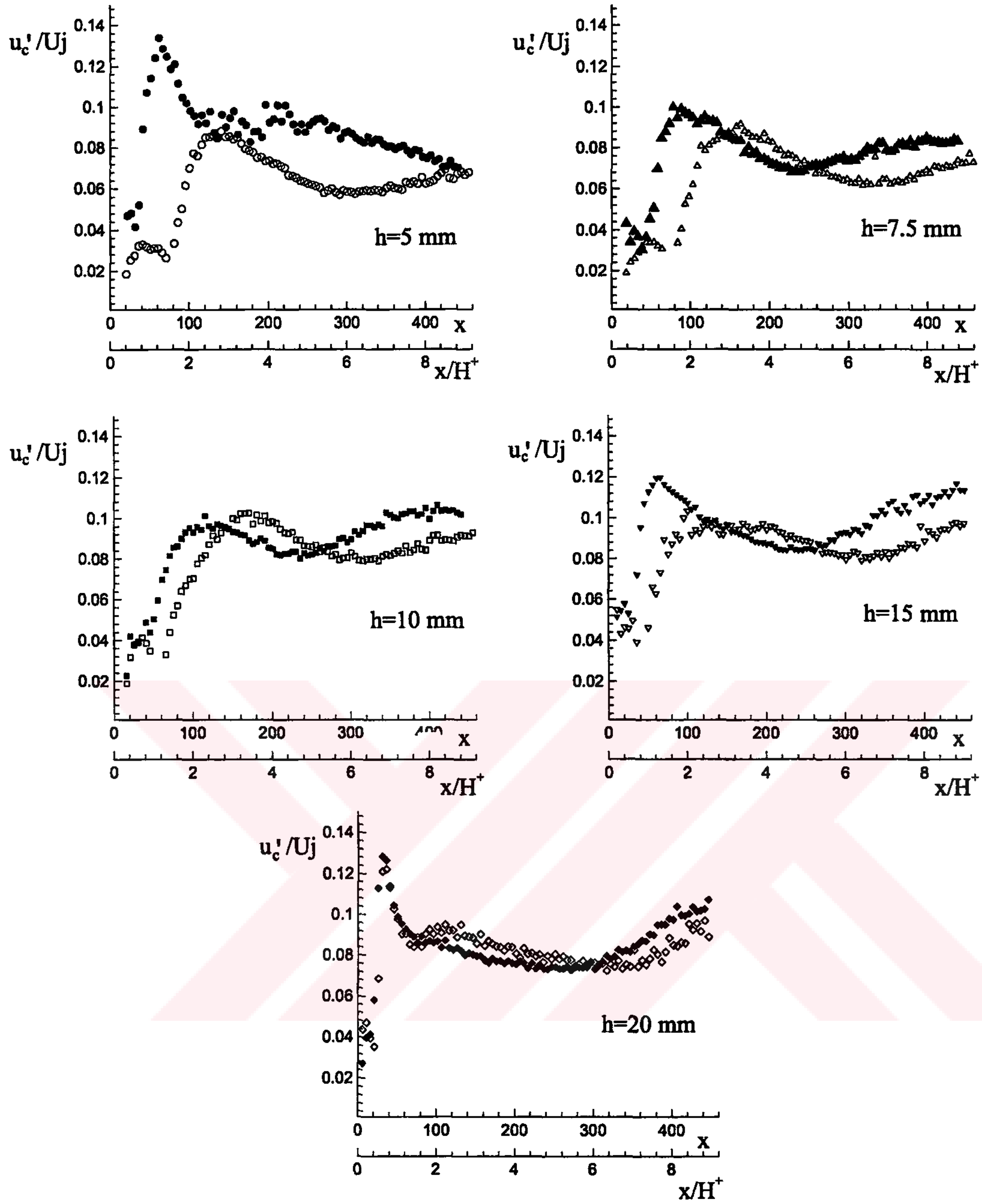

Figure 4.43 Jet centerline turbulence intensities of twin jets with (●,▲,■,▼,◆) and without (○,△,□,▽,◇) convex surface

Turbulence intensity variations along the x axis are presented in Figure 4.43. Similar shifted curves are observed for TJSC flow. Turbulence intensities are in the same magnitude except for the h=5mm case. Higher values obtained just after the merging point may be attributed to the strong interaction between the jets.

Merging and combined point locations are determined and compared with previous twin jet results in Figure 4.44 and 4.45 respectively. The equation between merging point locations X_{mp}/h and nozzle spacing S/h of the TJSC flow obeys again the power law. However the coefficients of the equation are different. The position of combined points does not follow the linear curve after S/h=4.

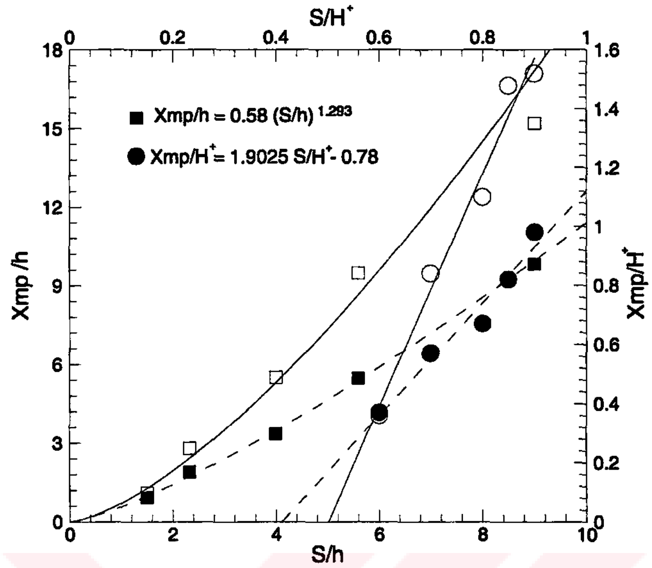

Figure 4.44 Merging point locations of twin jets with (●,■) and without (○, □) convex surface

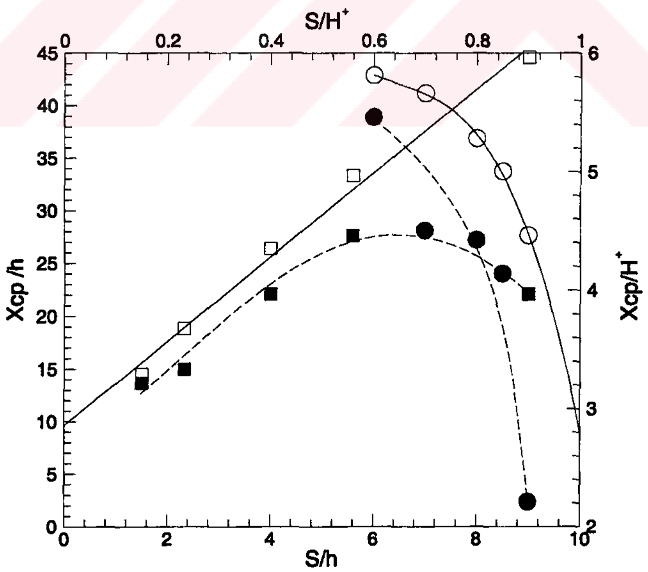

Figure 4.45 Combined point locations of twin jets with (●,■) and without (○, □) convex surface

4.7 Twin Jet Impingement

The impingement of two rectangular unventilated jets on a plane surface is investigated.

Flow field is of particular interest in the design of efficient VTOL aircraft. The flow field of two impinging parallel jets is classified into two types: Near field and far field flows[46]. Far field flows are encountered when the jets are placed close enough and when the jets are sufficiently far from the ground. Near field flows are encountered when the jets are placed far enough apart. Two jets impinging on the plate exhibit wall jet behaviors on the plate. The collision of the wall jets originates an upwash flow between the jets which affects the forces and moments induced on the aircraft when operating in ground effect. This study can be classified as a far field flow since the jets are placed very close.

Twin jet impingement experiments were carried out for three different nozzle to plate distances (Y). Non-dimensional nozzle to plate distances were $Y/H^{+}=2$, 4 and 8. Experimental parameters are listed in Table 4.3.

Table 4.3 Experimental parameters of twin jet impingement

	nozzle high (mm)	$Y/H^{+}=2$	$Y/H^{+}=4$	$Y/H^{+}=8$
without	5	X	X	X
convex	10			X
surface	20			X
with	5			X
convex	10			X
surface	20			X

Experimental results are compared with the flow visualizations obtained by the oil-film method.

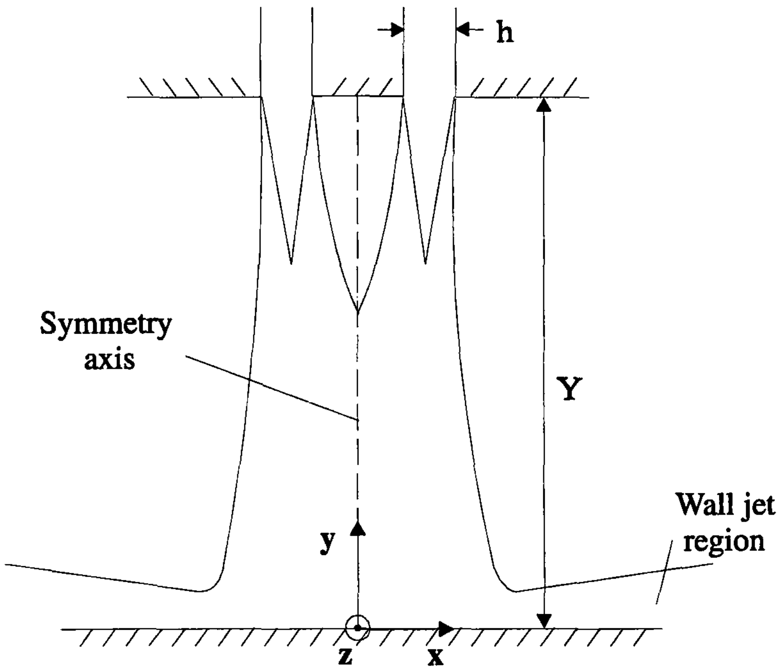

Figure 4.46 Cartesian coordinate system

Cartesian coordinate system used in jet impingement experiments is shown in Figure 4.46.

The velocity and turbulence profiles on the surface are presented in Figure 4.47 and 4.48 respectively, for jet nozzle exit high h=5mm case. Experiments are carried out for three different distances from nozzle to plate. For all three cases the converging process is terminated and merging point takes place before the impingement. For the first case ($Y/H^+=2$), jets are not combined yet. Hence, the flow impinging on the surface still retains its twin jet properties. For the second case ($Y/H^+=4$), plate position is very close to the combined point. Combining process has been terminated however the single jet has not yet been achieved its self similarity. For the third case ($Y/H^+=8$), self similarity has been reached and flow has been attained its final state before the impingement.

Figure 4.47 shows the development of the velocity profiles along the x-axis. As can be seen from the figure, jet half width $y_{1/2}$ approaches to the wall with increasing x distance from the origin up to the position where the wall jet region starts. Jet widths are plotted against to downstream distance x in Figure 4.49. Maximum velocities also accelerates near the impingement region and then shows a slowing down

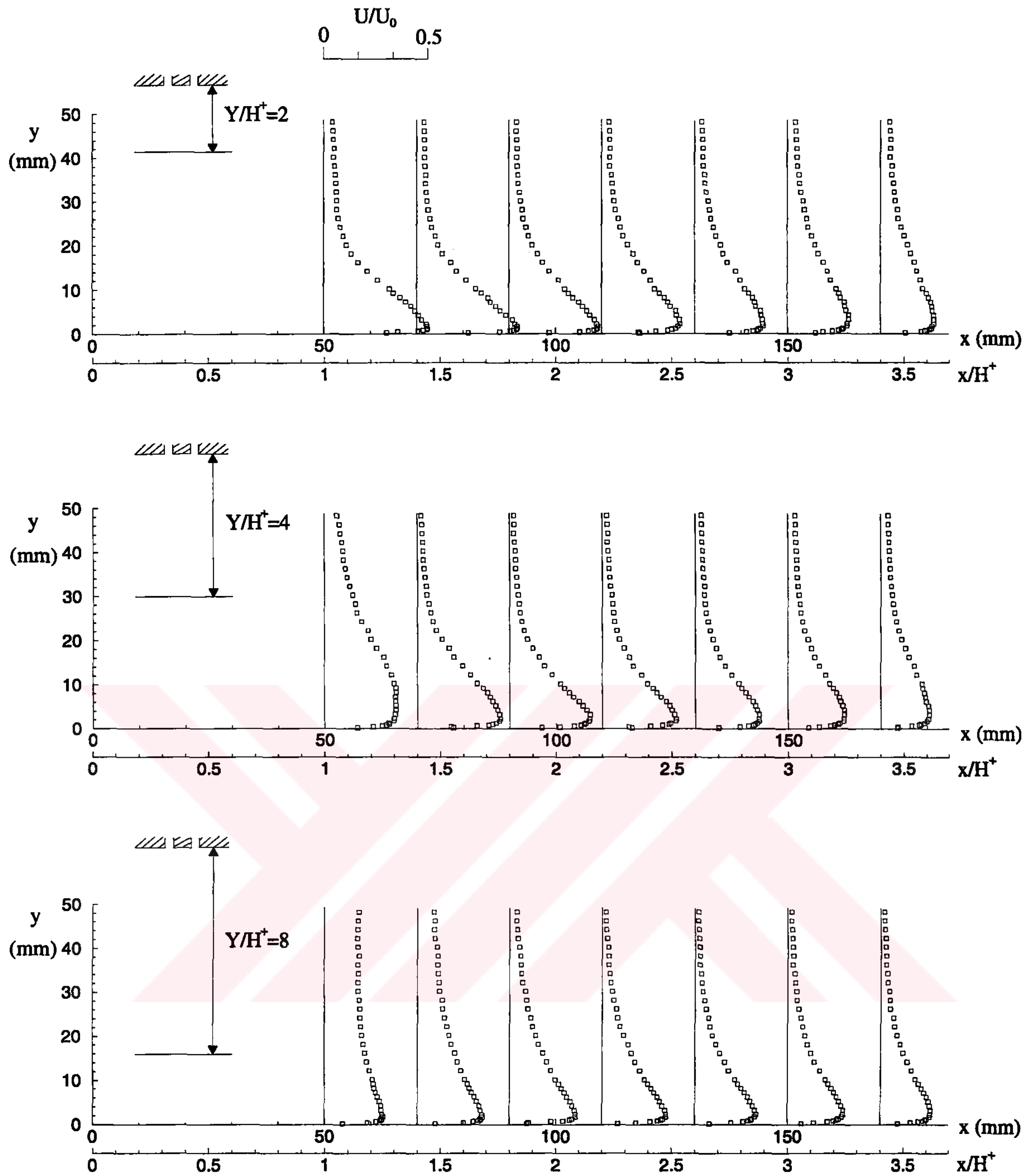

Figure 4.47 Velocity profiles on the impingement plate (h=5mm)

characteristic in the wall jet region. It should also be noted that, as the nozzle to plate distance increased maximum velocity values decrease.

Development of the turbulence intensity profiles along the x axis are presented in Figure 4.48. Maximum turbulence intensities (outer peak values) decrease with increasing nozzle to plate distance Y/H^+. In addition, as the downstream distance augments, the outer peak value becomes higher than the near-wall peak value.

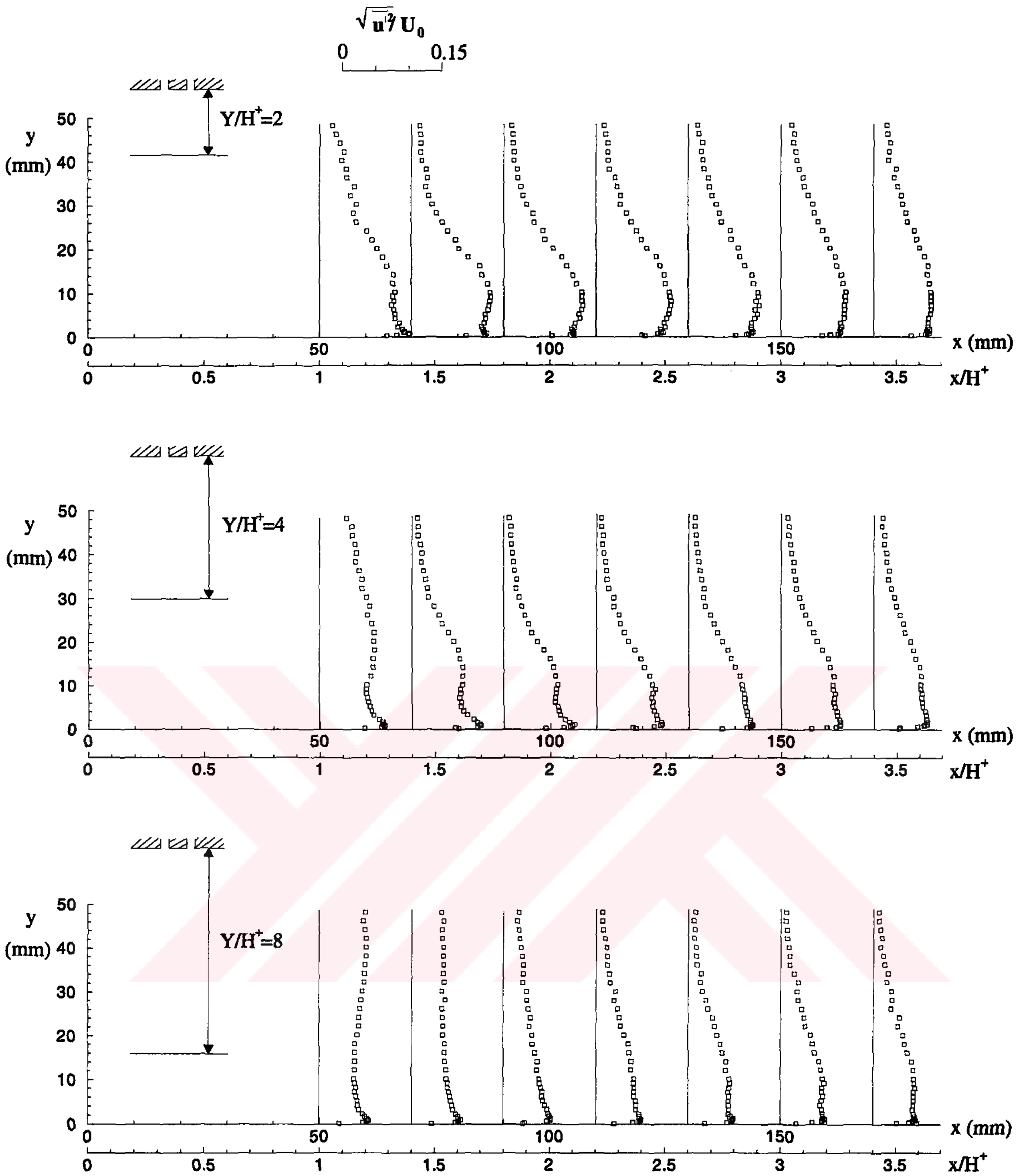

Figure 4.48 Turbulence intensities on the impingement plate (h=5mm)

Development of turbulence profiles show that the nozzle to plate distance act upon the evolution of the wall jet. This result is due to the broader free jet boundaries impinging on the surface, in the case of higher nozzle to plate distances.

Non-dimensional velocity and turbulence profiles of the wall jet region, are plotted in Figure 4.50 and 4.51. Normalized velocity profiles are similar after $x/H^+=1.0$ for nozzle to plate distances $Y/H^+=2$ and $Y/H^+=4$. Nevertheless, when the plate position is $Y/H^{+}=8$, normalized velocity profiles are reached self similarity at $x/H^{+}=1.8$. This result is consistent with Figure 4.49.

Non dimensional turbulence intensity profiles exhibit different maximum values in the wall region (Figure 4.51). With increasing distance turbulence profiles approaches to self-similar profiles.

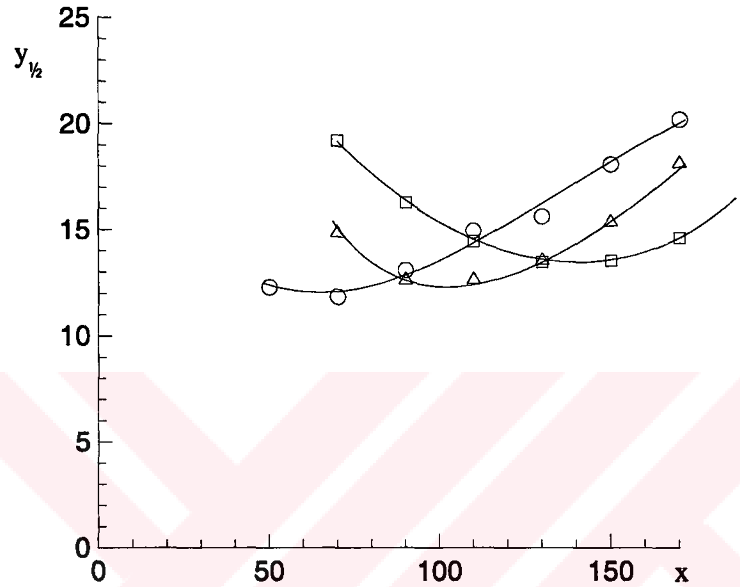

Figure 4.49 Jet growth on the impingement plate ($Y/H^{+}=2$(○),$Y/H^{+}=4$(△), $Y/H^{+}=8$(□)).

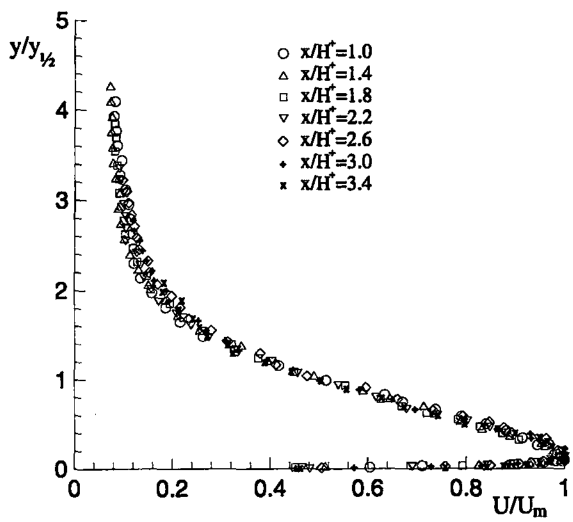

Figure 4.50.a Velocity profiles in the wall jet region of impinging jet ($Y/H^{+}=2$)

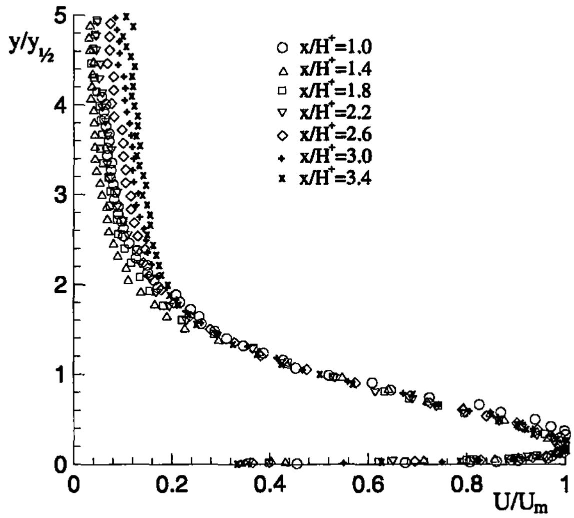

Figure 4.50.b Self-similar velocity profiles in the wall jet region of impinging jet (h=5mm, $Y/H^+=4$)

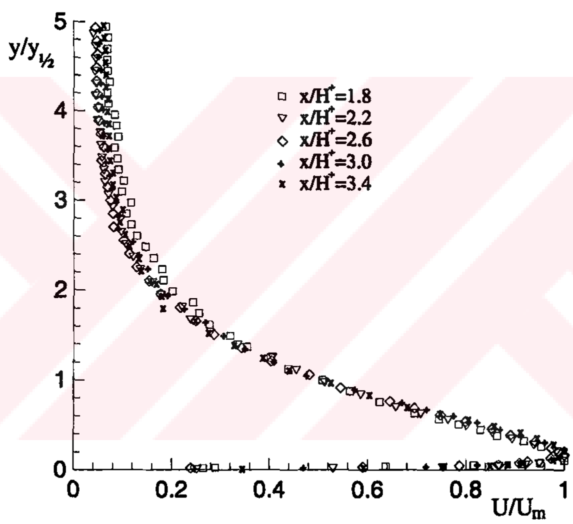

Figure 4.50.c Self similar velocity profiles in the wall jet region of impinging jet (h=5mm, $Y/H^+=8$)

Pressure distributions on the impingement surface are presented in Appendix E. Pressure coefficient C_p is defined as the ratio of the measured pressure difference between the pressure tab on the plate(p_i) and ambient pressure(p_∞) to the dynamic pressure at the nozzle exit.

$$C_p = \frac{p_i - p_\infty}{\frac{1}{2}\rho U_j^2} \tag{4.3}$$

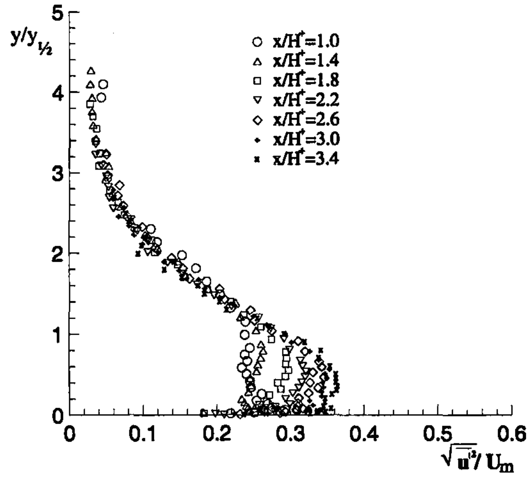

Figure 4.51.a Turbulence intensity profiles in the wall jet region of impinging jet (h=5mm, Y/H^{+}=2)

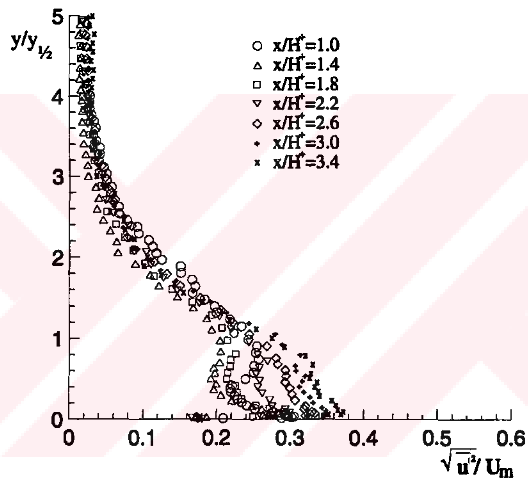

Figure 4.51.b Turbulence intensity profiles in the wall jet region of impinging jet (h=5mm, Y/H^{+}=4)

Pressure distribution on the plate at 100 mm distance from the nozzle exit (Y/H^{+}=2) is presented in Figure E.1. Pressure distribution contains four peaks which indicates the existence of saddle back shaped profiles in x-z plane of twin jets. When the plate is moved to downstream position Y/H^{+}=4, although the twin jets are combined saddle back shaped profile is preserved along a short distance (Figure E.2). Finally, pressure distribution gives a single peak at the origin and circular constant pressure lines for the plate distance of Y/H^{+}=8(Figure E.3). In that case, before the impingement, twin jet flow is formed a single (circular) free jet. Prevailing results

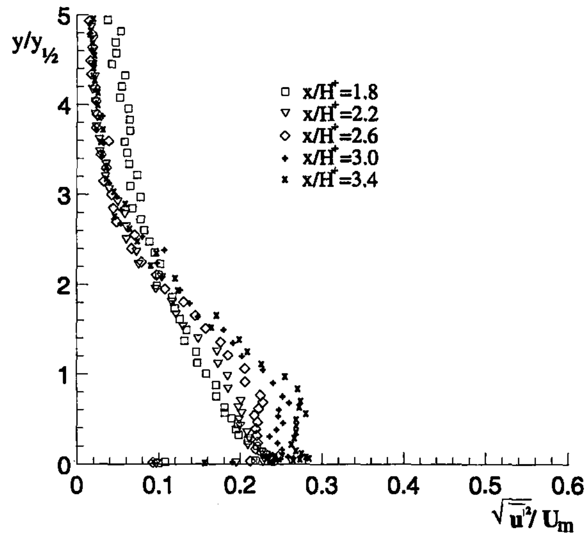

Figure 4.51.c Turbulence intensity profiles in the wall jet region of impinging jet ($Y/H^+=8$)

show that the maximum pressure has been decreased with increasing plate positions. Similar results are obtained for the twin jet issuing from 20 mm high slots (Figures E.4, E.5, E.6).

In fact, the maximal pressures on the surface are depend on the velocity field of the impinging jet. Centerline velocity evolution of the impinging jets nearby the surface

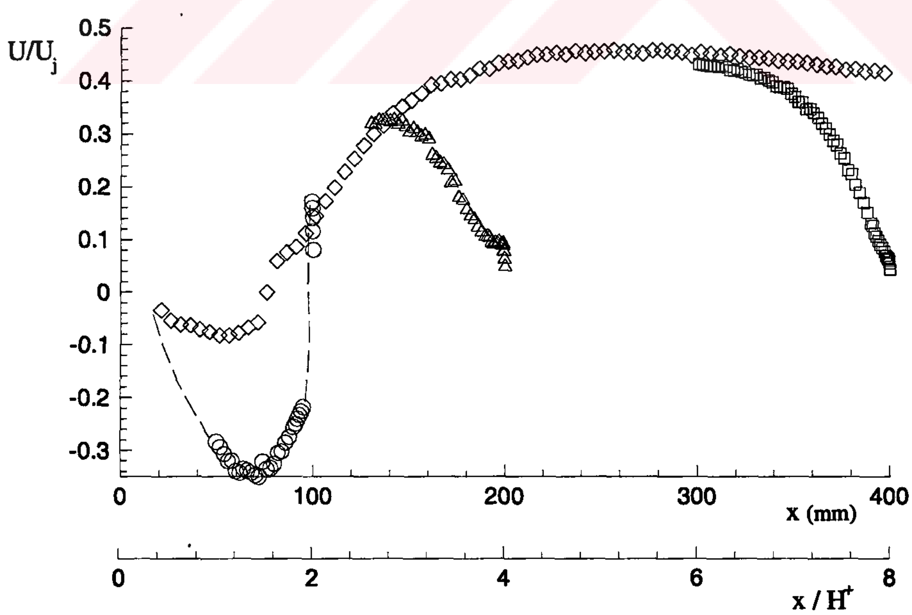

Figure 4.52 Jet centerline velocities of twin jet impinging on a surface at $Y/H^+=2$ (○) $Y/H^+=4$ (△), $Y/H^+=8$ (□) and twin jet without impingement plate (◇)

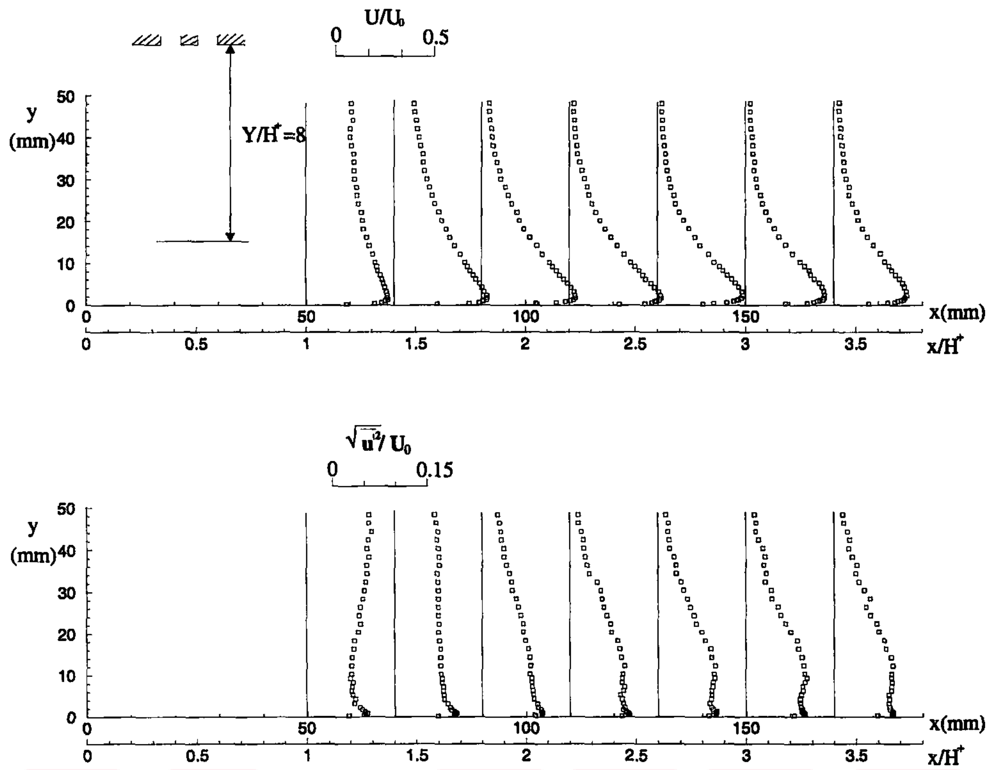

Figure 4.53 Velocity and turbulence intensity profiles on the impingement plate (h=10mm twin jet impingement).

are plotted in Figure 4.52. As the jet approaches to the surface it is affected by the presence of the plate and slows down. Higher deceleration rates indicate stronger impact, hence higher pressures on the surface. For $x/H^+=2$, whole flow field of the jet is affected by the existence of the plate.

Velocity and turbulence measurements are repeated for 10 and 20 mm height twin jet configurations and results are presented in Figure 4.53 and 4.54. As the jet slot height increases, velocity profiles of the wall jet flow on the impingement plate exhibit higher maximums. Turbulence intensities are also increased. However, flow structure is remained same. This can be seen from the normalized velocity and turbulence profiles (Figure 4.55 - 4.58). Velocity profiles reach the self similitude at the same point.

Pressure distributions on the impingement plate for the twin jets issued from 10mm high rectangular slots are presented in Figure E.7. The nozzle to plate distance is $Y/H^+=8$. The comparison of Figures E.3, E.6 and E.7 shows that maximum pressure increases with increasing slot height. Furthermore, in order to investigate the influence of the convex surface between jets two additional experiments has been performed. Figures E.8 and E.9 gives the pressure distributions on the impingement plate at $Y/H^{+}=8$ distance from the jet exit slots of 5 and 10 mm height respectively.

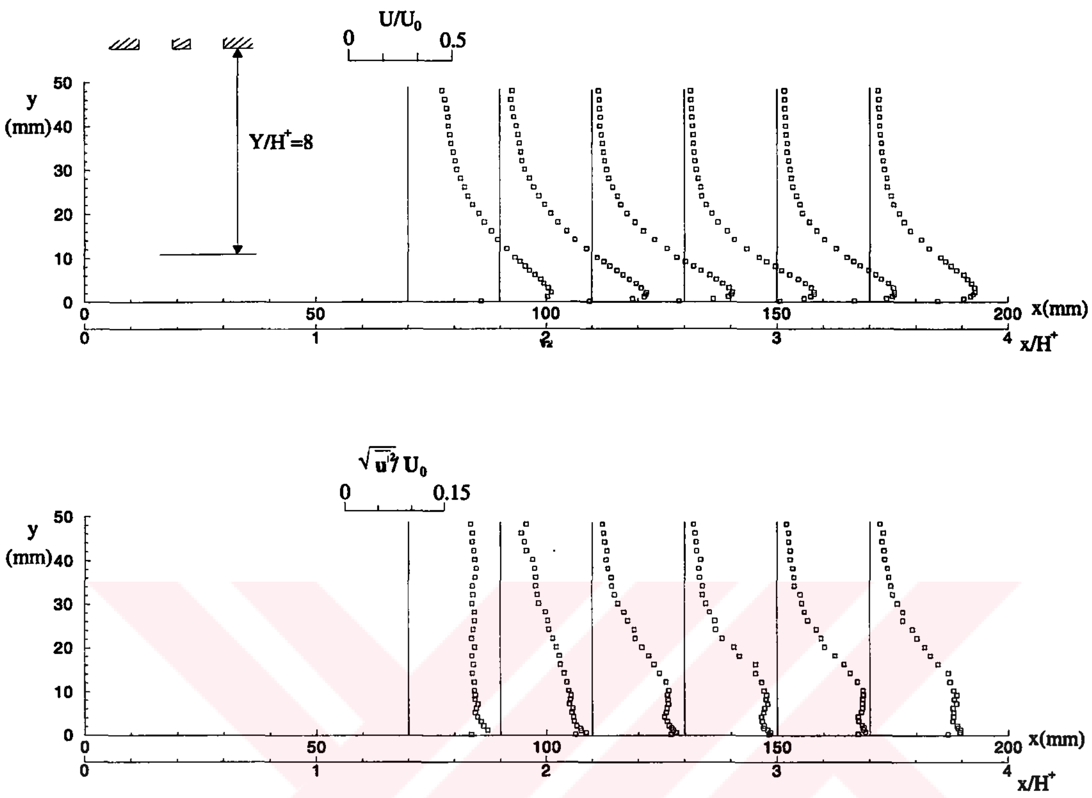

Figure 4.54 Velocity and turbulence intensity profiles on the impingement plate (h=20mm twin jet impingement).

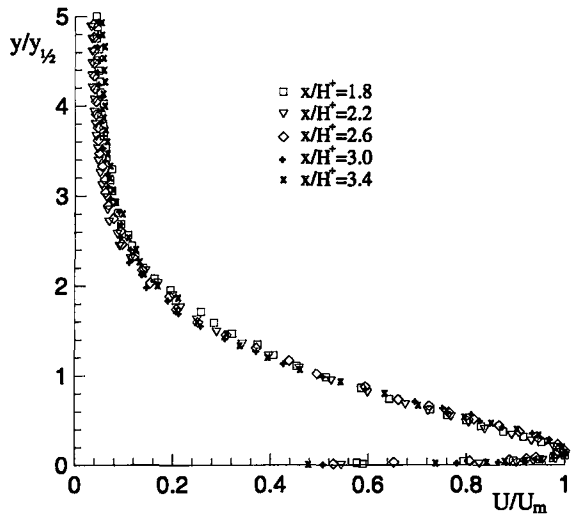

Figure 4.55 Self similar velocity profiles in the wall jet region of the impinging twin jet (h=10mm, $Y/H^{+}=8$)

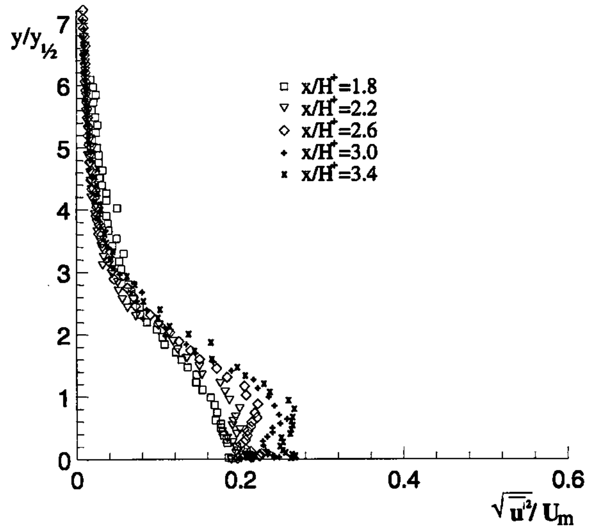

Figure 4.56 Turbulence intensity profiles in the wall jet region of the impinging twin jet (h=10mm, $Y/H^{+}=8$)

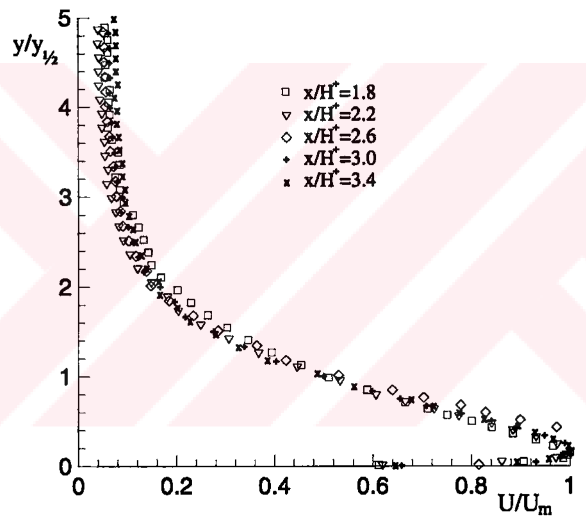

Figure 4.57 Self similar velocity profiles in the wall jet region of the impinging twin jet (h=20mm, $Y/H^{+}=8$)

Photographs of flow visualization on the impingement plate with surface oil flow technique are presented in Appendix F.

Flow visualization experiments are performed for 20 mm height twin jet case. Visualization photographs for all plate positions are presented in Figure E.1.On the plate at the nearest nozzle to plate position ($Y/H^{+}=2$), flow visualization photograph contains four stagnation points indicating the existence of four peaks in the velocity distribution of the impinging flow. When the plate is moved to downstream position

$Y/H^+=4$, two stagnation points are observed. Single jet impingement flow pattern is observed while the nozzle to plate distance is $Y/H^+=8$. The effect of the convex surface between two jet exit, is viewed in Figure E.2.

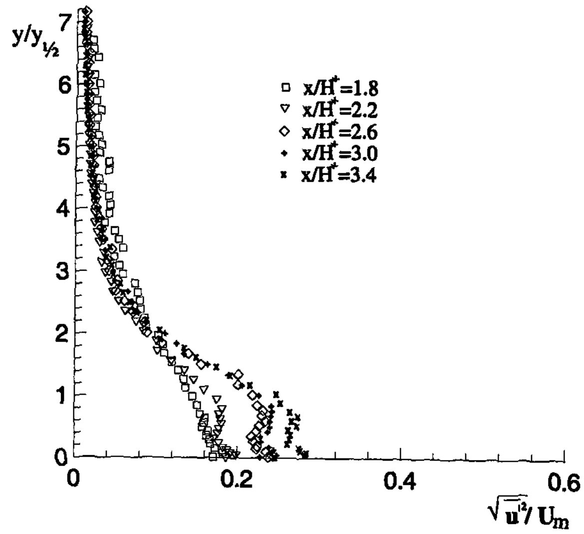

Figure 4.58 Turbulence intensity profiles in the wall jet region of the impinging twin jet (h=20mm, $Y/H^+=8$)

5. CONCLUSIONS

Subsonic, incompressible twin jet flow, emanating from identical rectangular slots is investigated experimentally. The velocity field of two parallel jets with five different nozzle heights and spacing has been measured using HWA.

In the present study, the initial boundary conditions of jets are examined first. Experiments revealed that, the initial velocity profiles agreed well with the laminar boundary layer profiles of Blasius. Even though the initial boundary layer is laminar, the flow in the mixing layer is highly unstable and quickly becomes turbulent. Displacement and momentum thicknesses and shape factors of initial boundary layer are presented in Table 4.1. The turbulence intensity at jet exit of each slot was 0.8% for the exit velocity of 30m/s. Spectral distribution measured inside the mixing layer close to the nozzle lip did not show any preferred frequency. This result demonstrates the absence of the facility dependent instabilities.

The dependence of the twin jet flow structure on the jet Reynolds number is investigated. 20 mm high and 100 mm long rectangular twin jet is used in order to study Reynolds number dependence of the flow. It is demonstrated by many researchers that the Reynolds number range substantially affects the flow properties at low Reynolds numbers. Nasr and Lai [9] who examined the effect of Reynolds number, reported that the flow was independent of the nozzle exit Reynolds number in the range 11000 to 19300.

Current experimental results indicated that, the distribution of mean velocity and turbulence intensities are virtually independent of the Reynolds number in the range 13422 to 40468.

In accordance with the previous results, jet exit velocity is maintained constant (V_j=30m/s) in twin jet experiments. General flow field characteristics of twin jets are observed by the smoke visualization experiments.

The flow field of two parallel jets is classified into three distinct regions; converging region which includes a recirculation region formed between the nozzle plate and the inner shear layers, the merging region which is the region between the merging point and the combined point and the combined region where two jets are combined to resemble a single jet.

Different twin jet configurations are investigated. The spatial distributions of the mean velocities and turbulence intensities clearly reveal the flow structure of converging, merging and combined regions.

Normalized velocity profiles in x-y plane of all twin jet configurations exhibit a high degree of similarity in the outer shear layer while they differ in the inner shear layer. Inner shear layers approach to the similarity with increasing downstream distance x and give similar profiles before the combined point. Downstream of the combined point, jets combine to spread like a free single jet. Non-dimensional velocity profiles in the fully developed single jet region agree with the theoretical curve of Gortler.

Saddle back shaped turbulence profiles indicate the appearance of the single jet flow. Non-dimensional turbulence profiles in combined region reach self similarity after the velocity profiles.

The normalized mean velocity and turbulence intensity profiles in the central x-z plane exhibit saddle shape velocity profiles up to the downstream location $4.8H^{+}$.

Flow characteristics such as spreading rates, maximum velocity decay rate and the variation of centerline velocity are examined. Maximum velocity decay, retains its rectangular jet characteristics and can be classified with three regions: potential core region, characteristic region and axisymmetric region. Jet growth rates of twin jets are related to the maximum velocity decay rate. Faster decay in the maximum velocity implies higher jet spreading.

The relation between the position of the merging point X_{mp} and the nozzle spacing S is expressed as follows;

$$\frac{X_{mp}}{h} = 0.7100(S/h)^{1.4506}$$

and the relation between the combined point and the nozzle spacing is obtained as follows;

$$\frac{X_{cp}}{h} = 4(S/h) + 9.62$$

Spectral measurements of velocity fluctuations show that the development of coherent structures in the outer shear layer is the same as that of a single jet.

The spectral measurements in the mixing layer gives frequency information of the vortex structure in the near region of the jet flow. Vortex passage frequencies of the initial shear layers, at a distance of x/H^{+}=0.2-0.3 from the nozzle, are measured. Corresponding Strouhal numbers based on the momentum thickness St_{θ} are obtained. Strouhal numbers of initial vortex formations are almost between 0.011 and 0.012.

The variation of the peak frequencies in the spectra, measured along the shear layer, shows a staging behavior. The initial peak value is halved at successive locations between the nozzle exit and the end of the potential core. These stages correspond to the pairing locations. At the end of the potential core a preferred frequency corresponding to the passage frequency of the dominant vortical structures can be detected. Consisting Strouhal numbers (based on the jet exit height) of preferred modes are obtained.

Common features of two parallel jets and the offset jets are investigated. The symmetry plane that exists between two parallel jets may appear to affect the flow field in the same way as a solid wall does in an offset jet. The symmetry plane between two parallel jets is replaced with a solid wall in order to obtain an offset jet. Therefore, identical initial conditions are provided for both flow structures.

Comparison of hot-wire measurements for twin jets and offset jet with the same offset ratio (2h/S=4.5) indicates that general flow behaviors are similar. Nevertheless, flow reversal occurs at slightly downstream position for the offset jet. In the reattachment region, the offset jet is subjected to strong interactions with the wall. Although the offset jet decay faster in the near field, in the far field the flow in the free jet region of twin jet, having broader velocity profiles than that of offset jet, grows faster. It is concluded that the additional momentum loses at the near wall region of the offset jet might cause lower spreading rates.

The effect of surface curvature is investigated by placing a cylindrical convex body between two jets. Velocity and turbulence intensity profiles are compared with the previous twin jet measurements in order to examine the convex surface effects. It is observed that the existence of the convex surface makes the recirculation region shorter. Thus merging point moves upstream positions. Merging process of jets results in the coalescence of two jets at upstream positions from the combined point of twin jets (without convex surface). Therefore, the function of such a convex surface between two jets, can be explained as follows: A convex surface deflects the jets towards the symmetry axis more strongly and accelerates the flow development procedure. As the curvature radius diminishes, the influence of the surface curvature on the flow field is vanished. HWA results indicate that the recirculation zone, merging length and combined length have been reduced by insertion of a convex surface between two jets while jet spreading and velocity decay have been enhanced.

Spreading rates of jets are affected by the convex surface. In the single free jet region of the twin jet with surface curvature flow, jet grows faster than that of the twin jet (without surface curvature). The highest growth rate augmentation is obtained for the highest curvature radius case.

Merging and combined point locations are determined and compared with previous results. It is found that the equation between merging point locations X_{mp}/h and nozzle spacing S/h of the TJSC flow obeys the power law.

Further experiments are intended to investigate the impingement of two rectangular unventilated jets on a plane surface. Twin jet impingement experiments were carried out for three different nozzle to plate distances (Y). Non-dimensional nozzle to plate distances were $Y/H^{+}=2$, 4 and 8.

Jet centerline velocity is affected by the existence of the wall. As the jet approaches to the surface, it is affected by the presence of the plate and slows down. There exists a stagnation point at the intersection point of the jet centerline and the wall.

The development of the velocity profiles along the x-axis shows that the jet width $y_{1/2}$ approaches to the wall with increasing x distance from the origin up to the position where the wall jet region starts. Maximum velocities also accelerate near the impingement region and then show a slowing down characteristic in the wall jet region.

Non dimensional velocity profiles show similarity in the wall jet region. Turbulence intensities are not fully reached self similarity inside the measurement area.

For all impinging plate locations the converging process is terminated and merging point takes place before the impingement. For the first case ($Y/H^+=2$), the flow impinging on the surface still retains its twin jet properties while for the $Y/H^+=8$ case flow shows fully developed single jet properties.

Pressure measurements on the impingement surface and oil film flow visualization technique give information about the impinging flow. Pressure distribution on the plate at $Y/H^+=2$ position, has four peaks. When the plate is moved to downstream position $Y/H^+=4$, two peaks are observed in x-z plane. Pressure distribution on the surface illustrates that the switching of axes, similar to elliptic jets also occurs in twin jet flows. After one switch of the major and minor axis; jet, attains fully developed single free jet flow characteristics. In this region pressure distributions give single peak value at the origin. The maximum pressure coefficient is decreased with increasing plate positions.

As the jet slot height increases, velocity profiles of the wall jet flow on the impingement plate exhibit higher maximums. Turbulence intensities are also increased. However, flow structure is remained the same.

Experimental results show that the three-dimensional twin jet spreading characteristics are different than that of two-dimensional case. Therefore, increasing number of studies on three-dimensional twin and multi-jets are needed. Multi jet configurations and its impingement on a flat or curved surface can be other related research subjects. Present study, proposes to utilize a convex surface between two jet exits for the passive control of the flow structure. However, only cylindrical surface is examined in the present study. Other convex surface possibilities may be investigated in future studies.

REFERENCES

[1] **Abramovich, G. N.,** 1963. The Theory of Turbulent Jets, The Massachusetts Institute of Technology Press, Cambridge.

[2] **Bradshaw, P., Ferriss, D.H., and Johnson, R. F.,** 1964. Turbulence in the noise-producing region of a circular jet, *Journal of Fluid Mechanics*, **Vol.19**, 591-624.

[3] **Mathieu, J. and Charnay, G.,** 1981. Structure and development of turbulent jets, AGARD, CP-308.

[4] **Yule, A. J.,** 1978. Large-scale structure in the mixing layer of a round jet, *Journal of Fluid Mechanics*, **Vol.89**, 413-432.

[5] **Liepmann, D.,** 1991. Streamwise vorticity and entrainment in the near field of a round jet, *Physics of Fluids A*, **Vol.3**, No.5, 1179-1185.

[6] **Moum, J. N., Kawall, J. G. and Keffer J. F.,** 1983. Coherent structures within the plane turbulent jet, *Physics of Fluids*, **Vol.26**(10), 2939-2945.

[7] **Liepmann, D. and Gharib, M.,** 1992. The role of streamwise vorticity in the near-field entrainment of round jets, *Journal of Fluid Mechanics*, **Vol.245**, 643-688.

[8] **Boguslawski, L. and Popiel, O.,** 1979. Flow structure of the free round turbulent jet in the initial region, *Journal of Fluid Mechanics*, **Vol.90**, 531-539.

[9] **Kotsovinos, N. E.,** 1978. A note on the conservation of the axial momentum of a turbulent jet, *Journal of Fluid Mechanics*, **Vol.87**, 55-63.

[10] **Abid, M. and Brachet, M. E.,** 1993. Numerical characterization of the dynamics of vortex filaments in round jets, *Physics of Fluids A*, **Vol.5**, No.11, 2582-2584.

[11] **Persen, L. N.,** 1981. The near field of a plane turbulent jet, AGARD, CP-308.

[12] **Gutmark, E. and Wygnanski, I.,** 1976. The planar turbulent jet, *Journal of Fluid Mechanics*, **Vol.73**, 465-495.

[13] **Hussain, A. K. M. F. and Clark A. R.,** 1977. Upstream influence on the near field of a plane turbulent jet, *The Physics of Fluids*, **Vol.20**, No.9, 1416-1426.

[14] **Bradshaw, P.,** 1977. Effect of external disturbances on the spreading rate of a plane jet, *Journal of Fluid Mechanics*, **Vol.80**, 795-797.

[15] **Bradbury, L. J. S.,** 1965. The structure of a self-preserving turbulent plane jet, *Journal of Fluid Mechanics*, **Vol.23**, 31-64.

[16] **Quinn, W. R.,** 1989. On mixing in an elliptic turbulent free jet, *The Physics of Fluids A*, **1**(10), 1716-1722.

[17] **Hussain, F. and Husain H. S.,** 1989. Elliptic jets. Part1. Characteristics of unexcited and excited jets. *Journal of Fluid Mechanics*, **Vol.208**, 257-320.

[18] **Husain H. S. and Hussain, F.,** 1991. Elliptic jets. Part 2. Dynamics of coherent structures: pairing. *Journal of Fluid Mechanics*, **Vol.233**, 439-482.

[19] **Quinn W. R.,** 1991. Passive near-field mixing enhancement in rectangular jets, *AIAA Journal*, **Vol.29**, No.4, 515-519.

[20] **Gutmark E. and Ho C. M.,** 1985. Near-field pressure fluctuations of an elliptic jet, *AIAA Journal*, **Vol.23**, No.3, 354-358.

[21] **Quinn W. R.,** 1995. Turbulent mixing in a free jet issuing from a low aspect ratio contoured rectangle nozzle, *Aeronautical Journal*, 337-342.

[22] **Krothapalli, A., Baganoff D. and Karamcheti, K.,** 1981. On the mixing of a rectangular jet, *Journal of Fluid Mechanics*, **Vol.107**, 201-220.

[23] **Sforza, P. M., Steiger, M. H. and Trentacoste, N.,** 1966. Studies on three-dimensional viscous jets, *AIAA Journal*, **Vol.4**, No.5, 800-806.

[24] **Trentacoste, N. and Sforza, P.,** 1967. Further experimental results for three dimensional free jets, *AIAA Journal*, **Vol.5**, No.5, 885-891.

[25] **Sfeir, A. A.,** 1979. Investigation of three-dimensional turbulent rectangular jets, *AIAA Journal*, **Vol.17**, No.10, 1055-1060.

[26] **Quinn, W. R., Polard, A. and Marsters, G. F.,**1985. Mean velocity and static pressure distributions in a three dimensional turbulent free jet, *AIAA Journal*, **Vol.23**, No.4, 971-973.

[27] **Tsuchiya, Y., Horikoshi, C. and Sato, T.,** 1986. On the spreading of rectangular jets, *Experiments in Fluids*, **4**, 197-204.

[28] **Namer, I., and Ötügen, M. V.,** 1988. Velocity measurements in a plane turbulent air jet at moderate Reynolds numbers, *Experiments in Fluids*, **6**, 387-399.

[29] **Lozanova, M. and Stankov, P.,** 1998. Experimental investigation on the similarity of a 3D rectangular turbulent jet, *Experiments in Fluids*, **24**, 470-478.

[30] **Kohigoe, S., Gutmark, E., Schadow, C. S. and Tubis, A.,** 1989. Initial development of noncircular jets leading to axis switching, *AIAA Journal*, **Vol.27**, No.4, 411-419.

[31] **Bourque C. and Newman G.,** 1960. Reattachment of a two-dimensional incompressible jet to an adjacent plate, *Aeronautical Q.*, **Vol.11**, 201-262.

[32] **Nasr, A. and Lai, J. C. S.,** 1998. A turbulent plane offset jet with small offset ratio, *Experiments in Fluids*, **Vol.24**, 47-57.

[33] **Koo, H-M. and Park, S. O.,** 1992. Prediction of a turbulent offset jet flows with an assessment of quicker scheme, *Int. J. of Numerical Methods*, **Vol.15**, 355-372.

[34] **Yoon, S. H., Kim K. C., Kim, D. S. and Chung, M. K.,** 1995. Effects of surface roughness on a wall-attaching offset jet, *Experiments in Fluids* , **Vol.19**, 38-42.

[35] **Kim, D. S. Yoon, S. H., Lee, D. H. and Kim, K. C.,** 1996. Flow and heat transfer measurements of a wall attaching offset jet, *Int. J. Heat and Mass Transfer*, **Vol.39**, No.14, 2907-2913.

[36] **Gu, R.,** 1996. Modeling two-dimensional turbulent offset jets, *J. of Hydraulic Engineering*, 617-624.

[37] **Song, H. B., Yoon, S. H. and Lee D. H.,** 2000, Flow and heat transfer characteristics of a two-dimensional oblique wall attaching offset jet, *International Journal of Heat and Mass Transfer*, **43**(13), 2395-2404.

[38] **Nasr, A. and Lai, J. C.,** 1997. Comparison of flow characteristics in the near field of two parallel plane jet and an offset plane jet, *Physics of Fluids*, **9**(10), 2919-2931.

[39] **Kotansky, D. R. and Bower, W. W.,** 1978. A basic study of the VTOL ground effect problem for planar flow, *Journal of Aircraft*, **Vol.15**, No.4, 214-221.

[40] Guillard, F., Fritzon, R., Revstedt, J., Tragardh, C., Alden, M. and Fuchs, L., 1998. Mixing in a confined turbulent impinging jet using planar laser-induced fluorescence, *Experiments in Fluids*, **Vol.24**, 143-150.

[41] Harman T. B., Cimbala, J. M. and Billet, M. L., 1994. Reduction in size and unsteadiness of VTOL ground vortices by ground fences, *Journal of Aircraft*, **Vol.31**, No.3, 579-584.

[42] Knowles, K. and Bray, D., 1993. Ground vortex formed by impinging in cross flow, *Journal of Aircraft,* **Vol.30**, No.6, 872-878.

[43] Barata, J. M. M., 1996. Fountain flows produced by multiple impinging jets in a cross flow, *AIAA Journal*, **Vol.34**, No.12, 2523-2530.

[44] Barata, J. M. M., 1993. Fountain flows produced by multijet impingement on a ground plane, *Journal of Aircraft*, **Vol.30**, No.1, 50-56.

[45] Schetz, J. A., Jakubowski, A. K. and Aoyagi, K., 1984. Surface pressures on a flat plate with dual jet configurations, *Journal of Aircraft*, **Vol.21**, No.7, 484-490.

[46] Elbanna, H. and Sabbagh, J. A., 1989. Flow visualization and measurements in a two-dimensional two-impinging-jet flow, *AIAA Journal*, **Vol.27**, No.4, 420-426.

[47] Miller, P. and Wilson, M., 1993. Wall jets created by single and twin high pressure jet impingement, *Aeronautical Journal*, 87-99.

[48] Chuang, S-H., Chen, M-H. and Tai, F-M., 1992,Numerical simulation of twin-jet impingement on a flat plate coupled with cross flow, *Int. J. of Numerical Methods in Fluids*, **Vol.14**, 459-475.

[49] Arjocu, S. C. and Liburdy, J. A., 1999. Near surface characterization of an impinging elliptic jet array, *Journal of Fluids Engineering*, **Vol.21**, 384-390.

[50] Ho, C-M. and Nosseir N. S., 1981. Dynamics of an impinging jet. Part 1. The feedback phenomenon, *Journal of Fluid Mechanics*, **Vol.105**, 119-142.

[51] Nosseir N. S. and Ho, C-M, 1982. Dynamics of an impinging jet. Part 2. The noise generation, *Journal of Fluid Mechanics*, **Vol.116**, 379-391.

[52] Looney, M. K. and Walsh, J. J., 1984. Mean-flow and turbulent characteristics of free and impinging jet flows, *Journal of Fluid Mechanics*, **Vol.147**, 397-429.

[53] **Bernard, A., Brizzi, L.-E. and Bousgarbies, J.-L.,** 2000, A comparison of flow visualization and wall pressure measurements for a jet impinging on a plane surface, *Experiments in Fluids*, **Vol.29**, 23-29.

[54] **Acar, H.,** 1998. An experimental investigation of a rectangular jet impinging on a flat surface. *PhD Thesis*. Istanbul Technical University, Institute of Technology and Science.

[55] **Raghunathan, S. and Reid I. M.,** 1981. A study of multiple jets, *AIAA Journal*, **Vol.19**, 124-126.

[56] **Krothapalli, A., Baganoff, D. and Karamcheti, K.,** 1980. Development and structure of a rectangular jet in a multiple jet configuration, *AIAA Journal*, **Vol.18**, No.8, 945-950.

[57] **Moustafa, G. H. and Rathakrishnan, E.,** 1993. Studies on the flowfield of multijet with square configuration, *AIAA Journal*, **Vol.31**, No.7, 1189-1190.

[58] **Coles, W. D. and Callaghan, E. E.,** 1957. Full-scale investigation of several jet-engine noise-reduction nozzles, *NACA Technical Note*, Report 1387, 1249-1271.

[59] **Krothapalli, A., Baganoff, D. and Karamcheti, K.,** Partially confined multiple jet mixing, *AIAA Journal*, **Vol.19**, No.3, 324-328.

[60] **Tanaka, E.,** 1970. The interference of two-dimensional parallel jets (1st report, Experiments on dual jet), *Bulletin of the JSME*, **Vol.13**, No.56, 273-280.

[61] **Tanaka, E.,** 1974. The interference of two-dimensional parallel jets (2nd report, Experiments on the combined flow of dual jet), *Bulletin of the JSME*, **Vol.17**, No.109, 920-927.

[62] **Lin, Y. F. and Sheu, M. J.,** 1990. Investigation of two plane parallel unventilated jets, *Experiments in Fluids*, **Vol.10**, 17-22.

[63] **Wang, C. S., Lin Y. F. and Sheu, M. J.,** 1993. Measurements of turbulent inclined plane dual jets, *Experiments in Fluids*, **Vol.16**, 27-35.

[64] **Lin,Y. F. and Sheu, M. J.,** 1991. Interaction of parallel Turbulent Plane Jets, *AIAA Journal*, **Vol.29**, No.9, 1372-1373.

[65] **Elangovan, S., Solaiappan, A. and Rathakrishnan, E.,** 1996. Studies on twin elliptic jets, *Aeronautical Journal*, 295-296.

[66] **Murai, K., Taga, M. and Akagawa, K.,** 1976. An experimental study on confluence of two two-dimensional jets, *Bulletin of the JSME*, **Vol.19**, No.134, 958-964.

[67] **Bourque, C.,** 1981. Recollement de deux jets sur eux-meme, AGARD, CP-308, 4.1-4.11.

[68] **Nasr, A. and Lai, J. C. S.,** 1997. Two parallel plane jets: mean flow and effects of acoustic excitation, *Experiments in Fluids*, **Vol.22**, 251-260.

[69] **Elbanna, H., Gahin, S. and Rashed, M. I. I.,** 1983, Investigation of two plane parallel jets, *AIAA Journal*, **Vol.21** , No. , 986-991.

[70] **Elbanna, H. and Sabbagh, J. A.,** 1987. Interaction of two nonequal plane parallel jets, *AIAA Journal*, **Vol.26** , No. ,12-13.

[71] **Marsters, G. F.,** 1977. Interaction of two plane parallel jets, *AIAA Journal*, **Vol.15**, No.12, 1756-1762.

[72] **Elbanna, H. and Sabbagh, J. A.,** 1985.Interaction of two nonequal jets, *AIAA Journal*, **Vol.24**, 686-687.

[73] **Elbanna, H., Sabbagh, J. A. and Rashed, M. I. I.,** 1985. Interception of two equal turbulent jets, *AIAA Journal*, **Vol.23**, No.7, 985-986.

[74] **Manjunath, A., Gowda, B. H. L. and Natarajan R.,** 1991. Studies on the mixing of two non-axial plane jets in a confined passage: mean flow characteristics, *Experiments in Fluids*, **Vol.11**, 17-24.

[75] **Goldstein, R. J.,** 1996. Fluid Mechanics Measurements, 2nd edition, Washington DC: Taylor & Francis.

[76] **Nigan, N. C. and Narayanan, S.,** 1994. Applications of Random Vibrations, Springer-Verlag.

[77] **Winant, C. D. and Browand, F. K.,** 1974. Vortex pairing: the mechanism of turbulent mixing layer growth at moderate Reynolds number, *Journal of Fluid Mechanics*, **Vol.63**, 237-255.

[78] **Gutmark, E. and Ho, C.-M.,** 1983. Preferred modes and the spreading rates of jets, Physics of Fluids, **26**(10), 2932-2938.

[79] **Mihalke, A.,** 1965. On spatially growing disturbances in an inviscid shear layer, *Journal of Fluid Mechanics,* **Vol.23**, 521-544.

[80] **Stuart, J. T.,** 1967. On the finite amplitude oscillations in laminar mixing layers, *Journal of Fluid Mechanics*, **Vol.29**, 417-440.

[81] Laufer, J., 1981. Instability and turbulence in jets, *Transition and Turbulence*, Academic Press, 63-76.

[82] Lilley, G. M., 1996. The radiated noise from isotropic turbulence with applications to the theory of jet noise, *Journal of Sound and Vibration*, **190**(3), 463-476.

[83] Tam, C. K. W., 1998. Jet noise: since 1952, *Theoret. Comput. Fluid Dynamics*, **Vol.10**, 393-405.

[84] Lau, J.C. and Fisher, M.J., 1975. The vortex-street structure of turbulent jets, *Journal of Fluid Mechanics*, **Vol.68**, 299-337.

[85] Shih, C., Krothapalli, A., and Gogineni, S., 1992. Experimental observations of instability modes in a rectangular jet, AIAA Journal, **Vol.30**, No.10, 2388-2394.

[86] Tam, C. K. W. and Chen, K. C., 1979. A statistical model of turbulence in two-dimensional mixing layer, *Journal of Fluid Mechanics*, **Vol.92**, 303-326.

[87] Hussain, A. K. M. F.,1986. Coherent structures and turbulence, *Journal of Fluid Mechanics*, **Vol.173**, 303-356.

[88] Bradshaw, P., 1973. Effects of streamline curvature on turbulent flow, *AGARDograph* no.169

[89] Lepretre, M. and Portier, C., 1981. Etude experimental d'un deviateur de jet, AGARD, CP-308, 23.1-23.20.

[89] Eriksson, J. G., Karlsson, R. I. and Persson, J., 1998. An experimental study of a two-dimensional plane turbulent wall jet, *Experiments in Fluids*, **Vol.25**, 50-60.

[90] Rodman, L. C., Wood,. N. J. and Roberts, L., 1989. Experimental investigation of straight and curved annular wall jets, AIAA Journal, **Vol.27**, No.8, 1059-1067.

[91] Guitton, D. E. and Newman, B. G., 1977. Self-preserving turbulent wall jets over convex surface, *Journal of Fluid Mechanics*, **Vol.81**, 155-185.

[92] Wilson, D.J. and Goldstein, R. J., 1976. Turbulent wall jets with cylindrical streamwise surface curvature, *Journal of Fluids Engineering*, 550-557.

[93] Newman, B. G., 1961. The deflection of plane jets by adjacent boundaries-Coanda effect, *Boundary Layer and Flow Control*, Pergamon.

[94] Launder, B. E., 1983. The turbulent wall jet-measurements and modeling, *Ann. Rev. Fluid Mechanics*,**15**, 4298-459.

[95] Shakouchi, T., Onohara, Y. and Kato, S., 1989. Analysis of a two-dimensional, turbulent wall jet along a circular cylinder, *JSME International Journal*, **Vol.32**, No.3, 332-339.

[96] Gibson, M. M. and Younis, B. A., 1983. Turbulence measurements in a developing mixing layer with mild destabilizing curvature, *Experiments in Fluids*, **Vol.1**, 23-30.

[97] Perry, A. E., 1982. Hot-wire Anemometry, *Oxford University Press.*

[98] Acrivlellis, M., 1978.An improved method for determining the flow field of multidimensional flows of any turbulence intensity, *DISA Information*, No.23, 11-16.

[99] Brunn, H. H., 1995. Hot-wire Anemometry Principle and Signal Analysis, *Oxford University Press.*

[100] Irwin, H. P. A. H. and Smith P. A., 1975. Prediction of the effect of streamline curvature on turbulence, *The Physics of Fluids*, **Vol.18**, No.6, 624-630.

[101] Fujisawa, N. and Kobayashi, R., 1987. Turbulence characteristics of wall jets along strong convex surface, *Int. J. Mech. Sci.*, **Vol.29**, No.5, 311-320.

[102] Newland D. E., 1993. An introduction to random vibrations, spectral and wavelet analysis. *Longman Scientific & Technical.*

APPENDIX A AUTO-CORRELATION AND SPECTRUM

a) Auto-Correlation

The autocorrelation function for a random process x(t) is defined as the average value of the product $x(t).x(t+\tau)$ [102];

$$R_{xx} = \overline{x(t)x(t+\tau)} \qquad (A.1)$$

Auto-correlation for a stationary process is;

$$\overline{x(t)x(t+\tau)} = \overline{x^2(t)}\rho(\tau) \qquad (A.2)$$

where ρ is correlation coefficient and;

$$|\rho(\tau)| \le 1 = \rho(0) \qquad (A.3)$$

Note: The random process is said to be stationary if the probability distribution do not depend on the absolute time. This implies that all averages are independent of absolute time.

b) Auto-Spectral Density

The spectral density is the Fourier transform of the Auto-correlation;

$$S_{xx}(\omega) = \frac{1}{2\pi}\int_{-\infty}^{\infty} R_{xx}(\tau)e^{-i\omega\tau}d\tau \qquad (A.4)$$

$$R_{xx} = \int_{-\infty}^{\infty} S_{xx}(\omega)e^{i\omega\tau}d\omega \qquad (A.5)$$

The most important property of S_{xx} becomes apparent when we put $\tau=0$ in equation(A.4),

$$R_{xx}(0) = \int_{-\infty}^{\infty} S_{xx}(\omega)d\omega \qquad (A.6)$$

and equation (A.1) gives;

$$R_{xx}(0) = \overline{x^2(t)} \qquad (A.7)$$

from (A.6) and (A.7);

$$\overline{x^2(t)} = \int S_{xx}(\omega)d\omega \qquad (A.8)$$

The area under a graph of spectral density gives the mean square value of a stationary random process x(t).

Although S_{xx} is defined as a infinite continuos function of ω in equation (A.4), experimental data of random processes are finite discrete time series. In order to estimate spectra from the measured data it is necessary to use discrete Fourier Transform. If x(t) is a periodic function with period T, spectrum can be written as;

$$S_k = \frac{1}{N}\sum_{r=0}^{N-1} R_r e^{-i(2\pi kr/N)} \qquad (A.9)$$

where;

$$R_r = \frac{1}{N}\sum_{s=0}^{N-1} x_s x_{s+r} \qquad (A.10)$$

It can easily be proved by using equation (A.9) and (A.10) that, S_k is related to X_s (Fourier Transform of x_s) by the simple equation;

$$S_k = X_s X_s^* \qquad (A.11)$$

Since we are calculating Fourier Transform of a periodic function which is actually measured in a single cycle $0<t<T$, it is necessary for improving the accuracy of calculations to use a window function. A window function modifies the data by weighting the middle of the record more heavily than the two ends.

Data windowing is available in "AcqWIRE" software. The data windows smooth discontinuities at the joints of the periodic function. This operation corresponds to convolving the original spectral estimate S_T with a filter window.

$$\overline{S_T}(f) = \int_{-\infty}^{\infty} S_T(f_1) W(f - f_1) df_1 \tag{A.12}$$

W is the Fourier Transform of the data window. Super Gaussian, Hanning, and Hamning windows are available in acqWIRE software. Gaussian Window is used in the experiments.

The coefficient of Fourier Transform of a discrete function (X_r) repeats themselves for $k>N-1$, so that the graphs of X_k versus ω_k repeat itself periodically. Therefore, we can conclude that the coefficients X_k calculated by the Fourier Transformation are correct only for frequencies up to $\omega_k=2\pi k/N\Delta=\pi/\Delta$. If there are frequencies above π/Δ present in the original signal, these introduce a distortion of the graph called aliasing.

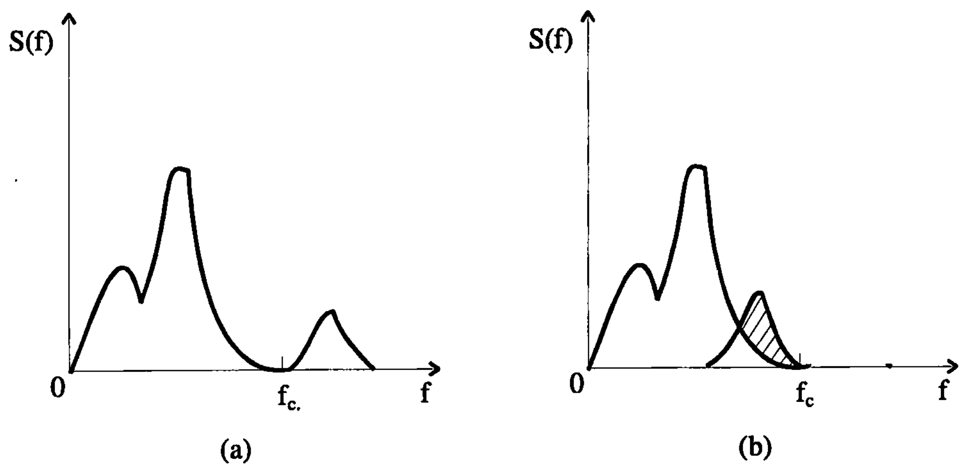

Figure A.1 Aliased auto spectrum due to folding (a) true spectrum, (b) aliased spectrum.

Aliasing problem is inherent in digital processing. This error may be explained by considering an experimental record with a sampling interval Δt (the sampling rate is 1/Δt). At least two samples per cycle are required to define a frequency component in the original data. Hence, the highest frequency that can be defined by a sampling rate of 1/Δt is 1/2Δt. Frequencies in the original data above this frequency (1/2Δt) will appear below it and be confused with the data in this range(Figure A.1)

The maximum frequency that can be detected from the data sampled at time spacing Δ is 1/2Δ. This frequency is called Nyquist frequency.

APPENDIX B VELOCITY AND TURBULENCE PROFILES OF TWIN JETS

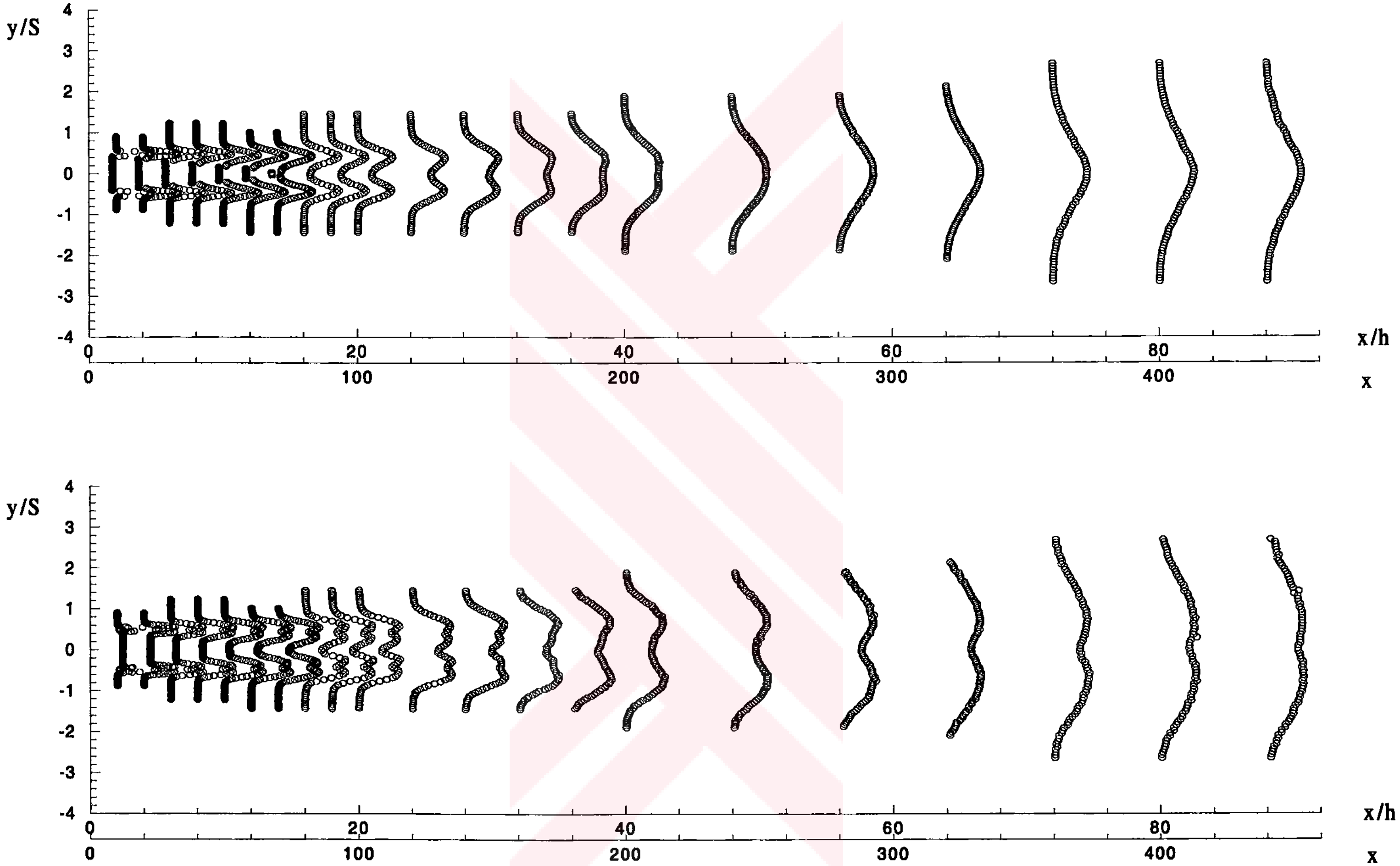

Figure B.1 Spatial development of the velocity and turbulence profiles of twin jet issued from 5 mm high rectangular jets.

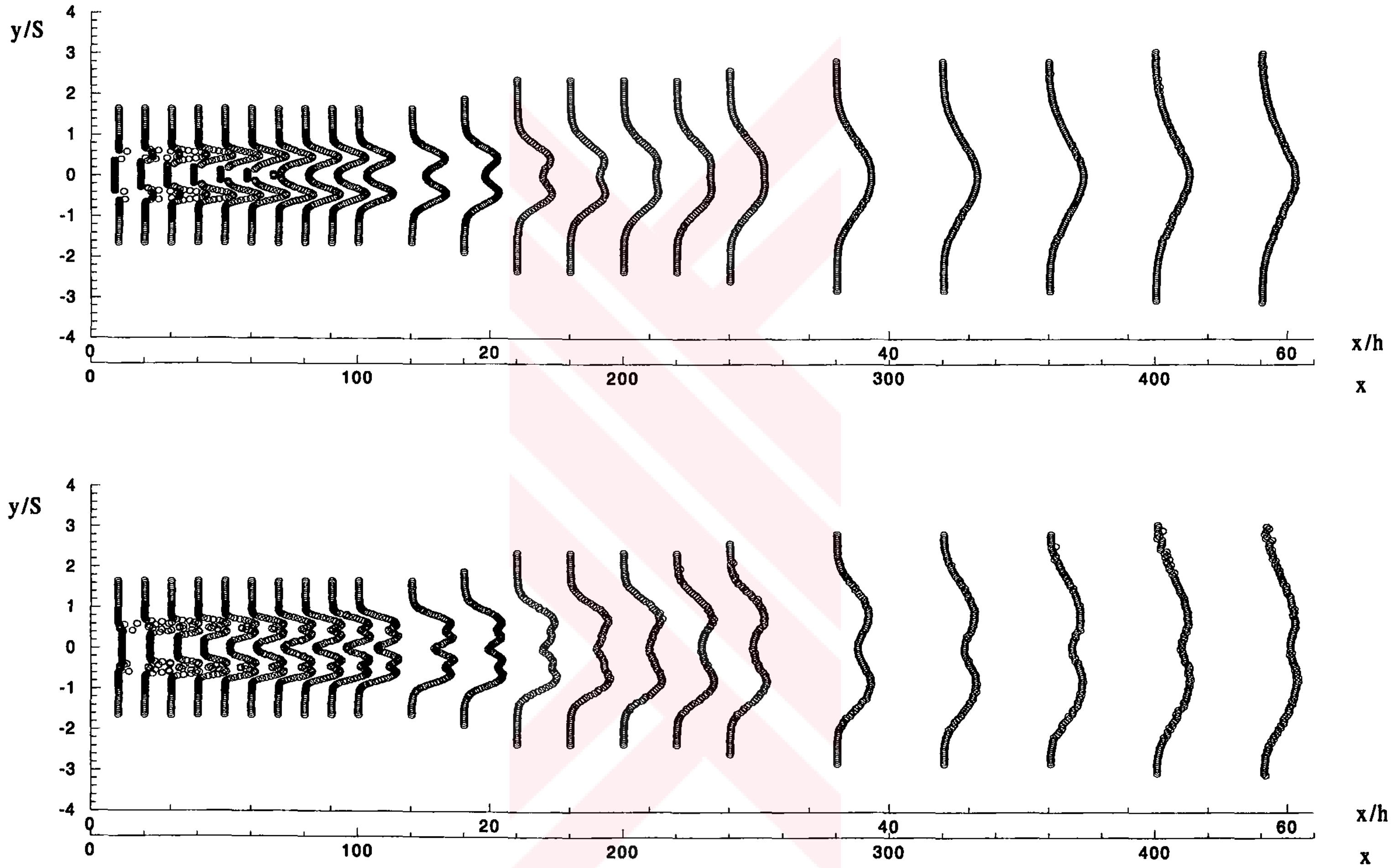

Figure B.2 Spatial development of the velocity and turbulence profiles of twin jet issued from 7.5 mm high rectangular jets.

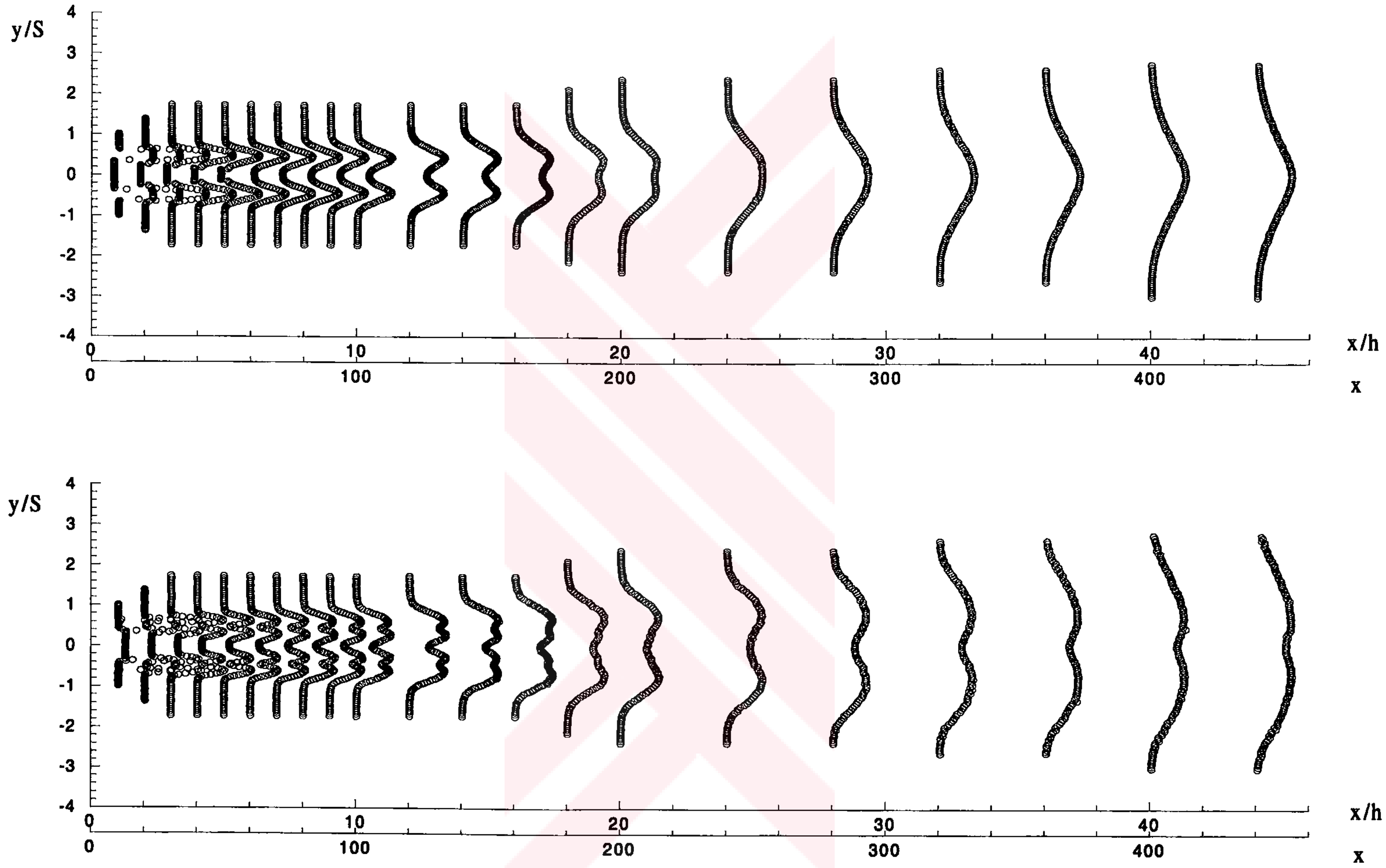

Figure B.3 Spatial development of the velocity and turbulence profiles of twin jet issued from 10 mm high rectangular jets.

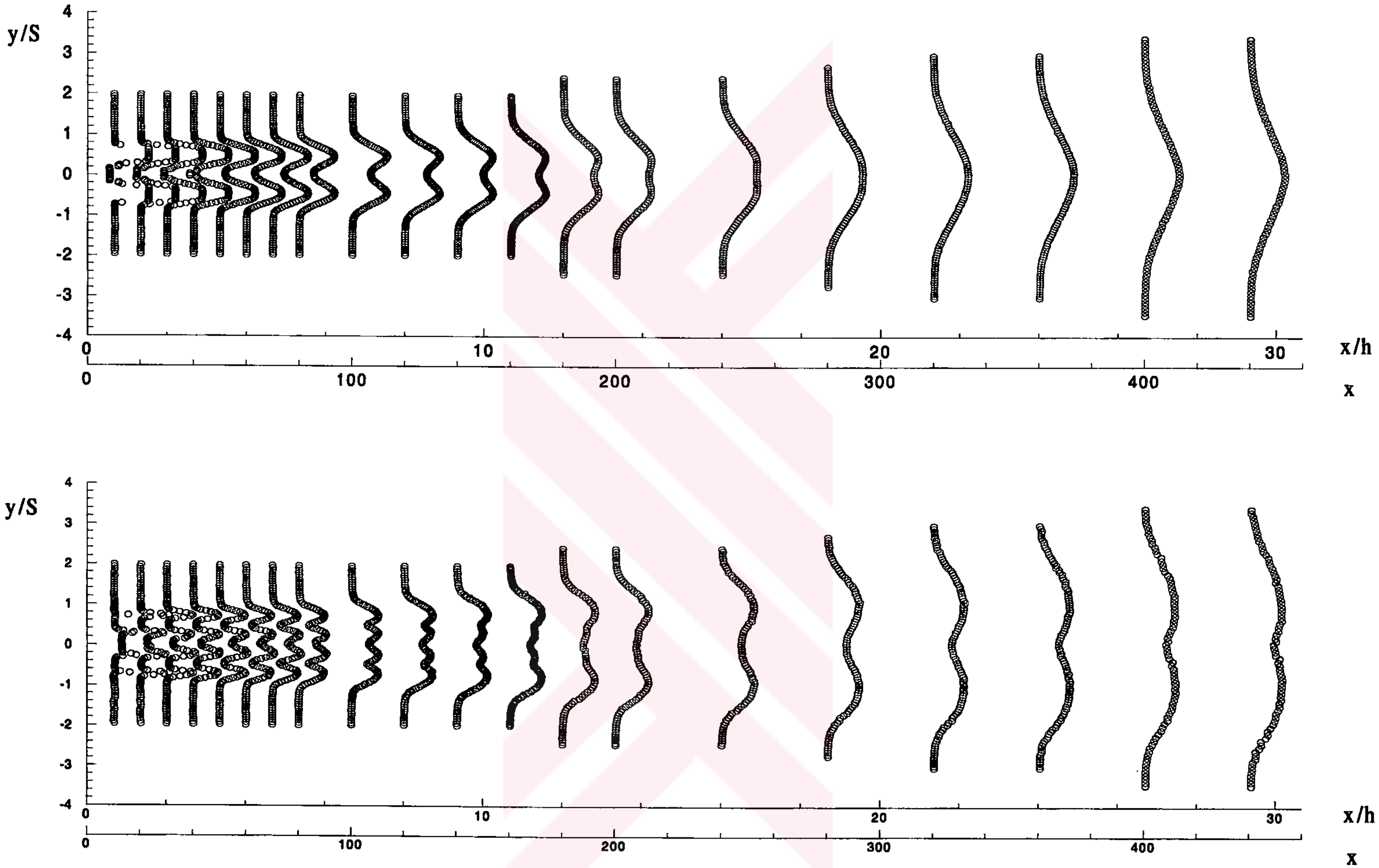

Figure B.4 Spatial development of the velocity and turbulence profiles of twin jet issued from 15 mm high rectangular jets.

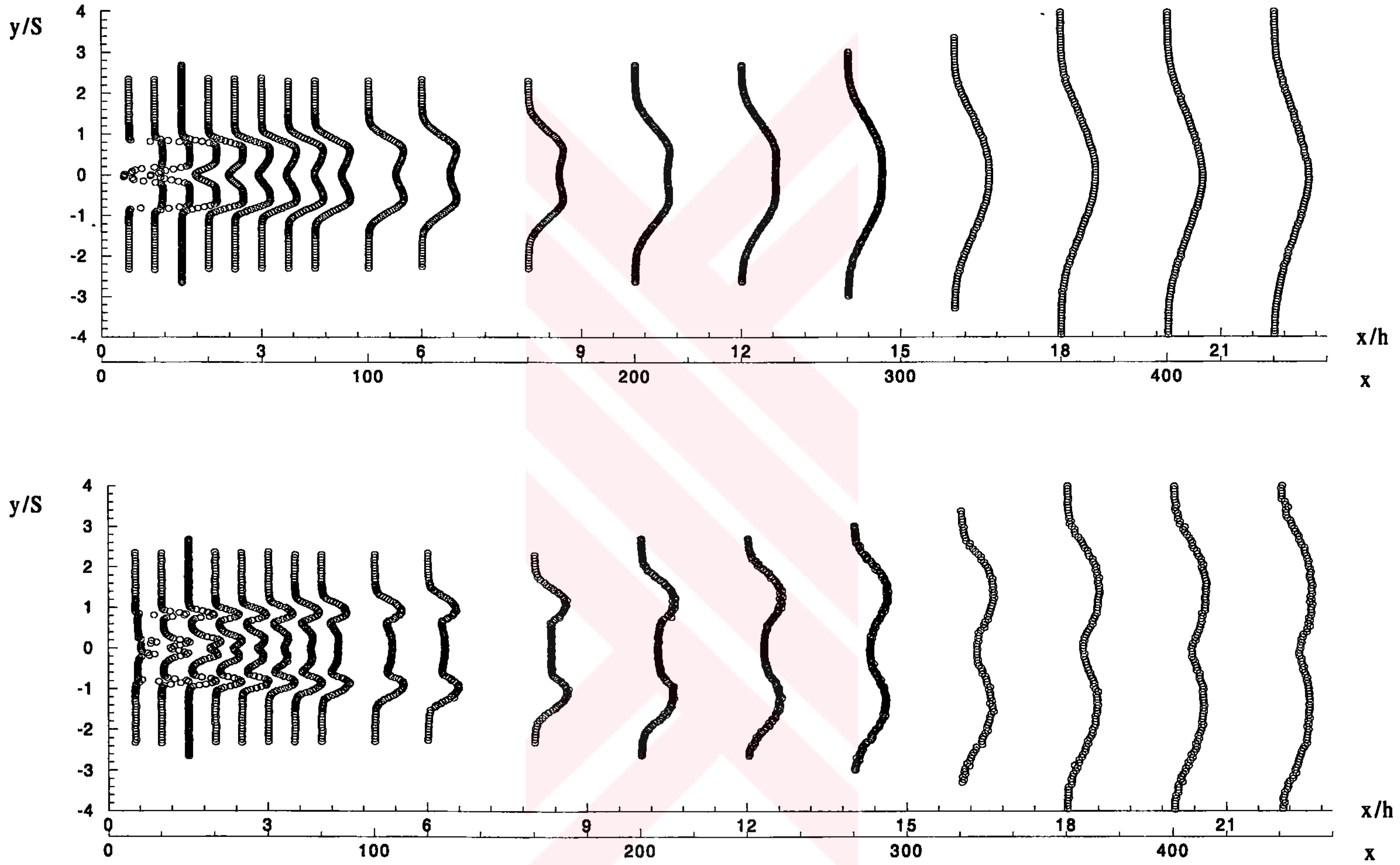

Figure B.5 Spatial development of the velocity and turbulence profiles of twin jet issued from 20 mm high rectangular jets.

APPENDIX C VELOCITY AND TURBULENCE PROFILES OF OFFSET JET

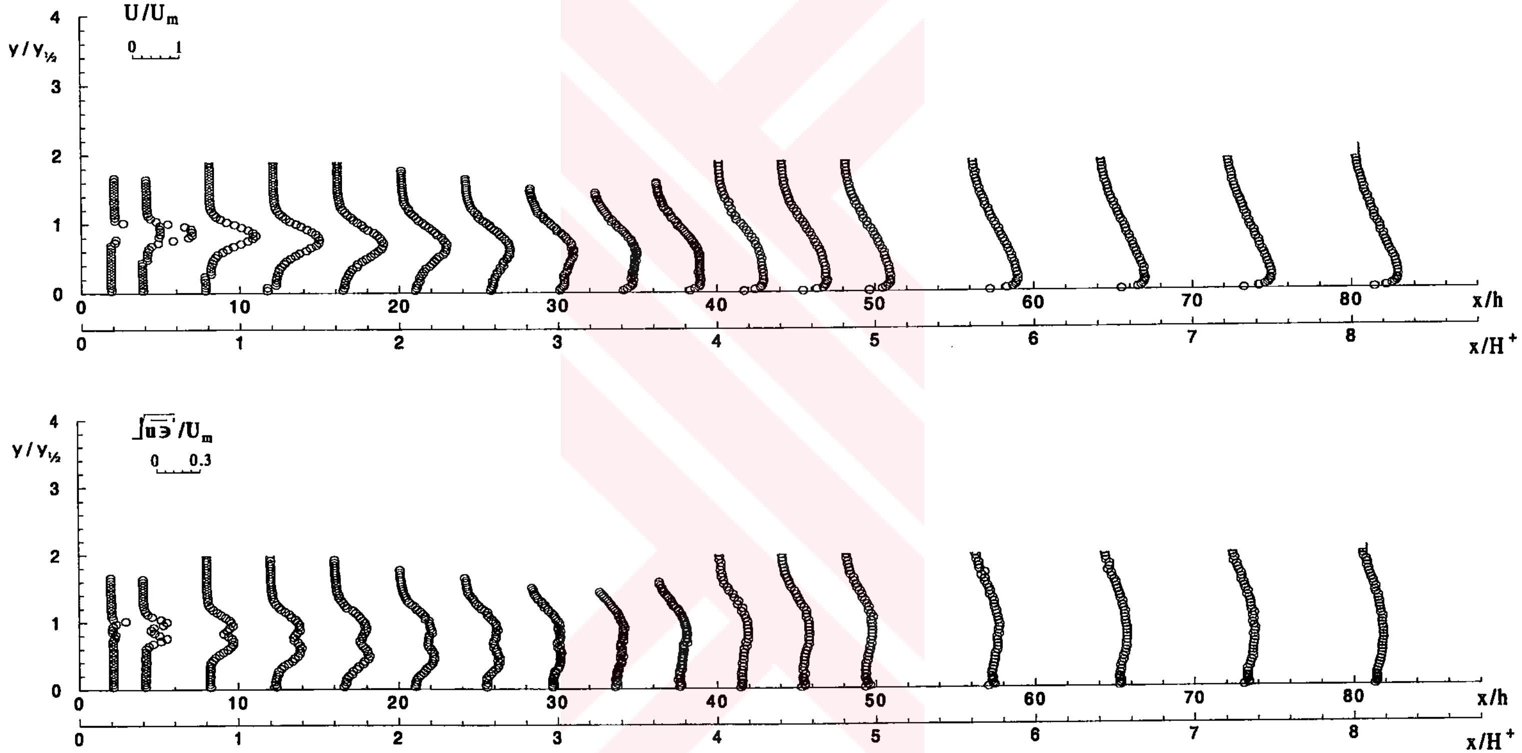

Figure C.1 Spatial development of the velocity and turbulence profiles of the offset jet issued from the 5 mm high rectangular slot with an offset ratio of 4.5.

APPENDIX D VELOCITY AND TURBULENCE PROFILES OF TWIN JET WITH CONVEX SURFACE

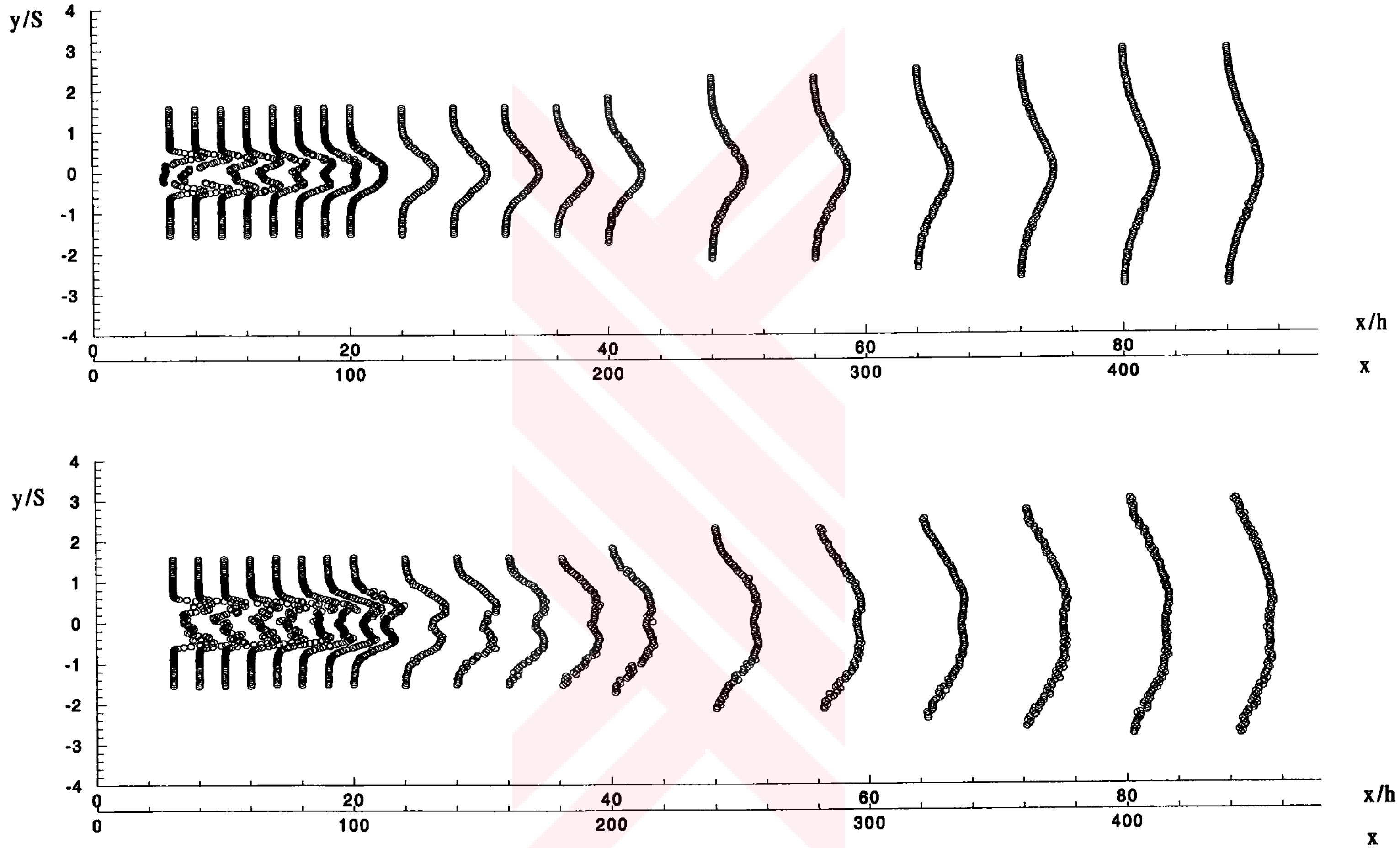

Figure D.1 Spatial development of the velocity and turbulence profiles of the twin jet issued from 5 mm high rectangular slots with a convex surface between them.

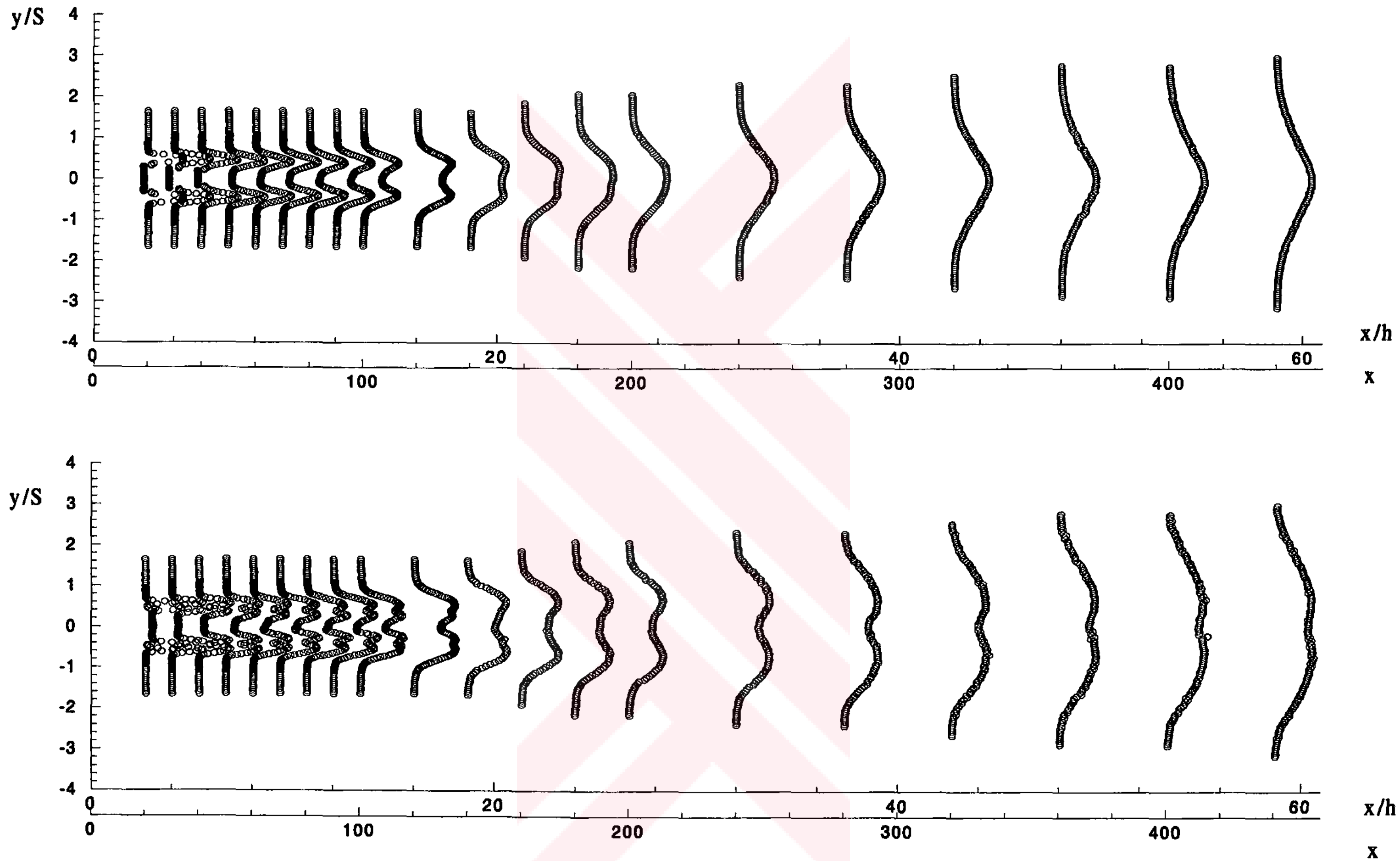

Figure D.2 Spatial development of the velocity and turbulence profiles of the twin jet issued from 7.5 mm high rectangular slots with a convex surface between them.

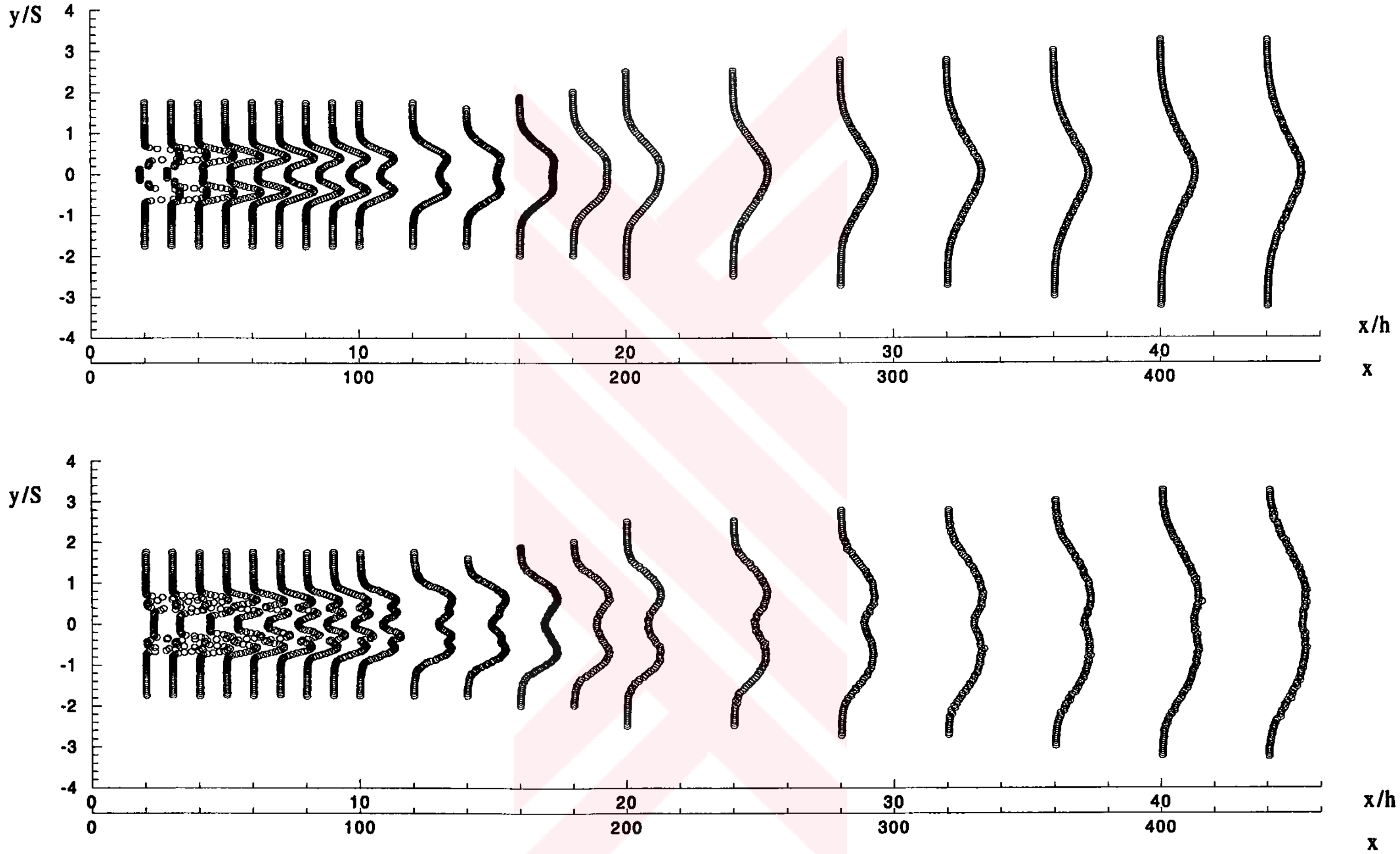

Figure D.3 Spatial development of the velocity and turbulence profiles of the twin jet issued from 10 mm high rectangular slots with a convex surface between them.

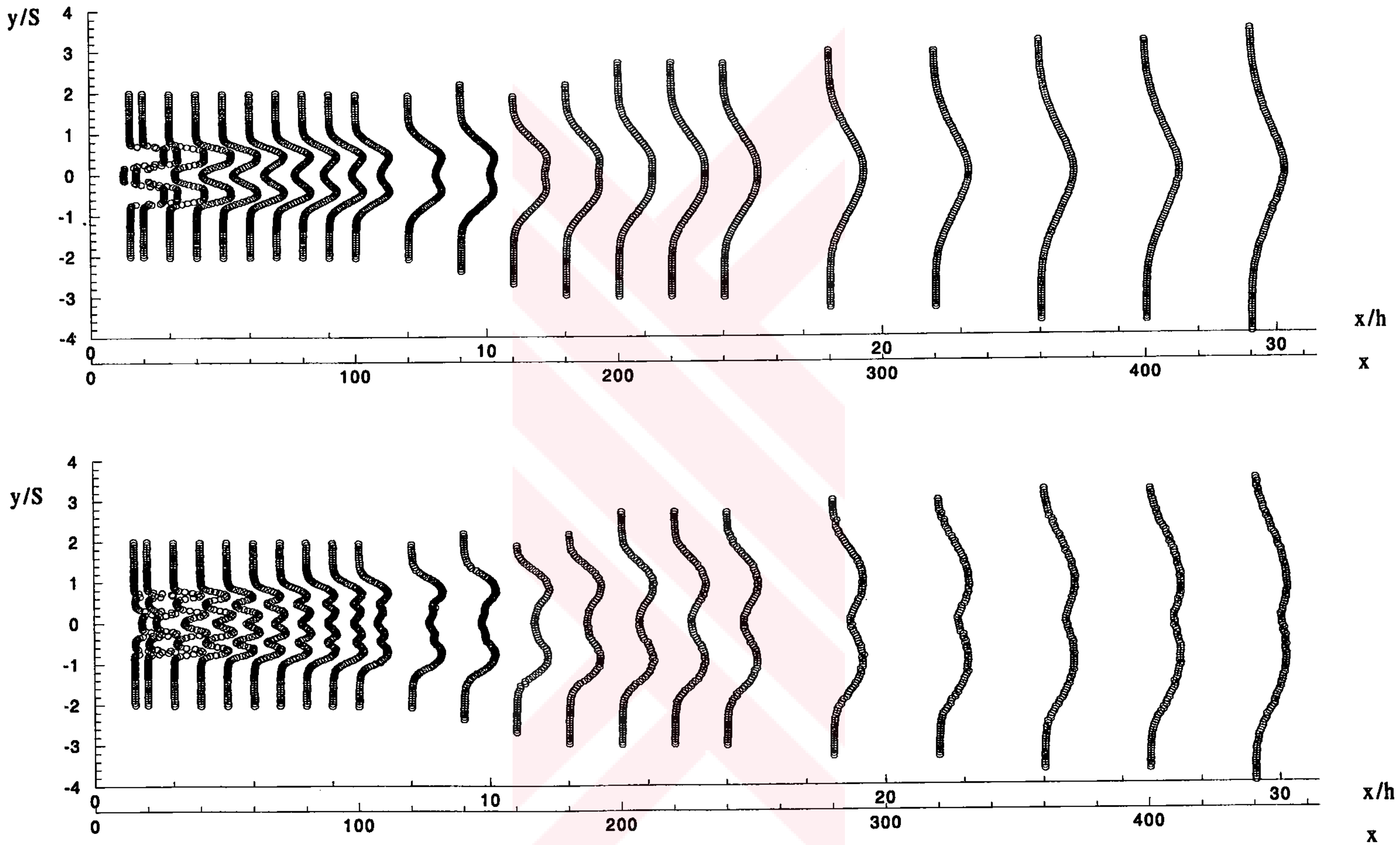

Figure D.4 Spatial development of the velocity and turbulence profiles of the twin jet issued from 15 mm high rectangular slots with a convex surface between them.

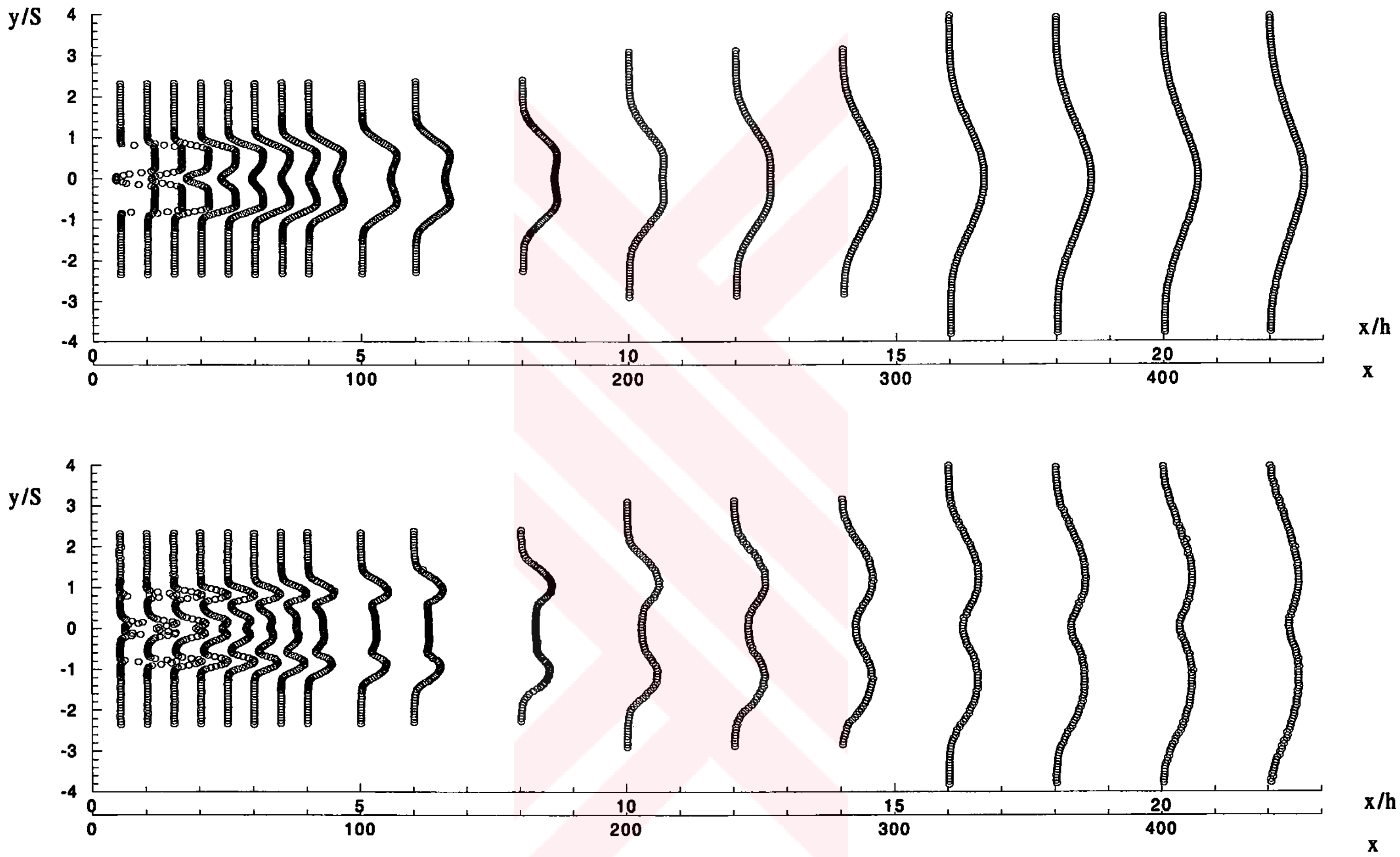

Figure D.5 Spatial development of the velocity and turbulence profiles of the twin jet issued from 20 mm high rectangular slots with a convex surface between them.

APPENDIX E PRESSURE DISTRIBUTIONS ON THE IMPINGEMENT SURFACE

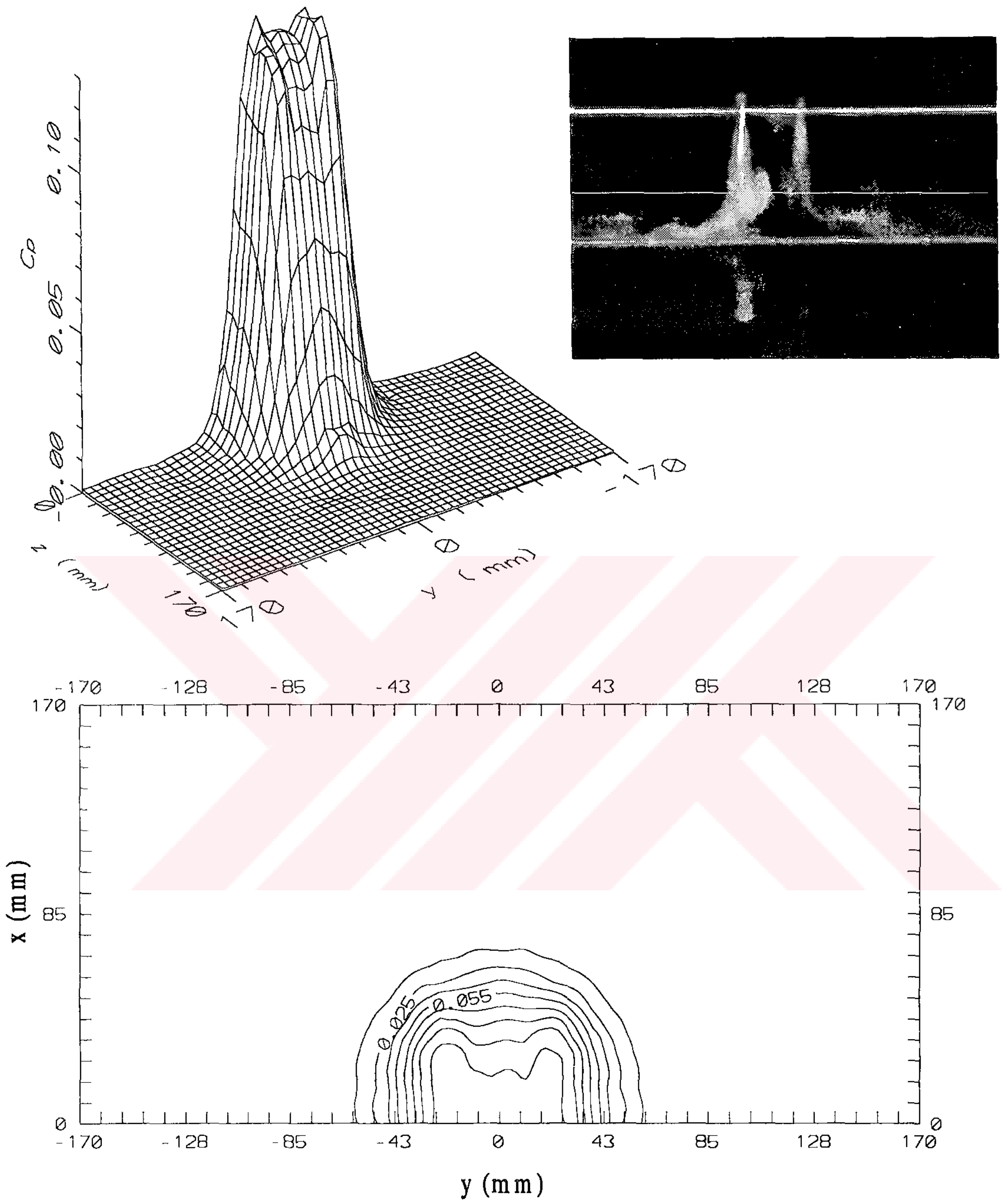

Figure E.1 Pressure distribution on the impingement plate (h=5mm, $Y/H^{+}=2$).

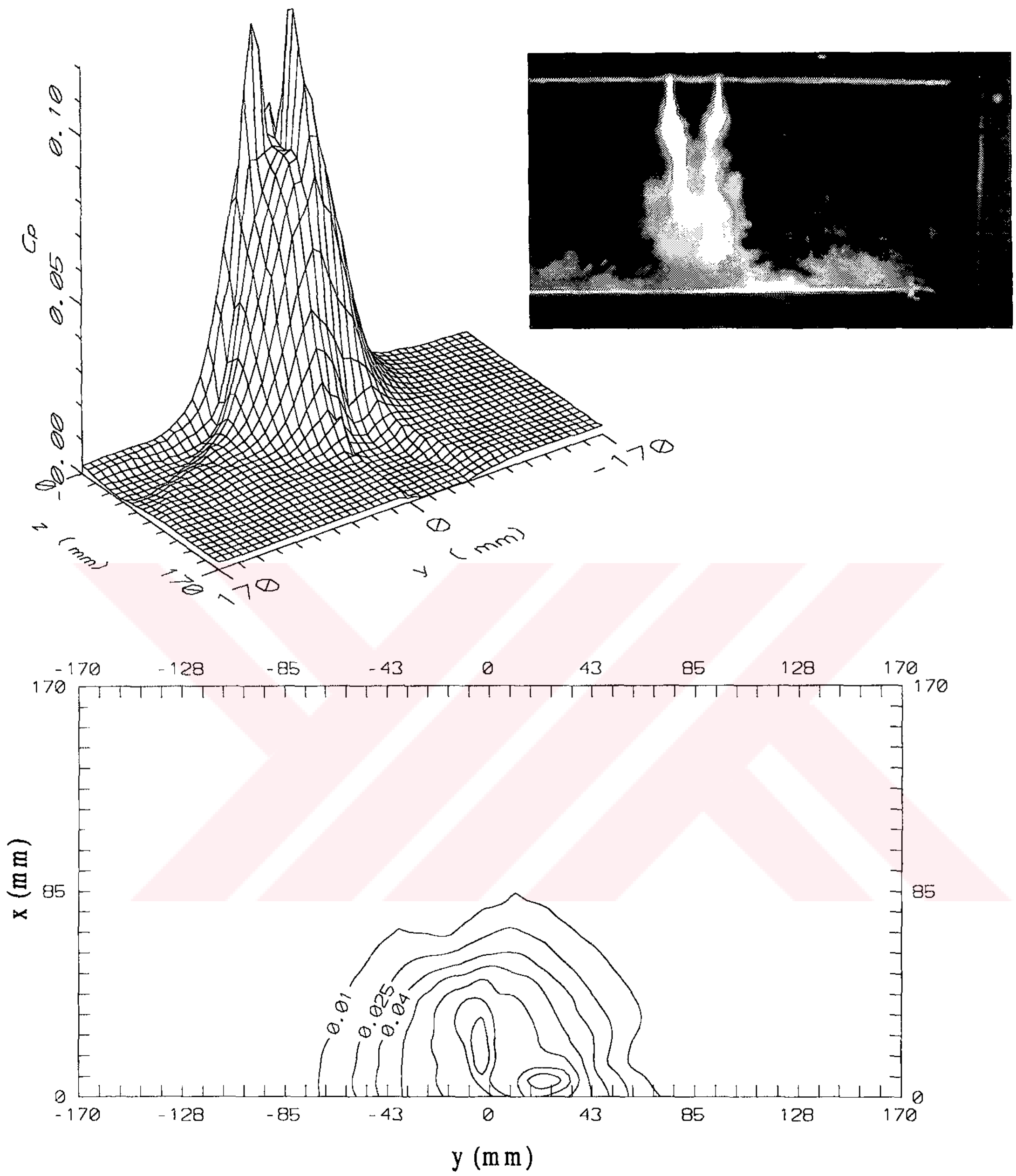

Figure E.2 Pressure distribution on the impingement plate (h=5mm, $Y/H^{+}=4$).

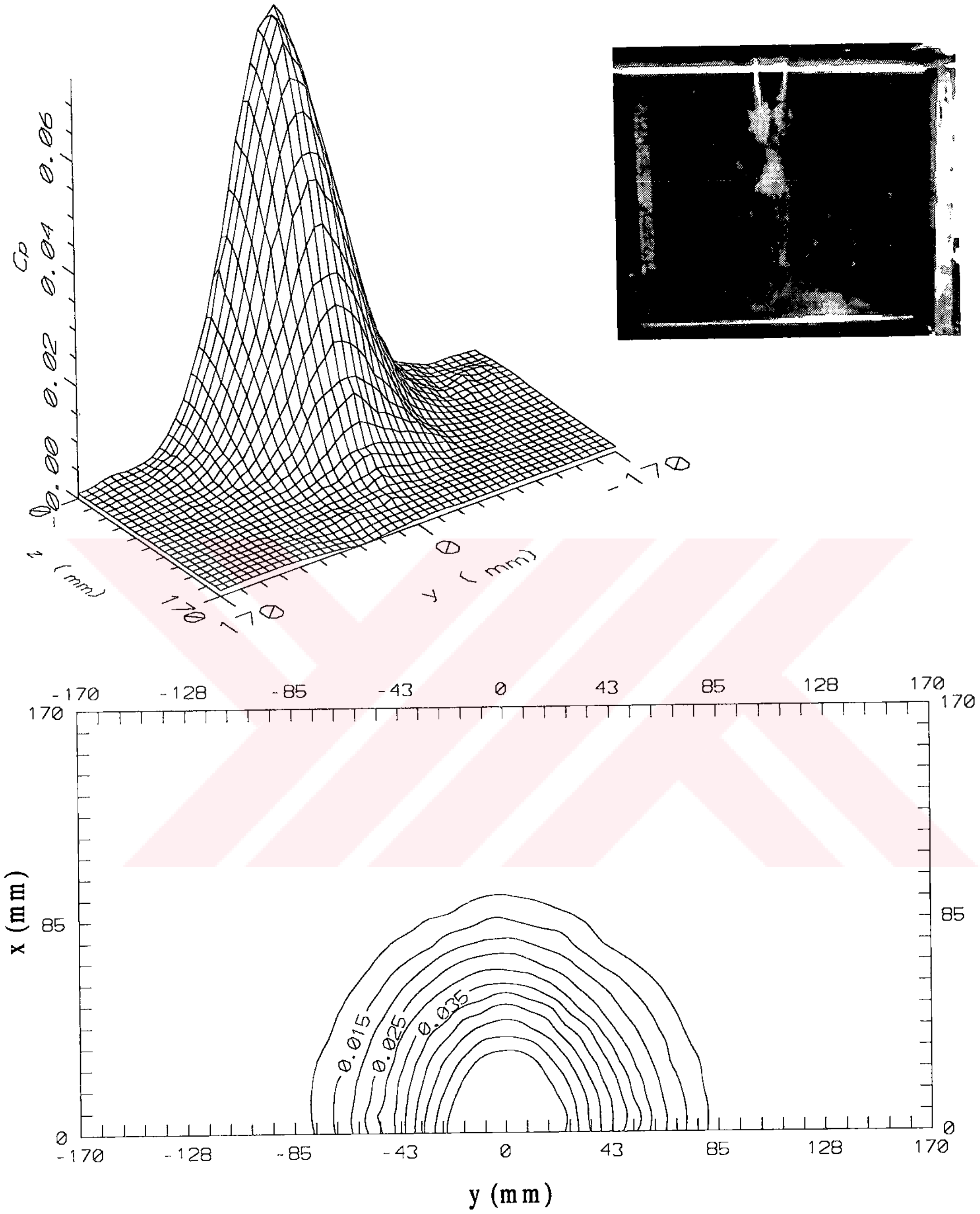

Figure E.3 Pressure distribution on the impingement plate (h=5mm, $Y/H^{+}=8$).

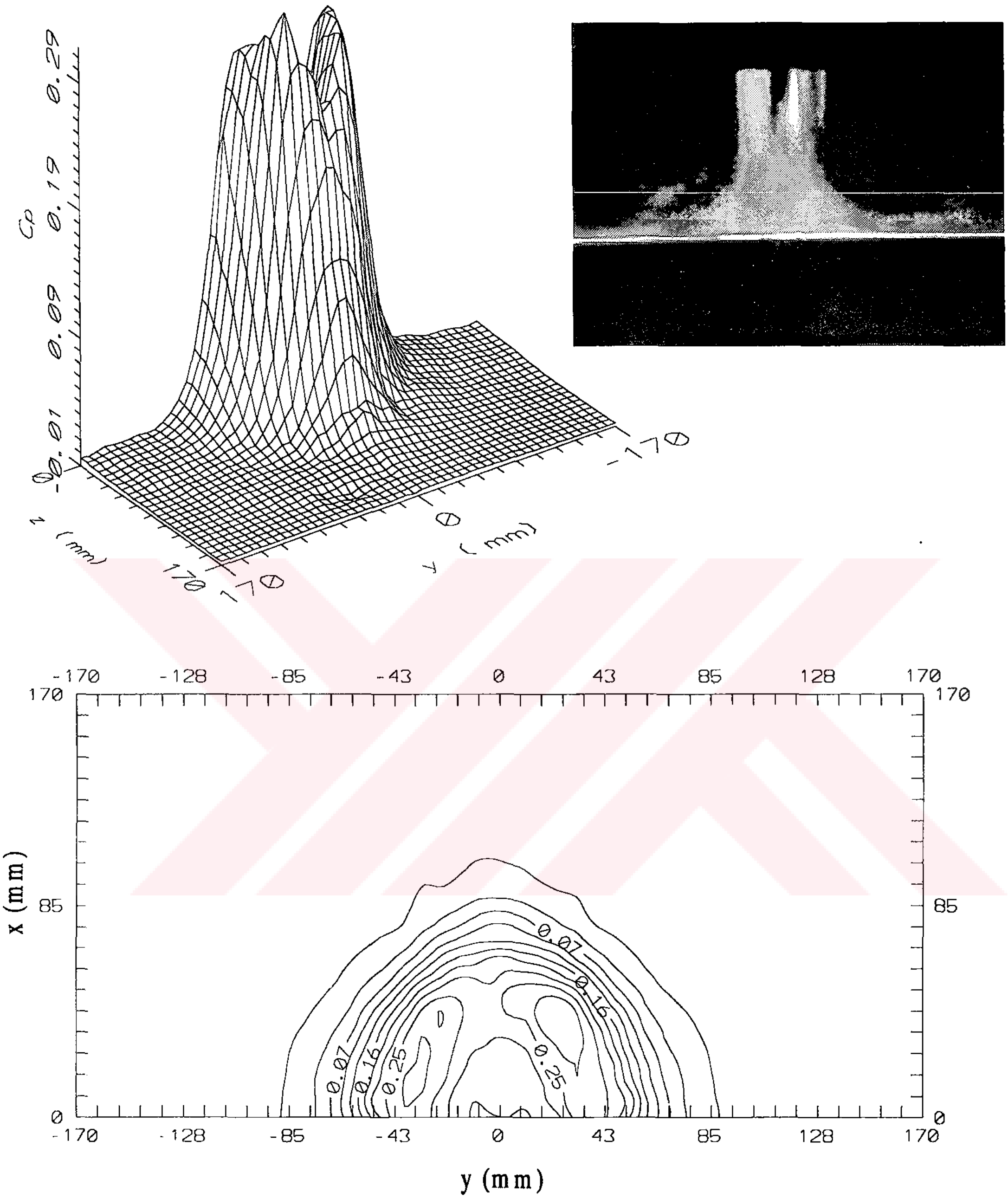

Figure E.4 Pressure distribution on the impingement plate (h=20mm, $Y/H^{+}=2$).

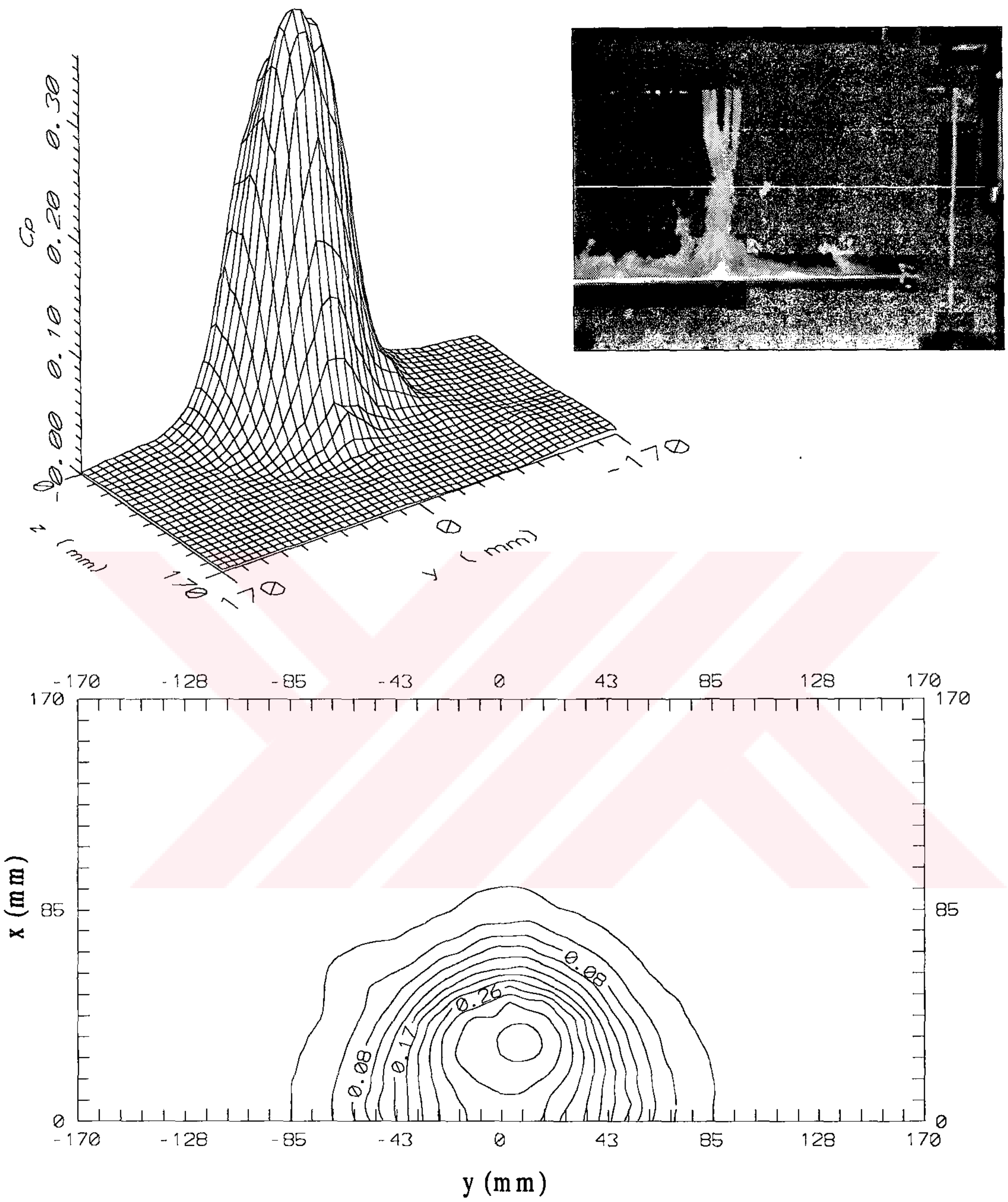

Figure E.5 Pressure distribution on the impingement plate (h=20mm, $Y/H^{+}=4$).

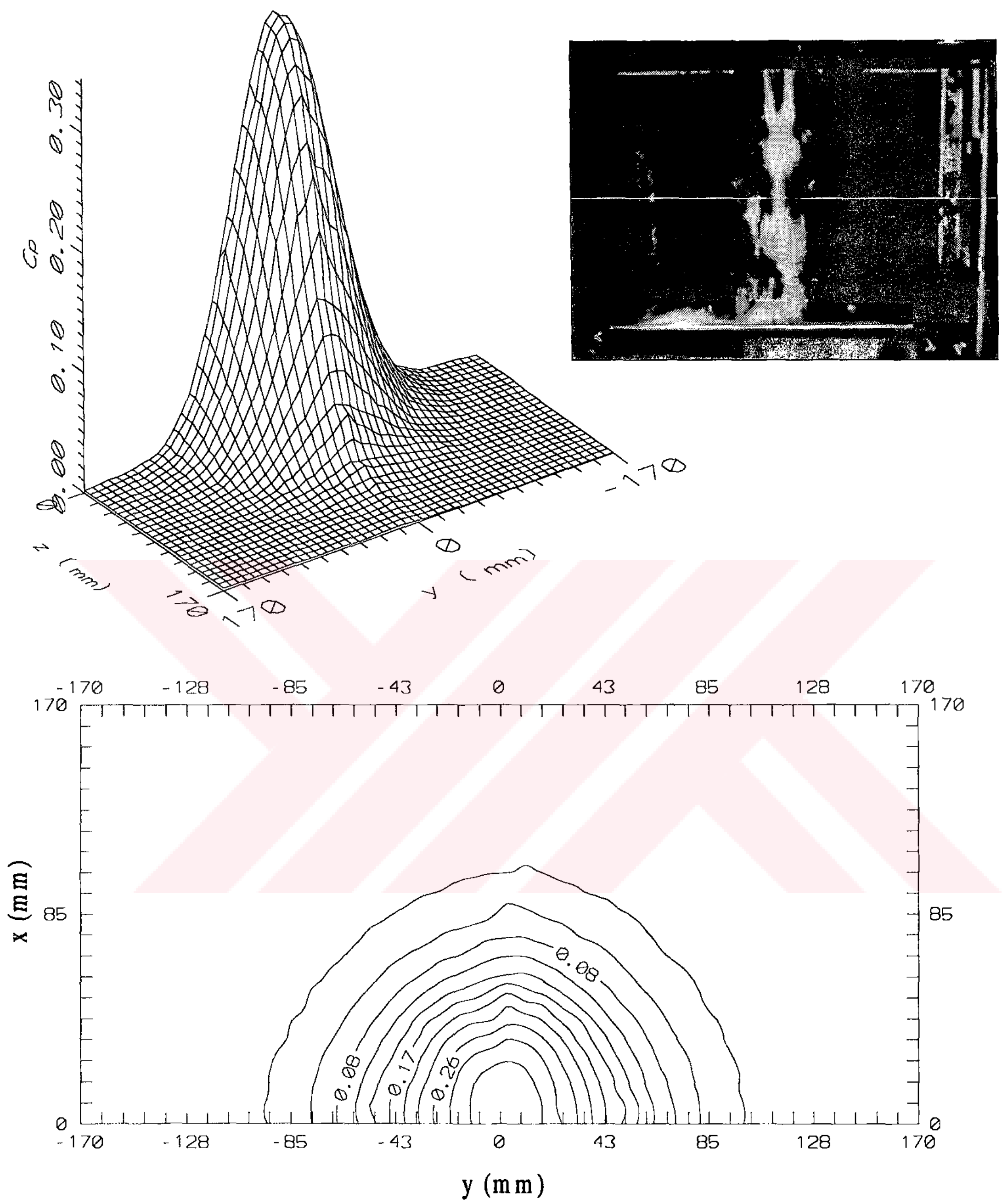

Figure E.6 Pressure distribution on the impingement plate (h=20mm, Y/H'=8).

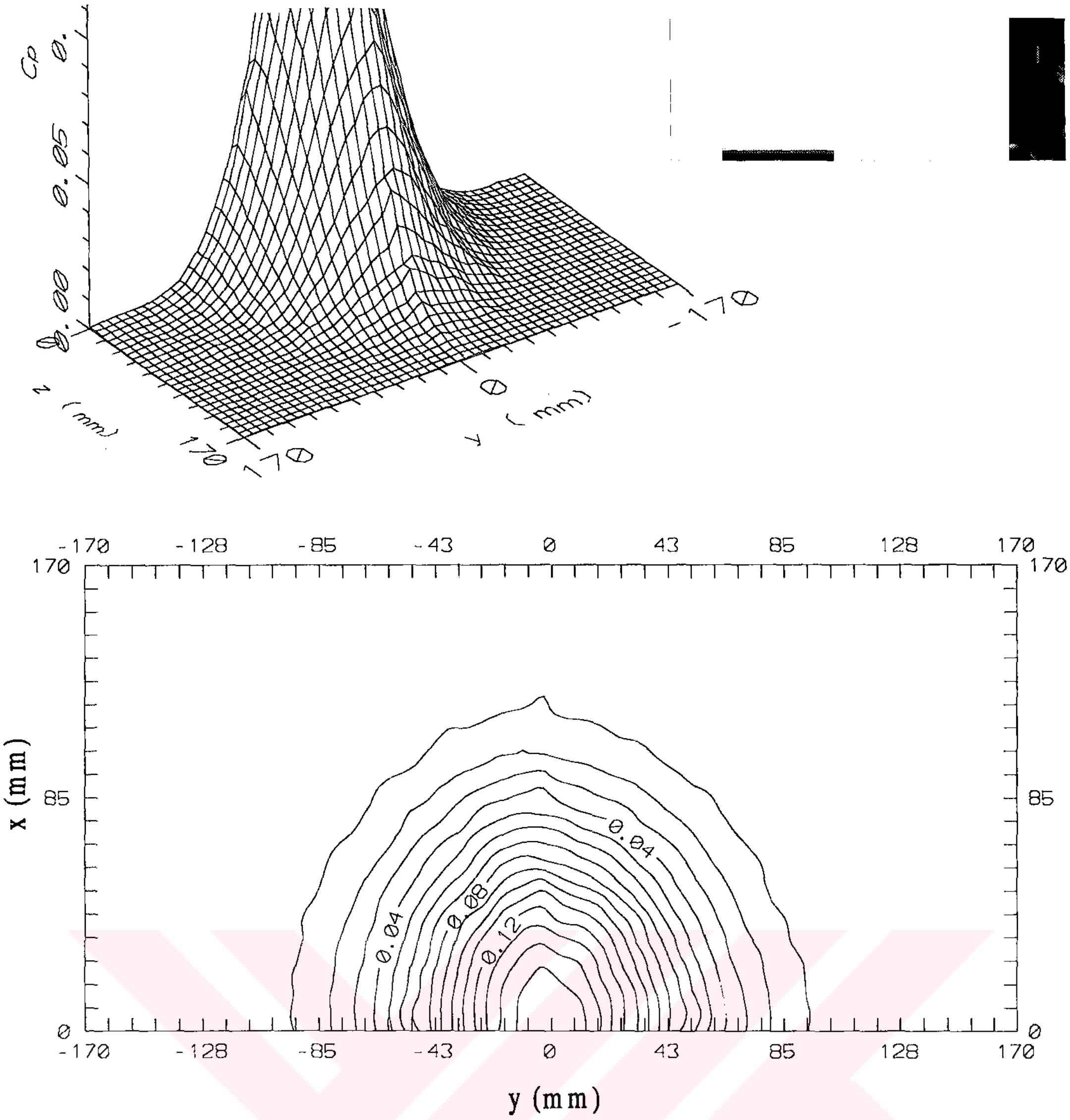

Figure E.7 Pressure distribution on the impingement plate (h=10mm, $Y/H^{+}=8$).

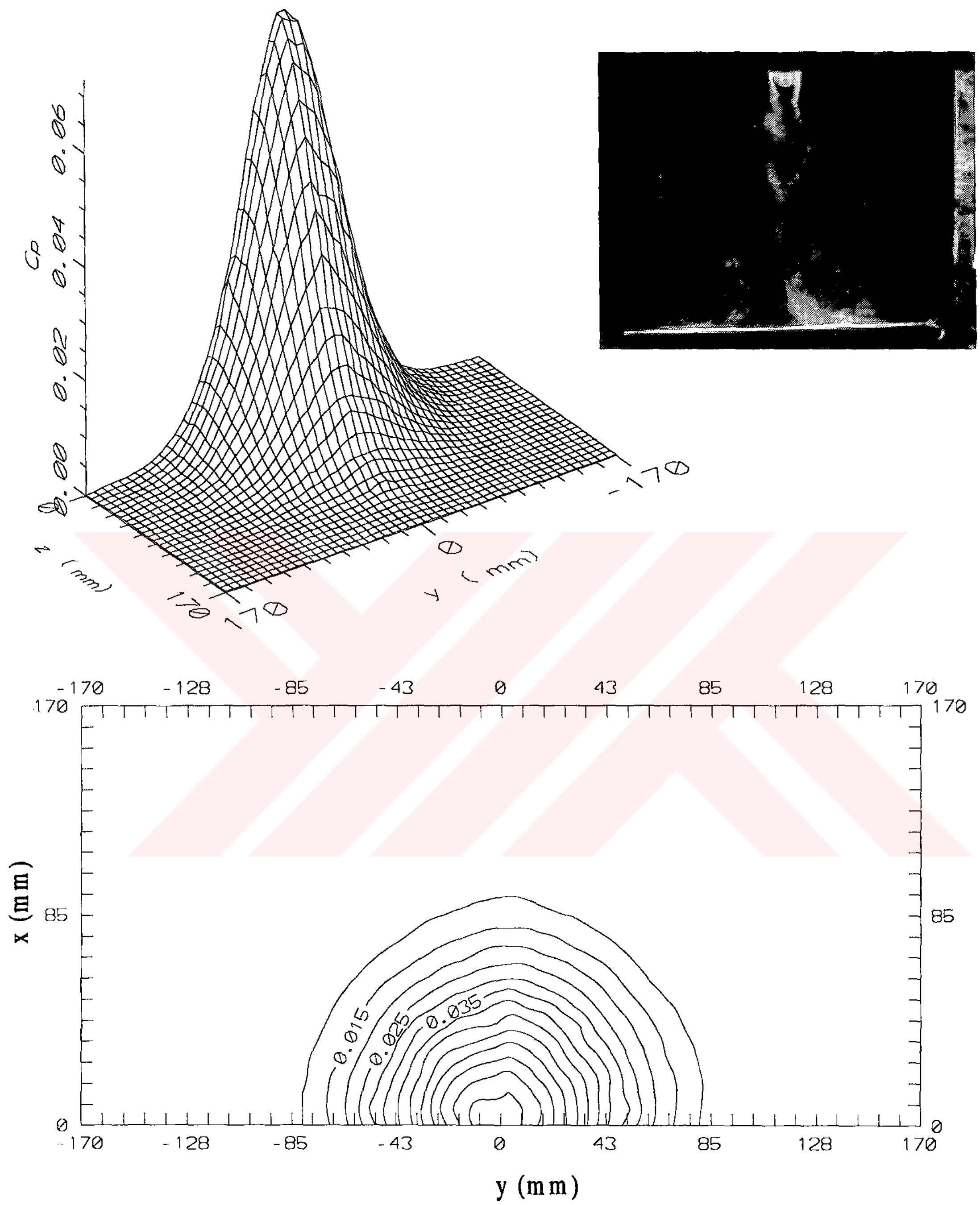

Figure E.8 Pressure distribution on the impingement plate (h=5mm, convex surface between jets, $Y/H^{+}=8$).

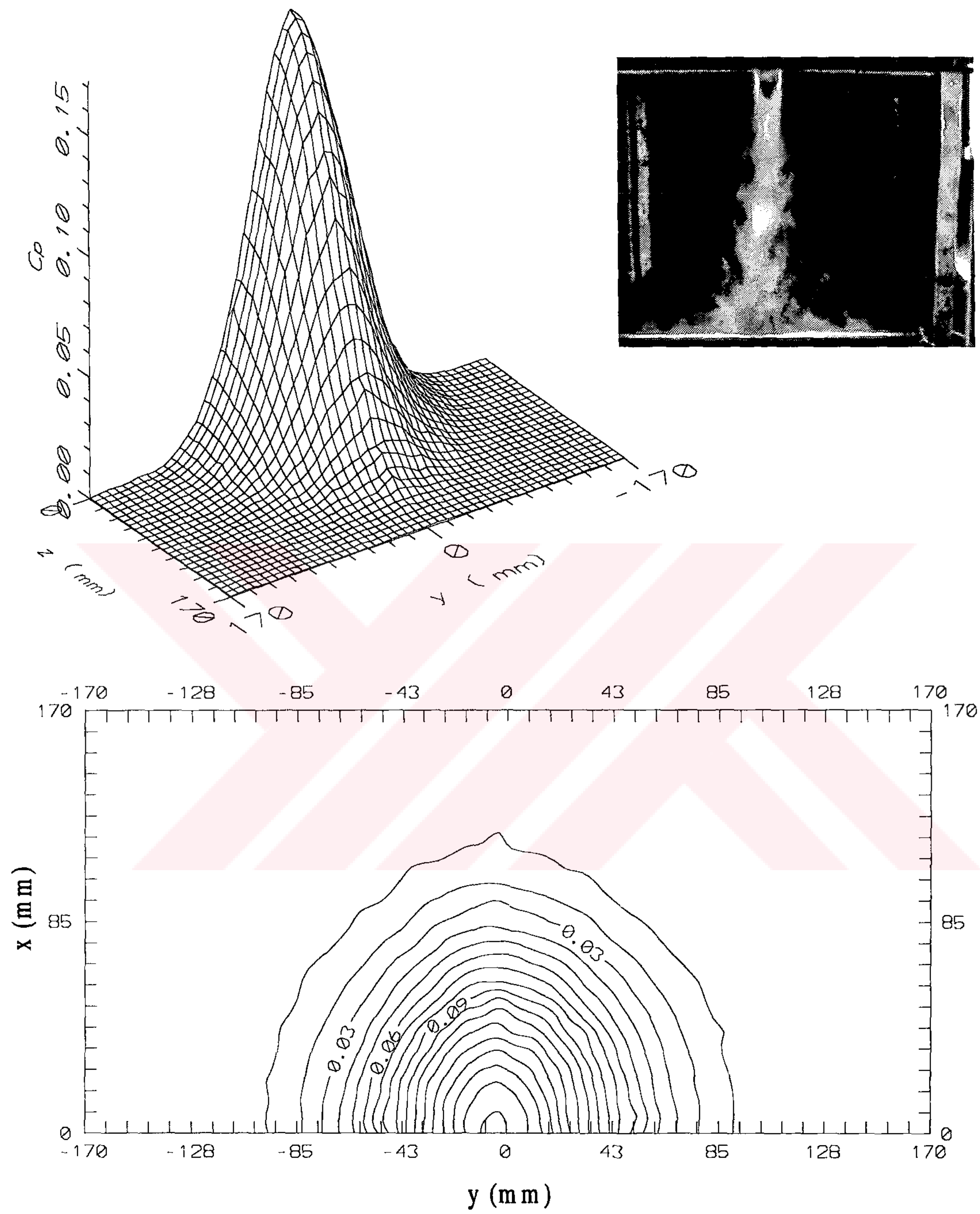

Figure E.9 Pressure distribution on the impingement plate (h=10mm, convex surface between jets, $Y/H^{+}=8$).

APPENDIX F FLOW VISUALIZATION ON THE IMPINGEMENT SURFACE

$Y/H^{+}=2$

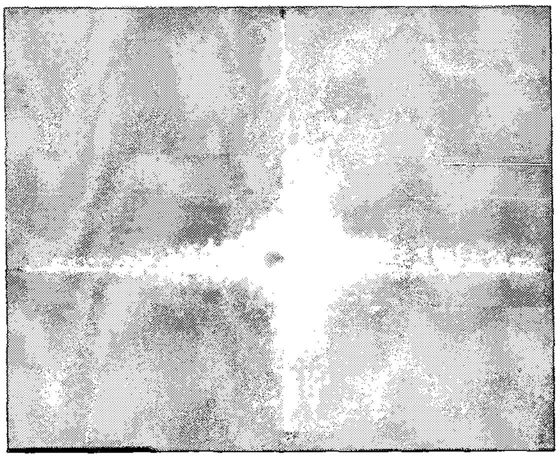

$Y/H^{+}=4$

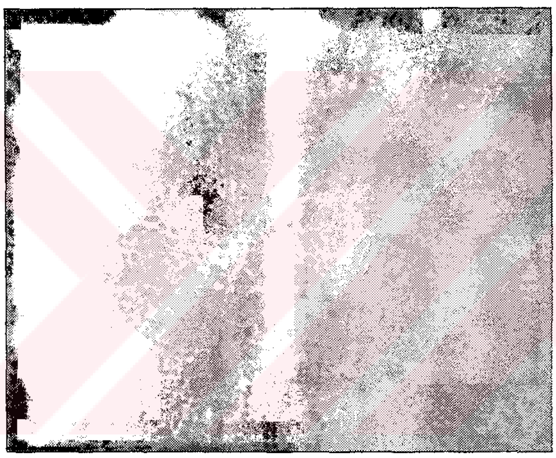

$Y/H^{+}=8$

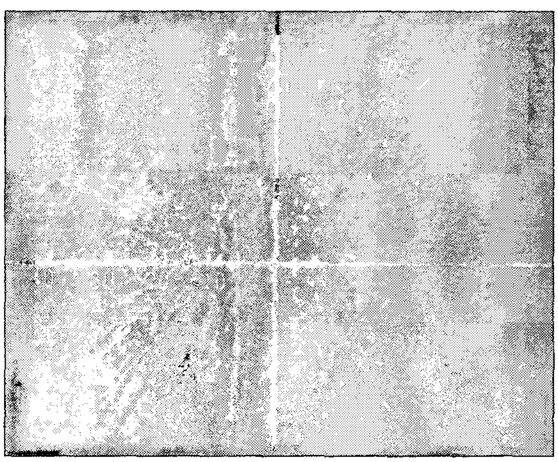

Figure F.1 Flow visualization photographs on the impingement surface (h=20mm, without convex surface)

Y/H$^+$=2

Y/H$^+$=4

Y/H$^+$=8

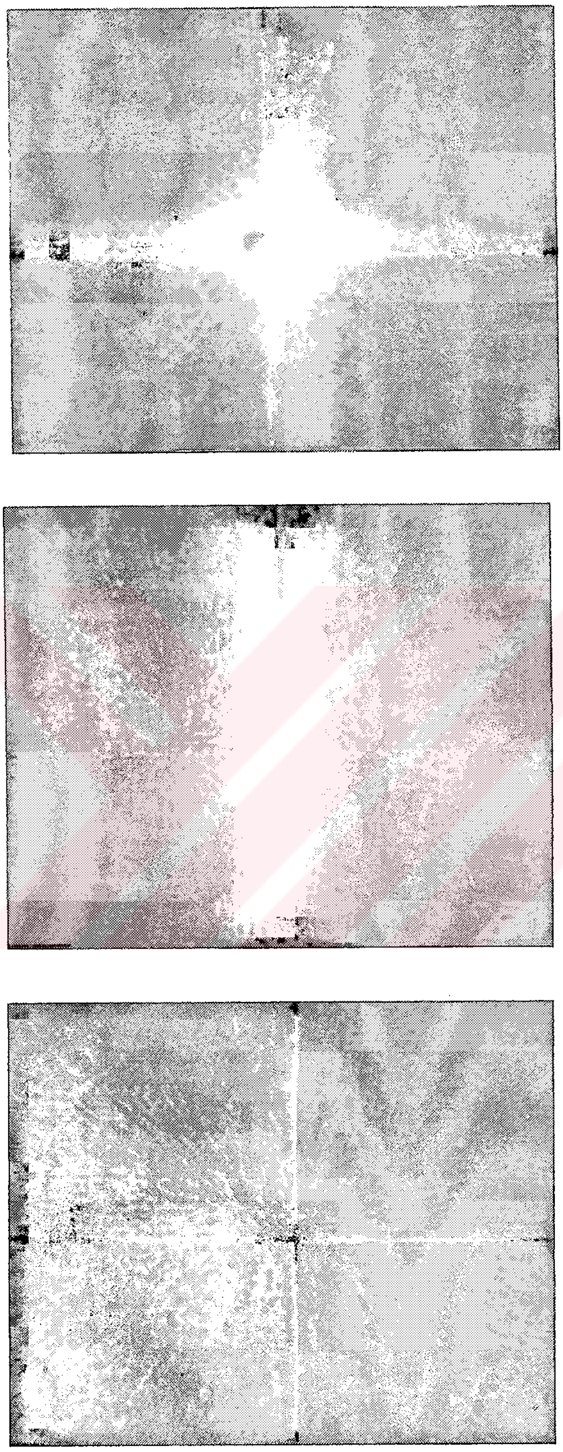

Figure F.2 Flow visualization photographs on the impingement surface (h=20mm, with convex surface)

CURRICULUM VITAE

Duygu ERDEM, was born in IZMIT-TURKIYE, in 1971. She completed her primary and secondary school education in Izmit. After having her lycée diploma from Lycée of Izmit, she continued her education in the Faculty of Aeronautics and Astronautics of Istanbul Technical University. She graduated from Istanbul Technical University with a B.Sc. degree in Aeronautical Engineering in 1992. In the same year, she started her graduate studies at ENSAE (Ecole Nationale Superiour de l'Aeronautique et de l'Espace)-Sup'Aero in France, with a scholarship from IAS. She received her M.Sc. Degree from ENSAE on December, 1993. She has been doing PhD in the Institute of Science and Technology of Istanbul Technical University since 1994. She has been employed by the Faculty of Aeronautics and Astronautics in 1995, as a research assistant.